NASA CR-72181

THIRD QUARTERLY REPORT

ELECTROCHEMICAL CHARACTERIZATION OF SYSTEMS FOR SECONDARY BATTERY APPLICATION

November, 1966 - January, 1967

by

M. Shaw, A. H. Remanick, R. J. Radkey

prepared for

NATIONAL AERONAUTICS AND SPACE ADMINISTRATION

February 17, 1967

CONTRACT NAS 3-8509

Technical Management
Space Power Systems Division
National Aeronautics and Space Administration
Lewis Research Center, Cleveland, Ohio
Mr. Robert B. King

NARMCO RESEARCH AND DEVELOPMENT DIVISION
OF
WHITTAKER CORPORATION
3540 Aero Court
San Diego, California 92123

TABLE OF CONTENTS

		Page
ABSTRACT		i
SUMMARY		ii
INTRODUCTION		iv
I.	RESULTS	
	A. Material Preparation	1
	B. Analysis of Cyclic Voltammograms	4
	1. Systems Involving Chloride Electrolytes	7
	2. Systems Involving Fluoride Electrolytes	15
	C. Tables of Cyclic Voltammetric Data	68
II.	EXPERIMENTAL	81
	A. Material Purification and Characterization	81
	1. Distillation of Solvents	81
	2. Solution Preparation	82
	3. Electrode Preparation	85
	B. Cyclic Voltammetric Measurements	86
III.	REFERENCES	87

CYCLIC VOLTAMMOGRAMS

Figure		Page
1.	Ag in Acetonitrile-$MgCl_2$	28
2.	Cu in Dimethylformamide-LiCl	29
3.	Cu in Dimethylformamide-LiCl + 1000 ppm H_2O	30
4.	Cu in Dimethylformamide-LiCl + 2000 ppm H_2O	31
5.	Cu in Dimethylformamide-$LiClO_4$	32
6	Cu in Dimethylformamide-$LiClO_4$ + 1000 ppm H_2O	33
7.	Cu in Dimethylformamide-LiCl+$LiClO_4$ + 1000 ppm water	34
8.	CuO in Propylene carbonate-LiCl+$AlCl_3$	35
9.	CuF_2 in Acetonitrile-$LiClO_4$	36
10.	CuF_2 in Butyrolactone-$LiClO_4$	37
11.	CuF_2 in Dimethylformamide-LiCl+$AlCl_3$	38
12.	CuF_2 in Dimethylformamide-$LiClO_4$	39
13.	CuF_2 in Propylene carbonate-$LiClO_4$	40
14.	Co in Acetonitrile-$LiClO_4$	41
15.	Co in Butyrolactone-$LiClO_4$	42
16.	AgF_2 in Butyrolactone-KPF_6	43
17.	AgF_2 in Propylene carbonate-$LiBF_4$	44
18.	Cu in Acetonitrile-$LiPF_6$	45
19.	Cu in Dimethylformamide-$Mg(BF_4)_2$	46
20.	CuO in Acetonitrile-$LiPF_6$	47
21.	CuO in Acetonitrile-KPF_6 + 1000 ppm H_2O	48
22.	CuO in Acetonitrile-KPF_6 + 2000 ppm H_2O	49
23.	CuF_2 in Acetonitrile-$LiPF_6$	50
24.	CuF_2 in Acetonitrile-$LiBF_4$	51
25.	CuF_2 in Acetonitrile-KPF_6	52
26.	CuF_2 in Acetonitrile-KPF_6+LiF	53
27.	CuF_2 in Butyrolactone-KPF_6	54

Figure		Page
28.	CuF_2 in Dimethylformamide-$LiPF_6$	55
29.	CuF_2 in Dimethylformamide-KPF_6	56
30.	CuF_2 in Dimethylformamide-$LiBF_4$	57
31.	CuF_2 in Propylene carbonate-$LiPF_6$	58
32.	CuF_2 in Propylene carbonate-KPF_6	59
33.	NiO in Acetonitrile-$LiPF_6$	60
34.	Co in Acetonitrile-$LiPF_6$	61
35.	Co in Dimethylformamide-$LiPF_6$	62
36.	Co in Dimethylformamide-$LiPF_6$	63
37.	CoO in Acetonitrile-$LiPF_6$	64
38.	CoO in Acetonitrile-KPF_6	65
39.	Zn in Dimethylformamide-KPF_6 (1.75 m)	66
40.	Zn in Dimethylformamide-KPF_6 (1.75 m) + 1000 ppm H_2O	67

Figure		
41.	Schematic of apparatus for preparing fluoride electrolytes	83

LIST OF TABLES

Table		Page
I.	Electrolyte Conductivities	2
II.	Electrochemical Systems Screened - Chloride (or Perchlorate) Electrolytes	5
III.	Electrochemical Systems Screened - Fluoride Electrolytes	6
IV.	Systems Causing Voltage Overload of Instrumentation	69
V.	Peak Current Density Range, Chloride and Perchlorate Electrolytes	71
VI.	Peak Current Density Range, Fluoride Electrolytes	72
VII.	Sweep Index	74
VIII.	Cathode Compatibility in Chloride Electrolytes	75
IX.	Cathode Compatibility in Fluoride Electrolytes	76
X.	ΔV_p and Charge-Discharge Efficiency, Chloride Electrolytes	78
XI.	ΔV_p and Charge-Discharge Efficiency, Fluoride Electrolytes	79
XII.	Fluorination Conditions	85

ELECTROCHEMICAL CHARACTERIZATION OF SYSTEMS FOR SECONDARY BATTERY APPLICATION

by

M. Shaw, A. H. Remanick, R. J. Radkey

ABSTRACT

Multisweep cyclic voltammograms have been obtained for an additional one hundred and ninety-three systems comprising silver, copper, nickel, cobalt, as well as the oxides and fluorides of these metals, in acetonitrile, butyrolactone, dimethylformamide, and propylene carbonate solutions of chlorides, perchlorates, and fluorides. Voltammograms are presented for thirty-nine of these systems. Tabular data includes peak current density, sweep index, charge-discharge efficiency, and cathode compatibility.

SUMMARY

The electrochemical characterization of non-aqueous battery systems by multisweep cyclic voltammetry has been continued. Cyclic voltammograms are now available on nearly four hundred systems comprising silver, copper, nickel, cobalt, zinc, cadmium, and molybdenum in chloride and fluoride solutions of acetonitrile, butyrolactone, dimethylformamide, and propylene carbonate. Solutes consist of $AlCl_3$, LiCl, $MgCl_2$, $LiClO_4$, LiF, MgF_2, $LiPF_6$, $LiBF_4$, and KPF_6. The cyclic voltammograms of thirty-nine systems are included in this report.

During this quarter, cyclic voltammetry was initiated on AgF_2, CuF_2, NiF_2, and CoF_3 electrodes. In general, nickel and cobalt fluoride electrodes exhibit low or negligible electrochemical activity in agreement with earlier data on nickel and cobalt metal. The possibility of high resistance due to excessive fluoride thickness cannot be discounted however, since similarly low currents are found for silver difluoride in certain cases, even though silver metal has demonstrated large currents during sweep cycling.

Cyclic voltammograms in general are not recordable in BF_3 and PF_5 solutions due to voltage overload of the instrumentation caused by a combination of appreciably high current and relatively low conductance (10^{-4} ohm^{-1} cm^{-1}) for these solutions. Sweep voltammetry of $LiBF_4$ and $LiPF_6$ solutions prepared <u>in situ</u> by the interaction of BF_3 and PF_5 with LiF suspensions in the solvents, demonstrate markedly different performance in terms of greater electrochemical activity compared with the commercially available complex fluorides.

Tables are presented listing system parameters derived from the cyclic voltammograms. These tables include data on peak current densities, sweep index, cathode compatibility, anodic to cathodic peak displacement and charge-discharge efficiency.

INTRODUCTION

The purpose of this program is to conduct a molecular level screening by the cyclic voltammetric method on a large number of electrochemical systems in nonaqueous electrolytes, and to characterize them as to their suitability for use in high energy density secondary batteries.

Since the release and storage of energy in a battery is initiated at the molecular level of the reaction, and therefore dependent on the charge and mass transfer processes, it is essential that screening be conducted at this level, in order to eliminate those systems whose electrode processes are inadequate for secondary battery operation.

I. RESULTS

A. MATERIAL PREPARATION:

During this period, attention was focused on the preparation of materials which were not commonly available in high purity.

The metal fluoride electrodes were prepared by direct fluorination of the metals. No direct measurement of coating thickness was made although measurement of weight gain indicated relatively thin coatings. Analysis of the coatings is in progress.

Since commercially available $LiBF_4$ and $LiPF_6$ were of doubtful purity, solutions of these salts were prepared by addition of BF_3 and PF_5 respectively to a suspension of LiF in the appropriate solvent. Formation of the desired material was evidenced by solution of essentially insoluble LiF, change in conductance, and alteration of the sweep curves from those in which only BF_3 and PF_5 were the only solutes present.

The addition of BF_3 or PF_5 in the absence of LiF did not appear to degrade acetonitrile, dimethylformamide or propylene carbonate. However, marked degradation of butyrolactone was observed. *In situ* preparation of $LiPF_6$ or $LiBF_4$ in this solvent was therefore not attempted.

Direct reaction of LiF and PF_5 at an elevated temperature, or by solution of LiF in liquid PF_5 was not successful. Attempted isolation and characterization of the salts prepared *in situ* is in progress.

Table I lists the conductivities of the solutions screened during this quarter.

TABLE I

ELECTROLYTE CONDUCTIVITIES

Electrolyte	Molality m	Conductivity $ohm^{-1} cm^{-1}$
Acetonitrile		
PF_5	0.5	2.2×10^{-3}
$LiPF_6$	0.5	1.7×10^{-2}
KPF_6	0.5(1)	1.5×10^{-2}
$LiF+KPF_6$	0.75(2)	3.7×10^{-2}
BF_3	0.5	1.9×10^{-4}
$LiBF_4$	0.5	1.6×10^{-2}
$Mg(BF_4)_2$	0.5(s)	9.2×10^{-4}
$LiClO_4$	0.75	3.0×10^{-2}
$MgCL_2$	0.5(s)	6.3×10^{-4}
Butyrolactone		
PF_5	5.6×10^{-2}	8.1×10^{-4}
KPF_6	0.75	7.1×10^{-3}
$LiF+KPF_6$	0.5(3)	1.4×10^{-2}
BF_3	0.5	5.0×10^{-4}
LiCl	0.5	7.1×10^{-4}
$LiClO_4$	0.75	1.1×10^{-2}
$LiCl+LiClO_4$	0.5	8.3×10^{-3}

TABLE I - Cont'd

Electrolyte	Molality m	Conductivity $ohm^{-1}\ cm^{-1}$
Dimethylformamide		
PF_5	0.5	3.9×10^{-4}
$LiPF_6$	0.5	2.7×10^{-3}
KPF_6	0.75	1.2×10^{-2}
	1.75(1)	1.3×10^{-2}
$LiF+KPF_6$	0.75(2)	1.2×10^{-2}
BF_3	0.5	1.7×10^{-3}
$LiBF_4$	0.5	5.7×10^{-3}
$Mg(BF_4)_2$	0.25	2.8×10^{-3}
LiCl	0.75	8.7×10^{-3}
$LiCl+AlCl_3$	0.5(s)	1.0×10^{-2}
$LiClO_4$	0.5	2.0×10^{-2}
$LiCl+LiClO_4$	0.75(1)	1.4×10^{-2}
Propylene Carbonate		
PF_5	5.6×10^{-2}	7.9×10^{-4}
$LiPF_6$	0.25	5.9×10^{-3}
KPF_6	1.0	4.5×10^{-3}
$LiF+KPF_6$	0.75(2)	4.4×10^{-3}
BF_3	0.5	1.1×10^{-4}
$LiBF_4$	0.5	4.2×10^{-3}
$LiCl+AlCl_3$	0.5	8.9×10^{-3}
$LiClO_4$	1.0	6.2×10^{-3}

(s) Saturated

(1) No measurable change in conductivity occurred on addition of 1000 or 2000 ppm H_2O

(2) Solution initially 0.75 m in KPF_6 and saturated with LiF. Solution was stirred overnight to equilibrate.

(3) Solution initially 0.5 m in KPF_6 and saturated with LiF. Solution was stirred overnight to equilibrate.

B. ANALYSIS OF CYCLIC VOLTAMMOGRAMS

Tables II and III list the electrochemical systems screened during the second quarter of this program. This represents a total of 193 systems. Curve analysis was accomplished by dividing all systems into two major groups:

1. Systems involving chloride electrolytes
2. Systems involving fluoride electrolytes

Each main group was then subdivided according to the identity of the working electrode. Each of these subgroups was further broken down according to the identity of the solvent portion of the solution. The cyclic voltammograms are then discussed in terms of the total solution. This classification facilitates data analysis, and has permitted a more significant correlation among the electrochemical systems.

Except in those cases where the metal is converted to a cathodic material prior to assembly in the measuring cell, the working electrode is the base metal itself. During the voltage sweep, the metal is oxidized to some species, this anodic product then serving as the cathode which is subsequently reduced during the cathodic portion of the sweep. Each sweep cycle thus corresponds to a charge-discharge cycle. In the absence of complicating factors, it is assumed that chloride cathodes would be formed in chloride electrolytes, and fluoride cathodes in fluoride electrolytes.

Each cyclic voltammogram is identified by a CV number and labelled according to the electrochemical system, sweep rate, temperature, and zero reference, respresenting the open circuit voltage (ocv) of the working electrode with respect to the indicated reference electrode. The current axis is in units of ma/cm^2, each unit being of variable scale depending on the X-Y recorder sensitivity setting. A maximum sensitivity of 0.1 $ma/cm^2/cm$ division has been established to avoid exaggerating the current background of poor systems. The sweep is always in a clockwise direction, the

TABLE II ELECTROCHEMICAL SYSTEMS SCREENED - CHLORIDE (or PERCHLORATE) ELECTROLYTES

Solute \ Solvent	Acetonitrile	Butyrolactone	Dimethylformamide	Propylene carbonate
LiCl	-	Co, CoO	Cu, Cu(a), Cu(b) Cu(c), Co, CoO	-
$LiCl+AlCl_3$	-	-	AgF_2, CuF_2, NiF_2 Co, CoF_3	AgO, CuO, NiO
$LiClO_4$	AgF_2, CuF_2, NiF_2 Co, CoO, CoF_3	AgF_2, CuF_2, NiF_2 Co, CoO, CoF_3	AgF_2, Cu(d), Cu(e) Cu(a, e), CuO, CuF_2 NiF_2, Co, CoO, CoF_3	AgF_2, CuF_2, NiF_2 Co, CoO, CoF_3
$LiCl+LiClO_4$	-	Co, CoO	Cu(a), Cu(b), Co CoO	-
$MgCl_2$	Ag, Cu, Ni	-	-	-

(a) Containing 1000 ppm water
(b) Containing 2000 ppm water
(c) Containing 3000 ppm water
(d) 0.5m
(e) 0.25m

TABLE III ELECTROCHEMICAL SYSTEMS SCREENED - FLUORIDE ELECTROLYTES

Solute \ Solvent	Acetonitrile	Butyrolactone	Dimethylformamide	Propylene carbonate
PF_5	Ag, Cu, Ni, Co	Ag, Cu, Ni, Co	Ag, Cu, Ni, Co	Ag, Cu, Ni, Co
$LiPF_6$	Ag, AgO, AgF_2, Cu CuO, CuF_2, NiF_2, Co CoO, CoF_3, NiO	-	AgO, AgF_2, CuF_2 Co, CoO, CoF_3 NiF_2	AgO, AgF_2, CuO CuF_2, NiO, NiF_2 Co, CoO, CoF_3
KPF_6	AgF_2, CuO(a), CuO(b) CuF_2, NiF_2, Co, CoO, CoF_3	AgF_2, CuF_2 NiF_2, Co, CoO CoF_3	AgF_2, CuF_2, NiF_2 Co, CoO, CoF_3, Zn, Zn(a), Zn(b)	AgF_2, CuF_2, NiF_2 Co, CoO, CoF_3
$LiF+KPF_6$	AgF_2, CuF_2, NiF_2 Co, CoF_3	AgF_2, CuF_2 NiF_2, Co, CoO CoF_3	AgO, AgF_2, CuO CuF_2, NiO, NiF_2 Co, CoO, CoF_3	AgO, AgF_2, CuO CuF_2, NiO, NiF_2 Co, CoO, CoF_3
BF_3	Ag, Cu, Ni, Co	Ag, Cu, Ni, Co	Ag, Cu, Ni, Co	Ag, Cu, Ni, Co
$LiBF_4$	Ag, AgF_2, CuF_2 Co, CoF_3	-	AgF_2, CuF_2, NiF_2 Co, CoF_3	AgF_2, CuF_2, NiF_2 Co, CoF_3
$Mg(BF_4)_2$	Ag, Cu, Ni, Co	-	Ag, Cu, Ni, Co	-

(a) Containing 1000 ppm water
(b) Containing 2000 ppm water

potential becoming more positive to the right. Positive currents represent anodic (charge) reactions, and negative currents represent cathodic (discharge) reactions. The voltage axis units are relative to the ocv so that voltage units are in terms of electrode polarization.

For comparative purposes, current density magnitude is classified according to very high (more than 300 ma/cm^2), high (100-300 ma/cm^2), medium high (50-100 ma/cm^2), medium low (10-50 ma/cm^2), low (1-10 ma/cm^2), and very low (less than 1 ma/cm^2).

Analysis is based on the cyclic voltammograms obtained at the lowest sweep rate, 40 mv/sec, except where additional information is required from the higher sweep rate curves to aid in the analysis.

1. Systems Involving Chloride Electrolytes

a. Silver Electrode

(1) Acetonitrile solutions

The cyclic voltammogram for silver in acetonitrile-$MgCl_2$ (Figure 1, CV-1147) exhibits a low anodic peak (3.3 ma/cm^2) and a flat cathodic plateau (1.0 ma/cm^2). Low conductivity indicates low chloride ion availability. Performance is therefore much poorer than the case for LiCl, which exhibits a well-formed cathodic peak, even though it is broad and of medium low height (Ref. 1, Figure 10).

b. Silver Oxide Electrode

(1) Propylene carbonate solutions

Silver oxide in $LiCl+AlCl_3$ solution results in current overload, comparing with silver in acetonitrile-$LiCl+AlCl_3$ reported earlier (Ref. 1).

c. Silver Difluoride Electrode

These represent the first reported data on silver difluoride electrodes prepared by direct fluorination of silver wire in fluorine gas.

Cyclic voltammetry of silver difluoride electrodes in lithium perchlorate solutions of acetonitrile, butyrolactone, dimethylformamide, and propylene carbonate, as well as in dimethylformamide-$LiCl+AlCl_3$, indicate excessively low currents in all cases. This may be due to high electrode resistance owing to a relatively deep conversion of metallic silver to the difluoride.

The sweep curve in butyrolactone solution is similar to that for silver oxide in the same solution (Ref. 1, Figure 9) except for having low current densities, 2.0 and 1.2 ma/cm^2 for the anodic and cathodic peak respectively, compared with 440.0 and 154.0 ma/cm^2 for the silver oxide electrode. Although a sharp anodic peak is formed in acetonitrile solution, the peak c.d. is less than 1 ma/cm^2.

The silver difluoride layer is apparently sufficiently stable in these solvents, otherwise typical silver curves would have been obtained (e.g. Ref. 1, Figures 9, 11, 15 and 22).

d. Copper Electrode

(1) Acetonitrile solutions

Copper in acetonitrile-$MgCl_2$ exhibits voltage overload.

(2) Dimethylformamide solutions

The cyclic voltammogram for copper in dimethylformamide-LiCl was determined earlier (Ref. 1, Figures 25 and 26). During this period, the effect of water on the curve characteristics was determined. Three separate solutions were prepared containing 1000, 2000 and 3000 ppm water respectively. Cyclic

voltammograms are shown in Figures 2-4 (CV's-1116, 1121, 1126). The presence of water has no appreciable effect on the curve shape. The initial anodic peak is slightly sharper, and there is a broadening at the base of the second anodic peak, which may or may not be significant.

The curve for copper in 0.25 m $LiClO_4$ solution is shown in Figure 5 (CV-1137). A similar curve is obtained for a 0.5 m solution, but the anodic and cathodic peak currents are three - and two-fold larger respectively. The effect of adding 1000 ppm water to 0.25 m $LiClO_4$ in dimethylformamide is shown in Figure 6 (CV-1142). Currents are greatly decreased, and multiple peaks are introduced. A similar curve, with less peaks but identical current density magnitude, is obtained for copper oxide in anhydrous dimethylformamide-$LiClO_4$ (Ref. 1, Figure 28). The reduction reaction for copper in this solution may involve a dissolved species. Suspension of product material in the solution, and discoloration of the latter, were observed.

The voltammogram for copper in dimethylformamide-LiCl+$LiClO_4$, containing 1000 ppm water, is shown in Figure 7 (CV-1298). The effect of water impurity is to eliminate the well-formed high anodic and cathodic peaks, with a peak-to-peak displacement (ΔV_p) of only 200 mv (Ref. 1, Figure 27). In addition, there is considerable concentration polorization. The deleterious effect of water is again evident. It is apparent that water impurity has a devastating effect on the sweep curves for copper in $LiClO_4$ solution, whereas the effect in LiCl is rather negligible.

e. Copper Oxide Electrode

(1) Dimethylformamide solutions

Copper oxide in 0.25 m $LiClO_4$ results in current overload, again accompanied by solution contamination. A 0.75 m solution was run during an earlier

period, but only low currents were obtained (Ref. 1, Figure 28). According to the results described for copper in dimethylformamide-$LiClO_4$ (Figure 6), the earlier solution must have contained water impurity.

(2) Propylene carbonate solutions

Copper oxide in $LiCl+AlCl_3$ solution exhibits two definite sharp anodic peaks, with only a single cathodic peak (Figure 8, CV-1111) corresponding to the reduction of the lower oxidation state to metallic copper. The system appears to be dependent on cycling.

f. Copper Fluoride Electrode

These represent the first reported data on copper fluoride electrodes prepared by direct fluorination of copper wire in fluorine gas.

(1) Acetonitrile solutions

The cyclogram for copper fluoride in $LiClO_4$ solution is shown in Figure 9 (CV-1619). The anodic peak is considerably broader than that for copper oxide in the same solution (Ref. 1, Figure 32). In both cases, the discharge reaction is accompanied by excessive activation polarization. A black reaction product forms on the copper fluoride electrode during voltammetry.

(2) Butyrolactone solutions

Copper fluoride in butyrolactone-$LiClO_4$ exhibits a cathodic peak indicative of high rate discharge and negligible activation polarization (Figure 10, CV-1639). The charge reaction, however, is not as efficient, and indicates two separate oxidations, although this is not evident at higher sweep rates (80 and 200 mv/sec). A black reaction product at the electrode was accompanied by a yellow discoloration of the solution. The invariance of the anode-cathode peak current ratio indicates a solid state reduction of insoluble cathode material (insoluble within the measurement time period. Refer to Ref. 1, page 11 for further discussion).

(3) Dimethylformamide solutions

The curve for copper fluoride in dimethylformamide-$LiCl+AlCl_3$ is shown in Figure 11 (CV-1814). A black reaction product was observed at the electrode with a yellow discoloration of the solution. The 40 mv/sec curve has not been reproduced here because of the erratic nature of the anodic portion. A reproducible sharp cathodic peak (305 ma/cm^2) was obtained however. CuF_2 in $LiClO_4$ solution gives a low value broad anodic peak, and a still lower poorly formed cathodic peak as shown in Figure 12 (CV-1560).

(4) Propylene carbonate solutions

The cyclic voltammogram for copper fluoride in propylene carbonate-$LiClO_4$ solution is shown in Figure 13 (CV-1419). This curve is of interest in that this system is under extensive development elsewhere in conjunction with a lithium negative for primary battery application. The sweep curve indicates that rechargeability should be possible. This curve has been compared with that obtained for copper oxide in the same electrolyte (Ref. 1, Figure 35), the cyclogram of which is comparable except that the second anodic peak is considerably reduced in height with respect to the first anodic peak. This may or may not be significant considering the earlier systems contained no fluoride. Visual examination of the fluorinated copper indicated that the surface had indeed been converted, but the possibility remains that the copper fluoride layer may have been discarded during the initial cycling prior to curve recording, leaving an etched copper metal surface corresponding to the air-oxidized copper measured in the earlier work. Measurements will be run using copper metal and copper fluoride in $LiClO_4$ containing fluoride (LiF). The resulting curves may be of help in interpreting the present data.

g. Nickel Electrode

Nickel in acetonitrile-$MgCl_2$ fails to show any anodic (and hence no cathodic) reaction, which is in accordance with earlier data.

h. Nickel Oxide Electrode

Nickel oxide in propylene carbonate-$LiCl+AlCl_3$ exhibits a low maximum anodic current with no peak, and negligible cathodic current.

i. Nickel Fluoride Electrode

Cyclic voltammetry of nickel fluoride electrodes, prepared by direct fluorination of nickel wire, was initiated during this period. Negligible anodic current is obtained in $LiClO_4$ solutions of all solvents. In the case of butyrolactone and propylene carbonate there is virtually zero cathodic current. Acetonitrile and dimethylformamide give very low cathodic currents with no peaks. Dimethylformamide-$LiCl+AlCl_3$ solution exhibits a broad anodic peak of low value, but virtually zero cathodic reaction.

j. Cobalt Electrode

(1) Acetonitrile solutions

Cobalt gives a very high anodic current (more than 800 ma/cm^2) in $LiClO_4$ at +1.0 volt, but virtually no cathodic current. The sweep curve is shown in Figure 14 (CV-1182). A black reaction product forms at the electrode, with a slight red coloration at the cell bottom.

(2) Butyrolactone solutions

Cobalt metal in LiCl solution results in voltage overload. A blue coloration of the solution was observed. $LiClO_4$ solution results in definite peak formation (Figure 15, CV-1172). Two anodic peaks occur, the second having a

current density of about 100 ma/cm^2. With increasing sweep rate, the initial oxidation peak moves to more anodic values, while the higher peak remains at a fixed potential. At a sweep rate of 200 mv/sec the initial peak occurs as an inflection on the ascending slope of the higher peak. The discharge reaction is accompanied by excessive activation polarization. A black reaction product forms at the electrode, and a slight red coloration appears at the cell bottom. A mixture of LiCl and $LiClO_4$ failed to produce appreciable current.

(3) Dimethylformamide solutions

An excessively high anodic current is obtained for cobalt in LiCl solution, causing current overload in the anodic direction only. The anodic product is soluble in the electrolyte, and reduction of a solid state material is indicated, since the cathodic current decreases rapidly with decreasing sweep rate. A blue discoloration was observed. Similarly, cobalt in $LiCl+AlCl_3$ solution results in voltage overload (maximum anodic current is 3.2 $amps/cm^2$) with a blue discoloration of the solution. On the other hand, solutions of $LiClO_4$ and $LiCl+LiClO_4$ result in excessively low currents (less than 0.1 $ma/cm^2/cm$ division current axis) indicating no electrooxidation of cobalt metal.

(4) Propylene carbonate solutions

Cobalt metal fails to undergo electrooxidation in propylene carbonate-$LiClO_4$.

k. Cobalt Oxide Electrode

(1) Acetonitrile solutions

Entirely unlike cobalt metal, which produces a very high anodic current in acetonitrile-$LiClO_4$, pre-oxidation of the metal passivates the surface, decreasing the anodic current density to less than 4 ma/cm^2. Again, no cathodic current is evident.

(2) Butyrolactone solutions

Cobalt oxide in LiCl solution exhibits a medium high anodic current at +1.0 volt (no peak), and a very low cathodic current, indicating that electrolytic oxidation occurs readily at this high positive potential, but with no significant reduction. Even at much higher sweep rates there is no appreciable cathodic current. Again, a blue discoloration was observed. A very low anodic peak is obtained in $LiClO_4$ solution, but again no reduction reaction is evident. A similar anodic peak is obtained in $LiCl+LiClO_4$ solution, as well as a very small cathodic peak.

(3) Dimethylformamide solutions

Results obtained for cobalt oxide in LiCl solution again indicate that pre-oxidation of cobalt metal passivates the surface, e.g. the maximum anodic current density is 0.16 ma/cm^2 compared with a current density in excess of 500 ma/cm^2 for the untreated metal. Very low anodic currents are also obtained in $LiClO_4$ and $LiCl+LiClO_4$ solutions.

(4) Propylene carbonate solutions

Current densities less than 0.1 $ma/cm^2/cm$ division current axis are obtained for cobalt oxide in $LiClO_4$ solution.

1. Cobalt Fluoride Electrode

The cyclic voltammetric results obtained for fluorinated cobalt metal are presented for the first time. In all cases, cobalt fluoride failed to give a cathodic reaction, and only very small anodic peaks were obtained, except that virtually zero current was obtained for propylene carbonate-$LiClO_4$. Solutions studied were $LiClO_4$ in all four solvents, and $LiCl+AlCl_3$ in dimethylformamide.

2. Systems Involving Fluoride Electrolytes

a. Silver Electrode

Silver in acetonitrile solutions of $LiPF_6$ and $LiBF_4$ results in current overloading of the instrumentation, due to excessively high currents accompanied by solution discoloration. Solutions of BF_3, PF_5 and $Mg(BF_4)_2$ give voltage overload with silver electrodes. Silver in butyrolactone, dimethylformamide and propylene carbonate solutions of BF_3 and PF_5, as well as dimethylformamide-$Mg(BF_4)_2$, also result in voltage overload.

When the maximum current does not exceed the amplifier rating, it can be read on a meter. In these cases, maximum anodic and cathodic current densities are obtainable even though curves cannot be recorded. Table IV lists the maximum current densities for a number of overloading systems. (Further details on instrument overloading are presented in the Experimental Section of this report).

Silver was also run in 1.0 m KPF_6 solution to determine the effect of concentration. Excessively high currents (accompanied by black discoloration of the solution) result in overload. This was not the case for 0.75 m KPF_6 (Ref. 1, Figure 38) for which a curve could be obtained. This is the same system which develops two distinct anodic and cathodic peaks as a result of continued cycling (Ref. 1, Figure 39).

b. Silver Oxide Electrode

(1) Acetonitrile solutions

Silver oxide in acetonitrile-$LiPF_6$ solution registers current overload due to extremely high current densities.

(2) Dimethylformamide solutions

Silver oxide in $LiF+KPF_6$ results in current overload accompanied by a black discoloration of the solution owing to reaction product dissolution. This compares with earlier results for pre-oxidized silver in KPF_6 solution alone (Ref. 1) where anodic peaks were obtained in excess of 650 ma/cm^2. Voltage overload is obtained in $LiPF_6$ solution.

(3) Propylene carbonate solutions

Silver oxide in $LiF+KPF_6$ solution compares with the untreated metal in the same solution (Ref. 1), indicating a two-step reduction reaction with low cathodic current densities. The two anodic reactions occur close together, with the higher oxidation reaction failing to reach a peak before +1.0 v. The solution turns black during the measurement. $LiPF_6$ solution results in voltage overload.

c. Silver Difluoride Electrode

(1) Acetonitrile solutions

Silver difluoride in acetonitrile solutions of $LiPF_6$ and $LiBF_4$ shows no cathodic reaction, and initiation of anodic reaction occurs only at +1.0 volt. Low anodic and cathodic peaks are obtained for the KPF_6+LiF system, and very low peaks for KPF_6. As indicated above, these low currents may be due to too thick a layer of AgF_2 on the silver substrate.

(2) Butyrolactone solutions

AgF_2 in KPF_6 and $LiF+KPF_6$ solutions again shows low currents, but very definite peaks are obtained reminiscent of those obtained by repetitive cycling of silver wire in propylene carbonate-KPF_6 (Ref. 1, Figure 39). The cyclic voltammogram for the KPF_6 solution is shown in Figure 16 (CV-1781).

(3) Dimethylformamide solutions

Prior to recording the voltammogram at 200 mv/sec in $LiPF_6$ solution, the

AgF_2 layer on the silver substrate went into solution (visual observation) during the first few cycles. During this initial cycling, the anodic and cathodic peaks were both very high, close together, and of equal area. The curve obtained subsequent to ten charge-discharge cycles, exhibits a very large anodic current density (800 ma/cm^2) failing to reach a peak in the scanning range, and a much lower cathodic c.d. (133 ma/cm^2). The cathodic peak current is proportionally much smaller at 40 mv/sec indicating a solid state reduction reaction, and confirming the solubility of AgF_2 in this solution. Anodic voltage overload is obtained in $LiBF_4$ solution. The cyclic voltammograms for KPF_6 and KPF_6+LiF are quite similar to that obtained in butyrolactone-KPF_6, except that the initial anodic peak is higher and sharper.

(4) Propylene carbonate solutions

Silver difluoride in $LiPF_6$ solution exhibits a low and very broad anodic peak at the higher oxidation potential, and a very low cathodic peak. No dissolution of cathode material was observed, nor evidenced by the sweep curves. The curve obtained in KPF_6 solution compares well with that obtained in dimethylformamide solution. The first anodic peak, in the case of KPF_6+LiF, is not as sharp as it was in dimethylformamide. Figure 17 (CV-1419) shows the effect of repeated cycling of AgF_2 in $LiBF_4$ solution, indicating the growth of the anodic and cathodic peaks with increased cycling. Comparison of the cathodic peak height of the earliest recorded cycle at 40 mv/sec with the peak heights at higher sweep rates, indicates a solid state reduction of a soluble cathode.

d. Copper Electrode

(1) Acetonitrile solutions

The cyclogram for copper in $LiPF_6$ solution is shown in Figure 18, (CV-1386), indicating high and sharp peak current densities for both the charge and discharge reactions, and an exceedingly small ΔV_p (90 mv). The peak height and shape,

indicative of high current density and very low activation polarization for each reaction, is characterized by the high sweep indices, 1414 and 251 for the anodic and cathodic peaks respectively. A black reaction product was evident on the working electrode, with no evidence of dissolution during measurement. This system is recommended for further study.

Copper in PF_5 solution of acetonitrile results in a very high anodic current density exhibiting two ill-defined peaks. No cathodic peaks are evident, the maximum reduction current density being 60 ma/cm^2 (compared to 450 ma/cm^2 for the anodic current density). Copper in BF_3 solution results in voltage overload. Overloading is also obtained in $Mg(BF_4)_2$ solution, but with relatively lower current.

(2) Butyrolactone solutions

Copper in BF_3 and PF_5 solutions of butyrolactone result in voltage overload during the anodic portion of the sweep.

(3) Dimethylformamide solutions

The cyclic voltammogram for copper in $Mg(BF_4)_2$ solution is shown in Figure 19 (CV-1455). This system is characterized by a small cathodic peak about 400 mv negative to the anodic peak, but with the major reduction occurring at much more negative potentials, indicating a complex reduction reaction. The system is of no interest since the first reduction reaction occurs with low current density, and the secondary reaction occurs at too negative a potential. Voltage overload results in the case of copper in BF_3 and PF_5 solutions of dimethylformamide.

(4) Propylene carbonate solutions

Copper in BF_3 and PF_5 solutions of propylene carbonate result in anodic voltage overload.

e. Copper Oxide Electrode

(1) Acetonitrile solutions

The cyclic voltammogram for copper oxide in acetonitrile-$LiPF_6$ is shown in Figure 20 (CV-1381). Compared to copper metal (Figure 18), the anodic peak has been greatly reduced in height and made considerably broader. The discharge reaction is correspondingly poor. This effect on peak height and shape by pre-oxidation in air, was unexpected since it was not observed with copper oxide in KPF_6 solution (Ref. 1, Figure 41).

The effect of adding water to acetonitrile-KPF_6 is shown in Figures 21 and 22 (CV-1303, CV-1308). The addition of 1000 ppm water (Figure 21) has no significant effect on the anodic reaction, but the discharge current density is considerably reduced. This is not due to anodic product dissolution since the anode-to-cathode peak ratio remains invariant with sweep rate (indicative of a solid state reduction reaction, with the cathode material being insoluble). The effect of adding 2000 ppm water is shown in Figure 22. There is a pronounced decrease in anodic peak current density (from 300 to 94 ma/cm^2). The cathodic peak c.d. remains relatively unchanged however.

(2) Dimethylformamide solutions

Copper oxide in LiF+ KPF_6 gives a similar type of curve as copper in KPF_6 (Ref. 1, Figure 45), very low anodic and cathodic current with no definite peak formation.

(3) Propylene carbonate solutions

The cyclic voltammogram of copper oxide in LiF+KPF_6 resembles that obtained for copper in KPF_6 solution (Ref. 1, Figure 47) but with much lower current densities. Copper metal in LiF+KPF_6 (Ref. 1) had resulted in voltage overload. A black reaction product formed at the electrode may have been responsible for spurious oscillations in the cyclograms at all three sweep rates

(200, 80, and 40 mv/sec), since a higher recorder sensitivity was necessary due to the low current densities. Copper oxide in $LiPF_6$ also gives poorly formed peaks with spurious oscillations, but the peaks are of medium low range.

f. Copper Fluoride Electrode

(1) Acetonitrile solutions

The cyclic voltammogram for copper fluoride in $LiPF_6$ solution (Figure 23, CV-1553) is identical in shape and current density to that obtained for copper oxide in the same solution (Figure 20). Comparison of this curve with copper metal in acetonitrile-$LiPF_6$ (Figure 18) shows the latter with much higher and sharper peaks, and a much smaller peak displacement (90 mv compared with 550 mv). The identical nature of the curves obtained for CuO and CuF_2 may possibly be due to a high electrode resistance absent at the copper metal electrode. The curves for CuF_2 in $LiBF_4$, KPF_6, and KPF_6+LiF are shown in Figures 24-26 (CV's-1468, 1683 and 1704) are comparable, except for the lower currents (approximately half) for KPF_6+LiF, and the appearance of a small second anodic peak for $LiBF_4$. These curves are also comparable with Cu in KPF_6+LiF (Ref. 1, Figure 42), except for a greater peak displacement in the latter due to a higher IR drop in the older measuring cell.

(2) Butyrolactone solutions

The sweep curve for copper fluoride in KPF_6 solution (Figure 27, CV-1786) shows a very low cathodic current, which is proportionately higher at the higher sweep rate, indicating a soluble cathode. Similar results were obtained for copper fluoride in KPF_6+LiF, except that the peak anodic current density was nearly three times larger (140 ma/cm^2). Copper metal in the same electrolyte gave a similar sweep curve, (Ref. 1, Figure 43) but with a still higher anodic peak current density (256 ma/cm^2).

(3) Dimethylformamide solutions

The cyclic voltammogram for CuF_2 in dimethylformamide-$LiPF_6$ is shown in Figure 28 (CV-1525). The extremely high and sharp cathodic peak gives this system the highest cathodic sweep index obtained to date, 2573 ohm^{-1} cm^{-2}. Also, the peak displacement is the smallest so far obtained (20 mv). This system is peculiar in that the cathodic current density at the lowest sweep is 50% higher than at the highest sweep rate (1.8 amps/cm^2 compared to 1.2 amps/cm^2). The anodic peak current density remains relatively independent of sweep rate. A minimum of 50 charge-discharge cycles at 200 mv/sec were required to stabilize the system prior to recording. This system requires further investigation because of its extremely high discharge current and minimal peak displacement.

Substitution of $LiPF_6$ by KPF_6 results in a vastly poorer system with greatly decreased currents and increased peak displacement, as shown in Figure 29, (CV-1424). A similar curve is obtained for CuF_2 in $LiF+KPF_6$, so that the unusually high currents cannot be explained by the presence of lithium ions, unless the explanation involves the absence of potassium ions. Solution conductivity plays no part, since the $LiPF_6$ solution has a lower conductivity (7.61×10^{-3} ohm^{-1} cm^{-1}) than the KPF_6 or $LiF+KPF_6$ solutions (1.22×10^{-2} ohm^{-1} cm^{-1}). The probable explanation lies in the method of solution preparation. The KPF_6 and KPF_6+LiF solutions were prepared from commercial salts (Ozark-Mahoning). The $LiPF_6$ solutions were prepared by adding PF_5 to dimethylformamide-LiF suspension. The conductivity of dimethylformamide-PF_5 is 3.87×10^{-4} ohm^{-1} cm^{-1}. Although CuF_2 has not yet been run in dimethylformamide-PF_5, copper metal has, and with resulting voltage overload due to a combination of high current and fairly high resistance. The decrease of electrolytic resistance by the addition of LiF (through PF_6^- formation) was probably just enough to prevent voltage overload, so that the high current cyclic voltammogram of Figure 28 was recordable.

The cyclic voltammogram for copper fluoride in $LiBF_4$ solution (Figure 30, CV-1481) shows a very high anodic peak, and medium low broad cathodic peak indicating poor discharge properties. The relatively small cathodic current may be due to dissolution of the cathode, which was also the case for copper in the same solution (Ref. 1, Figure 46). Higher sweep rate voltammograms could not be recorded due to anodic voltage overload. The $LiBF_4$ solutions were prepared by passing BF_3 into a dimethylformamide-LiF suspension. The high current obtained with this solution, compared to the $LiBF_4$ solution prepared from commercial material (and used in the earlier measurement (Ref. 1, Figure 46) is again indicative of the different results obtained by using different starting materials.

(4) Propylene carbonate solutions

Copper fluoride in $LiPF_6$ solution (Figure 31, CV-1614) exhibits high current densities and a broad anodic peak. Considerable concentration polarization is indicated. A sharper, but lower, anodic peak is obtained in KPF_6 solution (Figure 32, CV-1699). Solid state reduction of a soluble cathode is indicated. Results are comparable to copper in the same solution (Ref. 1, Figure 47). except that copper exhibits two anodic peaks. Current densities are comparable. Addition of LiF to the KPF_6 does not appreciably affect the sweep curve. Copper fluoride in propylene carbonate-$LiBF_4$ results in current overload, again confirming the high reaction currents obtainable from complex fluorides prepared directly from BF_3 or PF_5.

g. Nickel Electrode

(1) Acetonitrile solutions

Nickel in PF_5 solution shows a medium high anodic peak at +0.9 v with virtually zero cathodic current. Anodic voltage overload is obtained in BF_3 solution and a maximum cathodic current density of 40 ma/cm^2 is indicated.

A very high anodic current is recorded for $Mg(BF_4)_2$ solution at +0.6 v, with evidence of cathodic reaction occurring at -0.6v.

(2) Butyrolactone solutions

Nickel in BF_3 and PF_5 solution gives current densities considerably less than 0.1 $ma/cm^2/cm$ division, indicating no anodic or cathodic reaction.

(3) Dimethylformamide solutions

Nickel forms a black reaction product with BF_3 and PF_5 solutions, accompanied by anodic voltage overload. No cathodic reaction is evident. $Mg(BF_4)_2$ shows anodic current at +1.0 v (12 ma/cm^2) but virtually no cathodic reaction.

(4) Propylene carbonate solutions

Nickel in BF_3 shows no appreciable reaction. Nickel in PF_5 exhibits a low range anodic and cathodic current at +1.0 v and -1.0 v respectively. After cycling 30 time at 200 mv/sec, however, voltage overload is obtained in the PF_5 solution, and a light grey reaction product forms on the electrode.

h. Nickel Oxide Electrode

In line with the generally poor performance of nickel, nickel oxide gives current densities less than 0.1 $ma/cm^2/cm$ division current axis in dimethylformamide and propylene carbonate solutions of $LiF+KPF_6$. Only in the presence of $LiPF_6$, which gives very high currents in other systems, does nickel oxide show some appreciable current, and only during the oxidation phase of the cycle. Two anodic peaks of low current density result in acetonitrile-$LiPF_6$ (Figure 33, CV-1366), but the discharge reaction is very poor. A double anodic peak also occurs in the propylene carbonate solution, but not before +0.9 volts.

i. Nickel Fluoride Electrode

As has been found generally true for nickel and nickel oxide electrodes,

the cyclic voltammograms for nickel fluoride electrodes indicate the absence of electrochemical reactions having any significant current density. In nearly all cases screened, discharge (cathodic reaction) of nickel fluoride electrodes did not occur up to -1.0 volt relative to ocv. The maximum anodic current densities, which occur at highly positive potentials (except for some dimethylformamide solutions), are in the low current density range. Nickel fluoride in dimethylformamide-$LiBF_4$ gives a peak at +0.45 v, whose base extends the entire anodic range, and having a peak c.d. of 4.0 ma/cm^2. A poorly formed cathodic peak (1.4 ma/cm^2) exists at -0.7 v. $LiPF_6$ in the same solvent exhibits multiple anodic peaks, the highest having a peak c.d. of 11.2 ma/cm^2. No cathodic current is evident however.

j. Cobalt Electrode

(1) Acetonitrile solutions

Cobalt in PF_5 solution results in anodic voltage overload due to anodic current densities in excess of 1.0 amp/cm^2. In spite of such a high anodic current density, there is virtually no cathodic reaction. A black reaction product is formed on the electrode. Cobalt in $LiPF_6$ solution exhibits an anodic peak of medium high magnitude, but with no evidence of cathodic reaction until -1.0 v (Figure 34, CV-1371). No appreciable anodic currents are obtained for KPF_6 or $LiF+KPF_6$ solutions. Cobalt in BF_3 solution gives both anodic and cathodic voltage overload. $Mg(BF_4)_2$ exhibits anodic voltage overload. A very high c.d. anodic peak at +1.0 v is obtained in $LiBF_4$, but again there is virtually zero cathodic current.

(2) Butyrolactone solutions

Cobalt in BF_3 solution results in voltage overload due to very high anodic current densities. No anodic peak is obtained in PF_5 solution, although a maximum current density of 18 ma/cm^2 is reached. The cathodic current

density is much lower with no peak formation. Cobalt fails to yield appreciable anodic currents in KPF_6 or $LiF+KPF_6$ solutions.

(3) Dimethylformamide solutions

Very high anodic currents are generally indicated for cobalt in dimethylformamide solutions of BF_3, PF_5, and $Mg(BF_4)_2$, resulting in voltage overload. A well-defined anodic peak is obtained in $LiPF_6$ solution, but no cathodic reaction is evident until about -0.9 v. The cyclic voltammogram is shown in Figure 35 (CV-1398). Curves obtained at higher sweep rates (80 and 200 mv/sec) also show no cathodic reaction, but multiple anodic peaks are evident indicating three separate anodic reactions. Figure 36 (CV-1395) shows the 200 mv/sec sweep curve. If the three anodic peaks are indicative of the sequential oxidation, $Co \longrightarrow Co^{+1} \longrightarrow Co^{+2} \longrightarrow Co^{+3}$, then only the first oxidation occurs at the lowest sweep rate (Figure 35) which is nearest in time to steady state conditions. Cobalt in $LiBF_4$ solution shows virtually no anodic current until +0.95 v where a high range peak is obtained. A medium low cathodic peak is obtained at -0.95 v, representing a peak displacement of nearly 2.0 v. No appreciable anodic currents are obtained in KPF_6 and $LiF+KPF_6$ solutions.

(4) Propylene carbonate solutions

Cobalt in KPF_6 and $LiF+KPF_6$ solutions results in current densities less than 0.1 $ma/cm^2/cm$ division, indicating the inability to be electrooxidized in these solutions. Voltage overload is obtained in BF_3 solution. In PF_5 solution, cobalt exhibits a low anodic current density peaking out broadly at +1.0 volt, and a negligible cathodic current. Cobalt in $LiBF_4$ solution gives a low anodic peak at +0.75 v and zero cathodic current. $LiPF_6$ solution shows low anodic and cathodic peaks at +0.9 v and -0.9 v respectively.

k. Cobalt Oxide Electrode

(1) Acetonitrile solutions

Low current peaks are obtained for cobalt oxide in $LiPF_6$ solution (Figure 37, CV-1376), and medium high peaks in KPF_6 solution (Figure 38, CV-1259). The excessive activation polarization makes these systems undesirable for battery application.

Cobalt oxide undergoes negligible reaction in butyrolactone, propylene carbonate, and dimethylformamide solutions of KPF_6 and $LiF+KPF_6$, as well as in propylene carbonate-$LiPF_6$ solution. In dimethylformamide-$LiPF_6$, the cyclic voltammogram is similar to that for cobalt in the same solution (Figure 35) except that the anodic peak is much broader.

l. Cobalt Fluoride Electrode

In all systems studied, cyclic voltammograms of cobalt fluoride exhibit negligible currents.

m. Zinc Electrode

The effect of solute concentration was determined in the case for zinc in dimethylformamide-KPF_6. A 1.75 m solution gives the cyclic voltammogram shown in Figure 39 (CV-1313). The corresponding curve for 0.75 m was reported earlier (Ref. 1, Figure 52). The higher concentration electrolyte gives a cyclic voltammogram whose peak current densities are half that for the lower concentration. In addition the ΔV_p value is decreased from 320 to 70 mv. These results confirm the high reversibility of the Zn/dimethylformamide-KPF_6 system.

The addition of 1000 ppm water to dimethylformamide-KPF_6 solution results in the very peculiar cyclic voltammogram shown in Figure 40 (CV-1318).

Peaks A and B are the original peaks (in the absence of water) with an additional reaction occurring 0.70 volt negative to this. The secondary cathodic peak C is shifted 0.3 volts more cathodic at the 200 mv sweep rate. Addition of 2000 ppm water results in poorly reproducible curves, but which are consistent in exhibiting two pronounced cathodic peaks of very high current density at about 0.0 and -0.9 volts. Only low spurious anodic peaks are obtained. Obviously, the presence of water impurity is detrimental to this system. The anodic-cathodic reaction occurring at -0.7 v may involve formation and subsequent discharge of zinc oxide. Investigation of zinc fluoride as a cathode material would therefore require rigid exclusion of water.

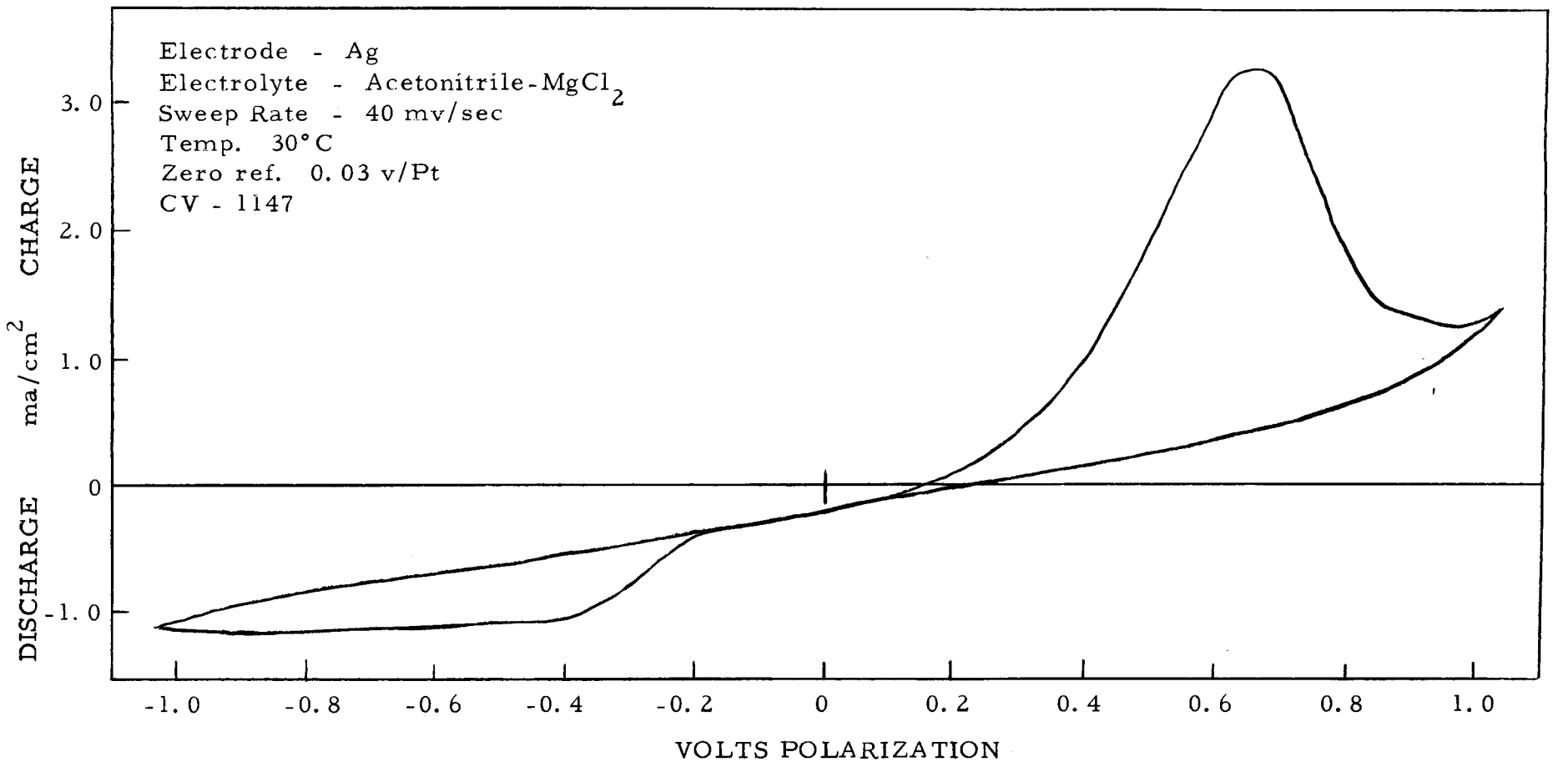
Electrode - Ag
Electrolyte - Acetonitrile-MgCl2
Sweep Rate - 40 mv/sec
Temp. 30°C
Zero ref. 0.03 v/Pt
CV - 1147
3.0
2.0
1.0
0
-1.0
CHARGE
ma/cm2
DISCHARGE
-1.0
-0.8
-0.6
-0.4
-0.2
0
0.2
0.4
0.6
0.8
1.0
VOLTS POLARIZATION

Figure 1

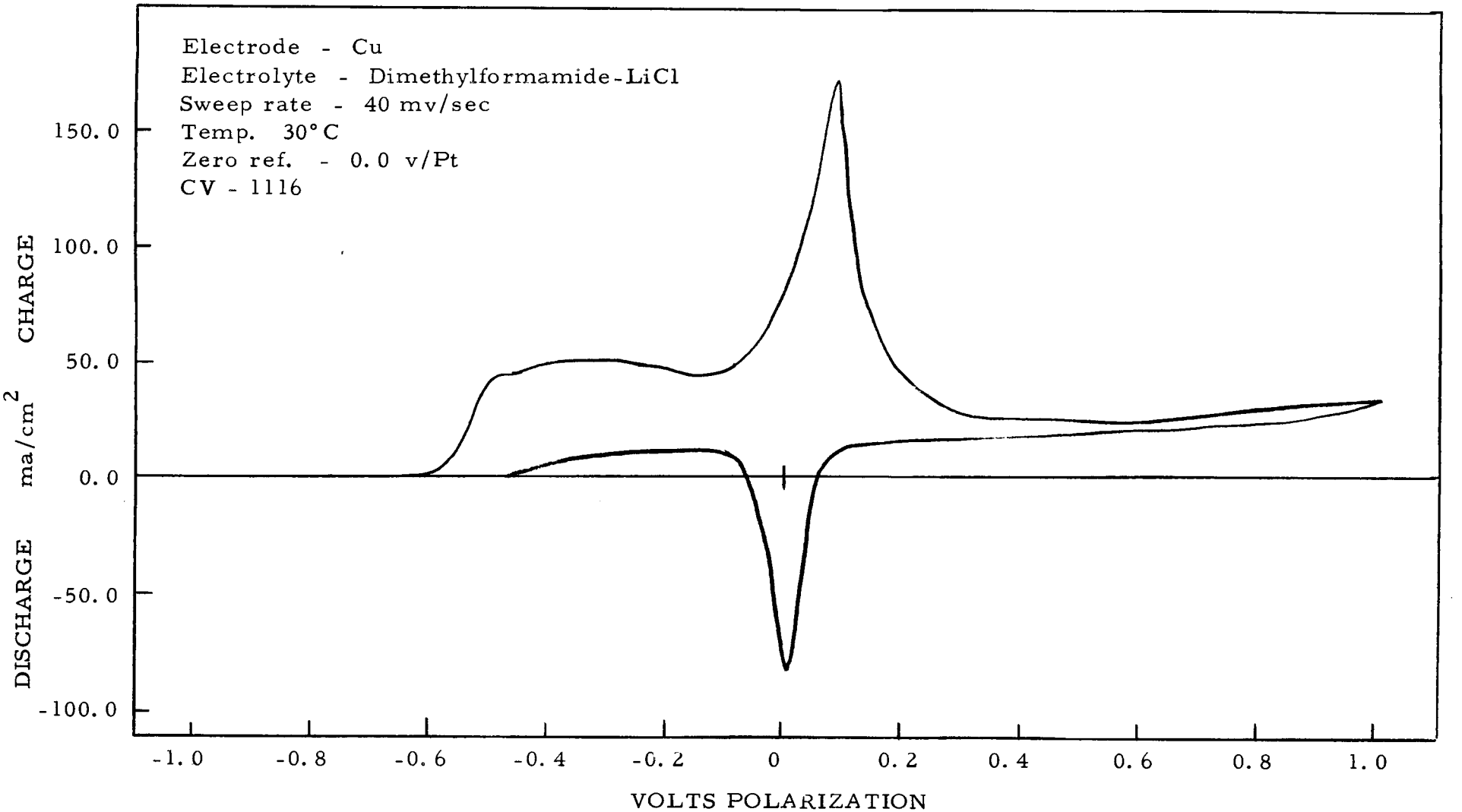
Electrode - Cu
Electrolyte - Dimethylformamide-LiCl
Sweep rate - 40 mv/sec
Temp. 30°C
Zero ref. - 0.0 v/Pt
CV - 1116
150.0
100.0
50.0
0.0
-50.0
-100.0
CHARGE
ma/cm2
DISCHARGE
-1.0
-0.8
-0.6
-0.4
-0.2
0
0.2
0.4
0.6
0.8
1.0
VOLTS POLARIZATION

Figure 2

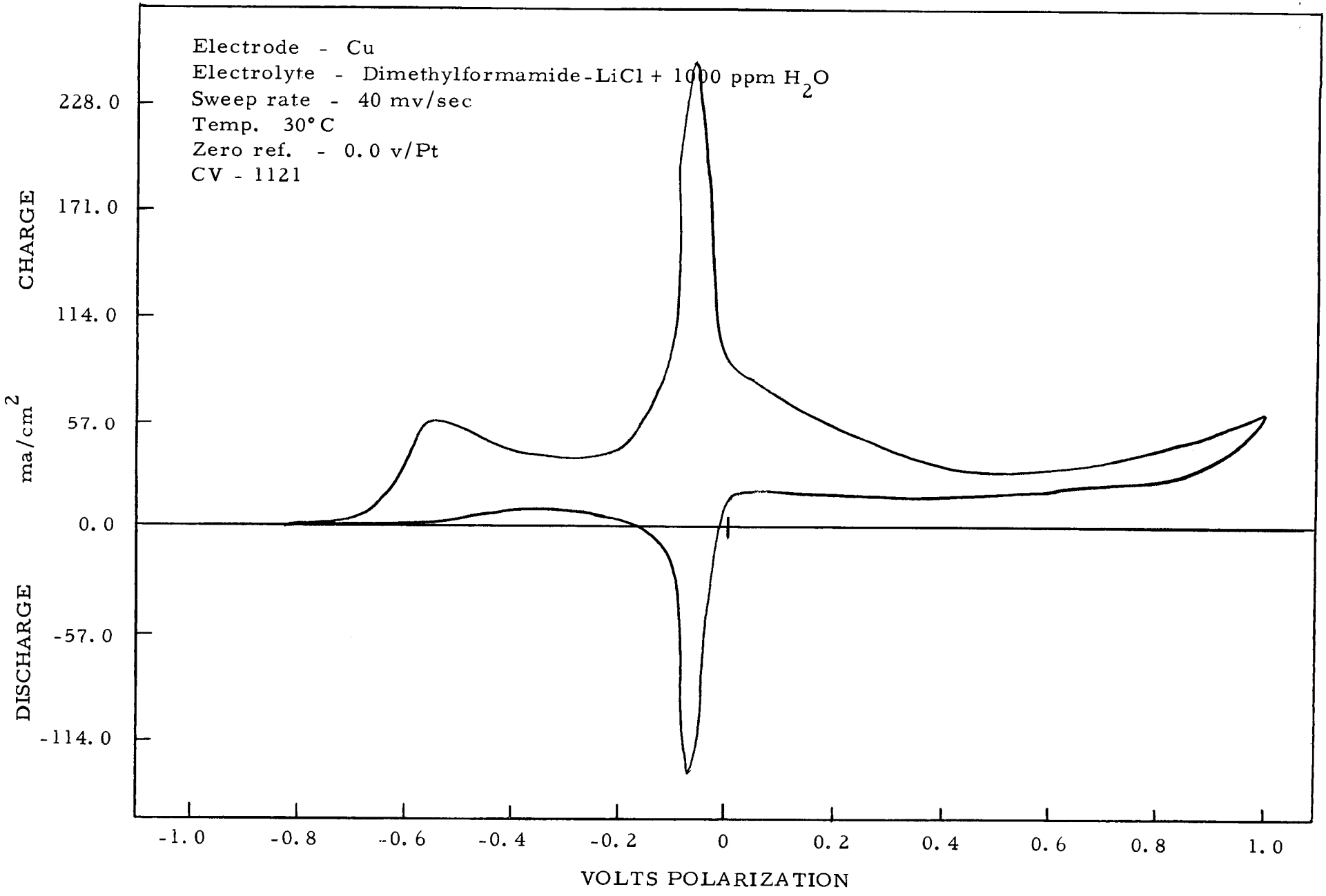
Electrode - Cu
Electrolyte - Dimethylformamide-LiCl + 1000 ppm H_2O
Sweep rate - 40 mv/sec
Temp. 30° C
Zero ref. - 0.0 v/Pt
CV - 1121
CHARGE
DISCHARGE
ma/cm^2
228.0
171.0
114.0
57.0
0.0
-57.0
-114.0
-1.0
-0.8
-0.6
-0.4
-0.2
0
0.2
0.4
0.6
0.8
1.0
VOLTS POLARIZATION

Figure 3

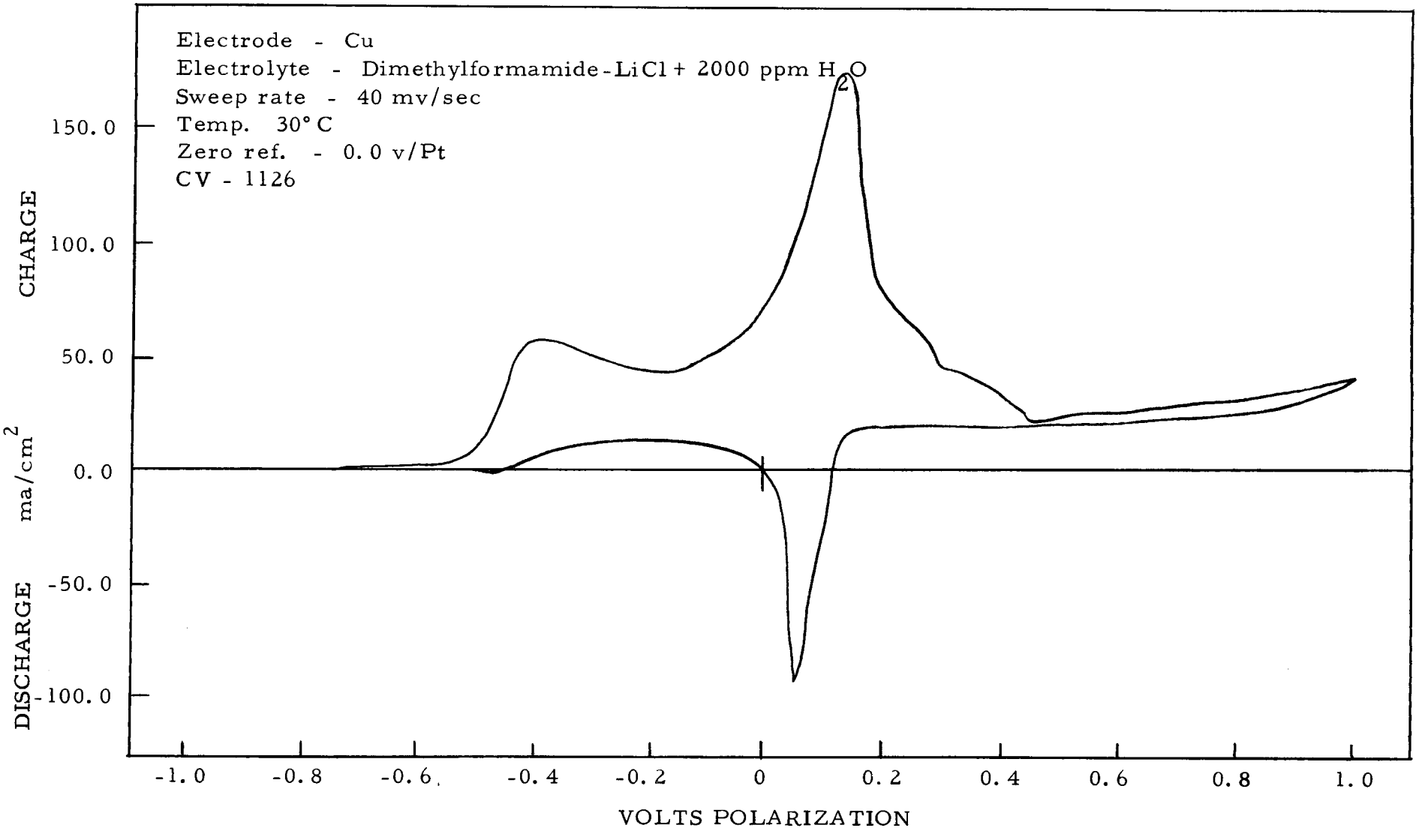
Electrode - Cu
Electrolyte - Dimethylformamide-LiCl + 2000 ppm H_2O
Sweep rate - 40 mv/sec
Temp. 30° C
Zero ref. - 0.0 v/Pt
CV - 1126
150.0
100.0
50.0
0.0
-50.0
-100.0
CHARGE
DISCHARGE
ma/cm^2
-1.0
-0.8
-0.6
-0.4
-0.2
0
0.2
0.4
0.6
0.8
1.0
VOLTS POLARIZATION

Figure 4

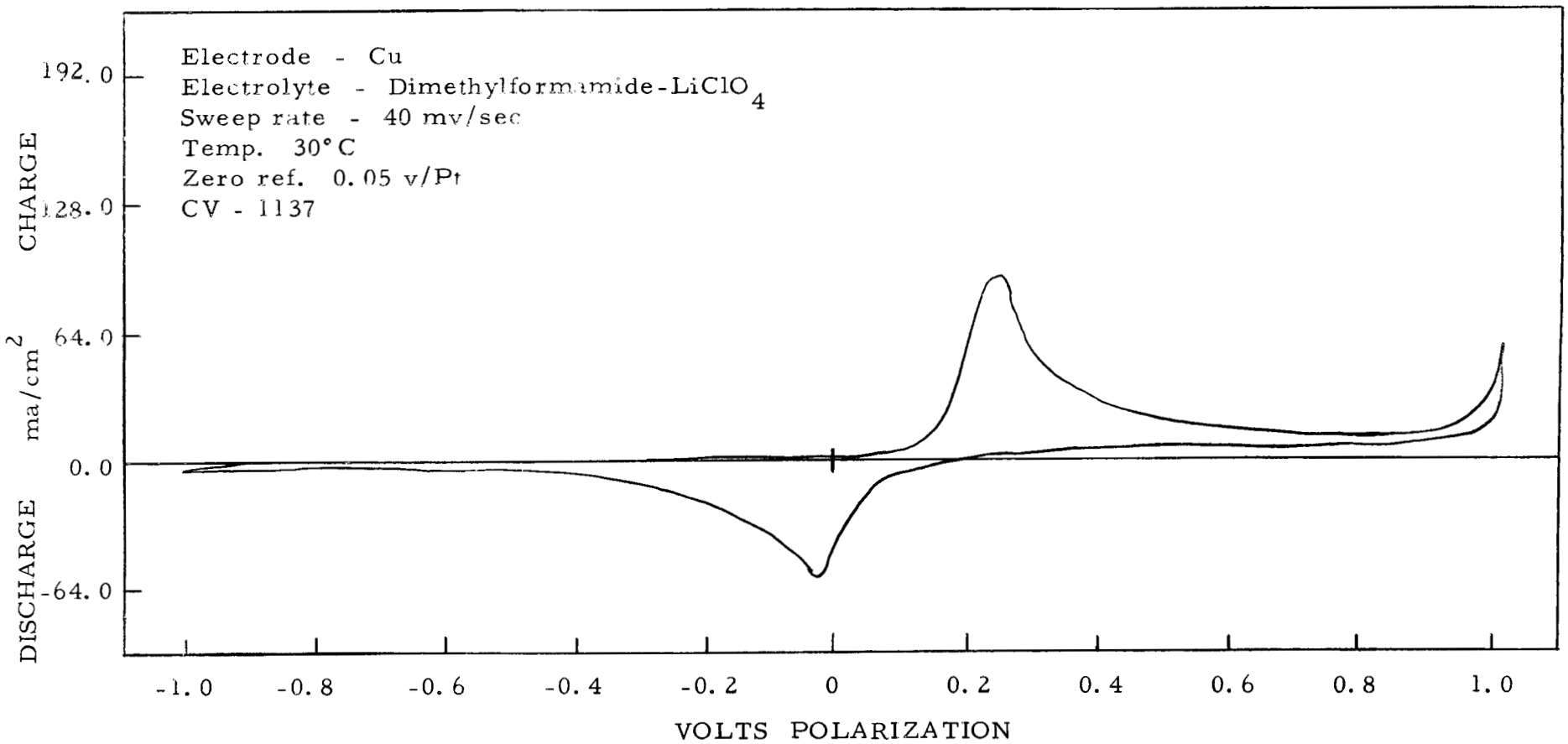
Electrode - Cu
Electrolyte - Dimethylformamide-LiClO4
Sweep rate - 40 mv/sec
Temp. 30°C
Zero ref. 0.05 v/Pt
CV - 1137
192.0
128.0
64.0
0.0
-64.0
CHARGE
ma/cm2
DISCHARGE
-1.0
-0.8
-0.6
-0.4
-0.2
0
0.2
0.4
0.6
0.8
1.0
VOLTS POLARIZATION

Figure 5

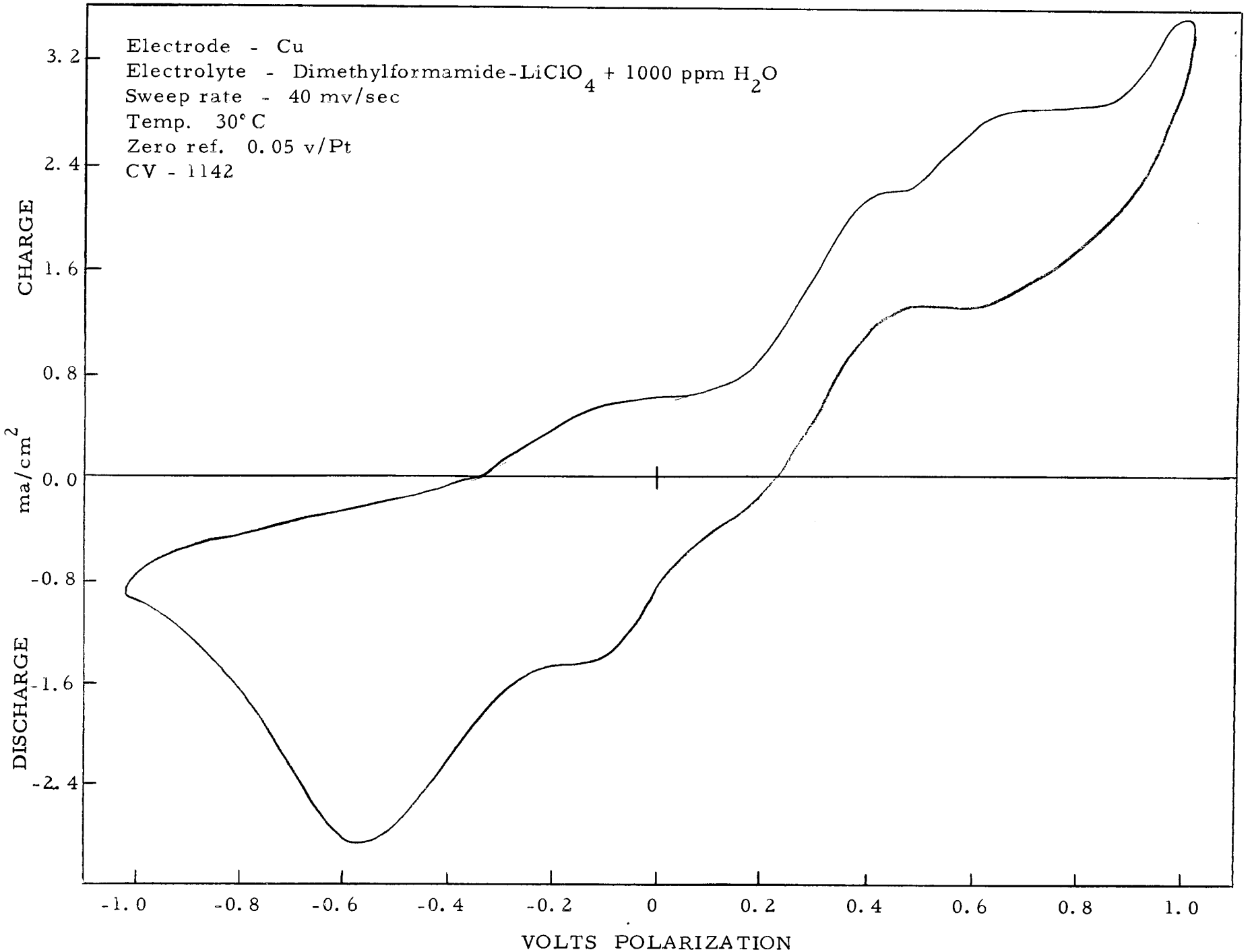
Electrode - Cu
Electrolyte - Dimethylformamide-$LiClO_4$ + 1000 ppm H_2O
Sweep rate - 40 mv/sec
Temp. 30° C
Zero ref. 0.05 v/Pt
CV - 1142
CHARGE
DISCHARGE
ma/cm^2
3.2
2.4
1.6
0.8
0.0
-0.8
-1.6
-2.4
-1.0
-0.8
-0.6
-0.4
-0.2
0
0.2
0.4
0.6
0.8
1.0
VOLTS POLARIZATION

Figure 6

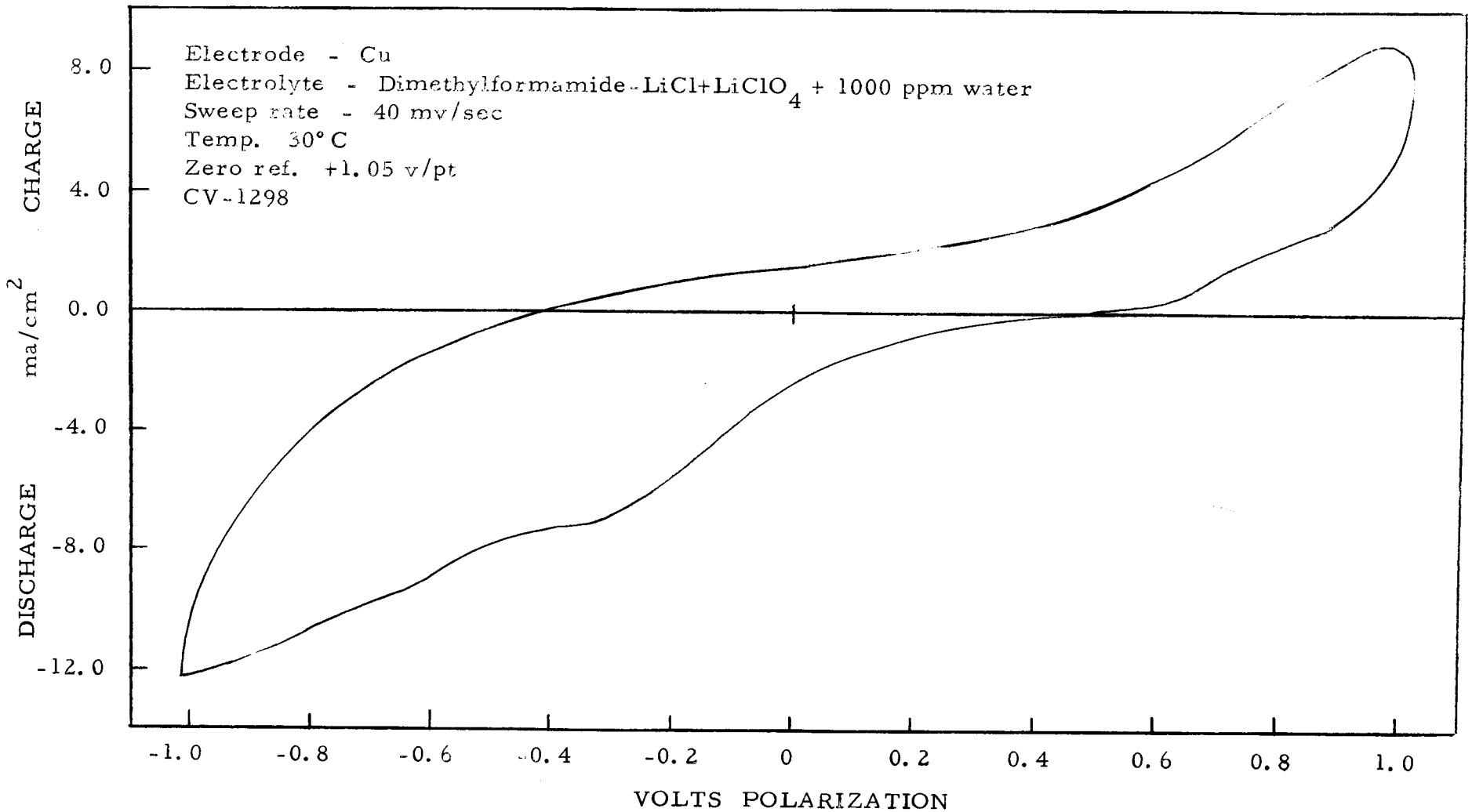
Electrode - Cu
Electrolyte - Dimethylformamide-LiCl+LiClO4 + 1000 ppm water
Sweep rate - 40 mv/sec
Temp. 30° C
Zero ref. +1.05 v/pt
CV-1298
CHARGE
ma/cm2
DISCHARGE
8.0
4.0
0.0
-4.0
-8.0
-12.0
-1.0
-0.8
-0.6
-0.4
-0.2
0
0.2
0.4
0.6
0.8
1.0
VOLTS POLARIZATION

Figure 7

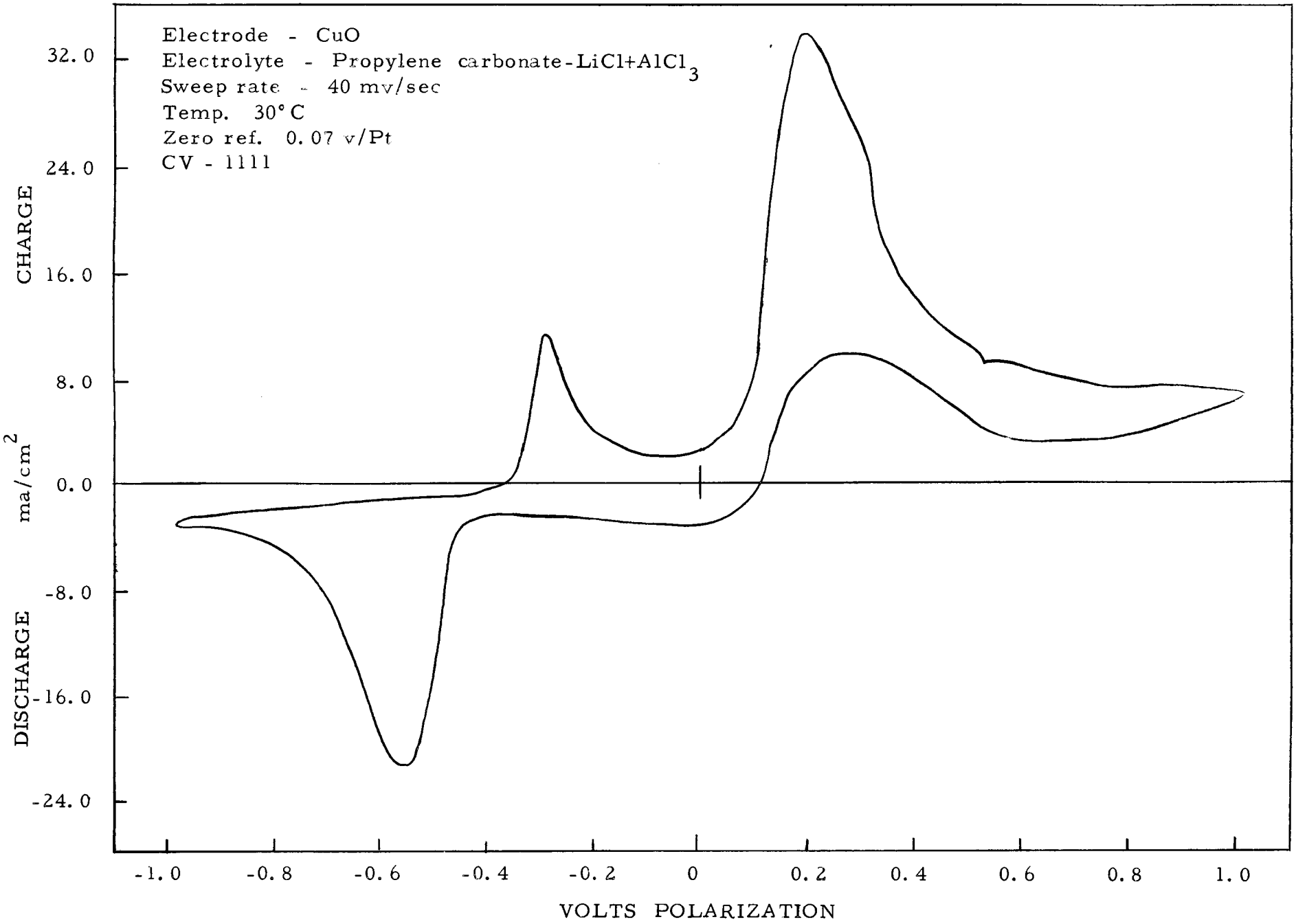
Electrode - CuO
Electrolyte - Propylene carbonate-LiCl+AlCl3
Sweep rate - 40 mv/sec
Temp. 30° C
Zero ref. 0.07 v/Pt
CV - 1111
32.0
24.0
16.0
8.0
0.0
-8.0
-16.0
-24.0
CHARGE
DISCHARGE
ma/cm2
-1.0
-0.8
-0.6
-0.4
-0.2
0
0.2
0.4
0.6
0.8
1.0
VOLTS POLARIZATION

Figure 8

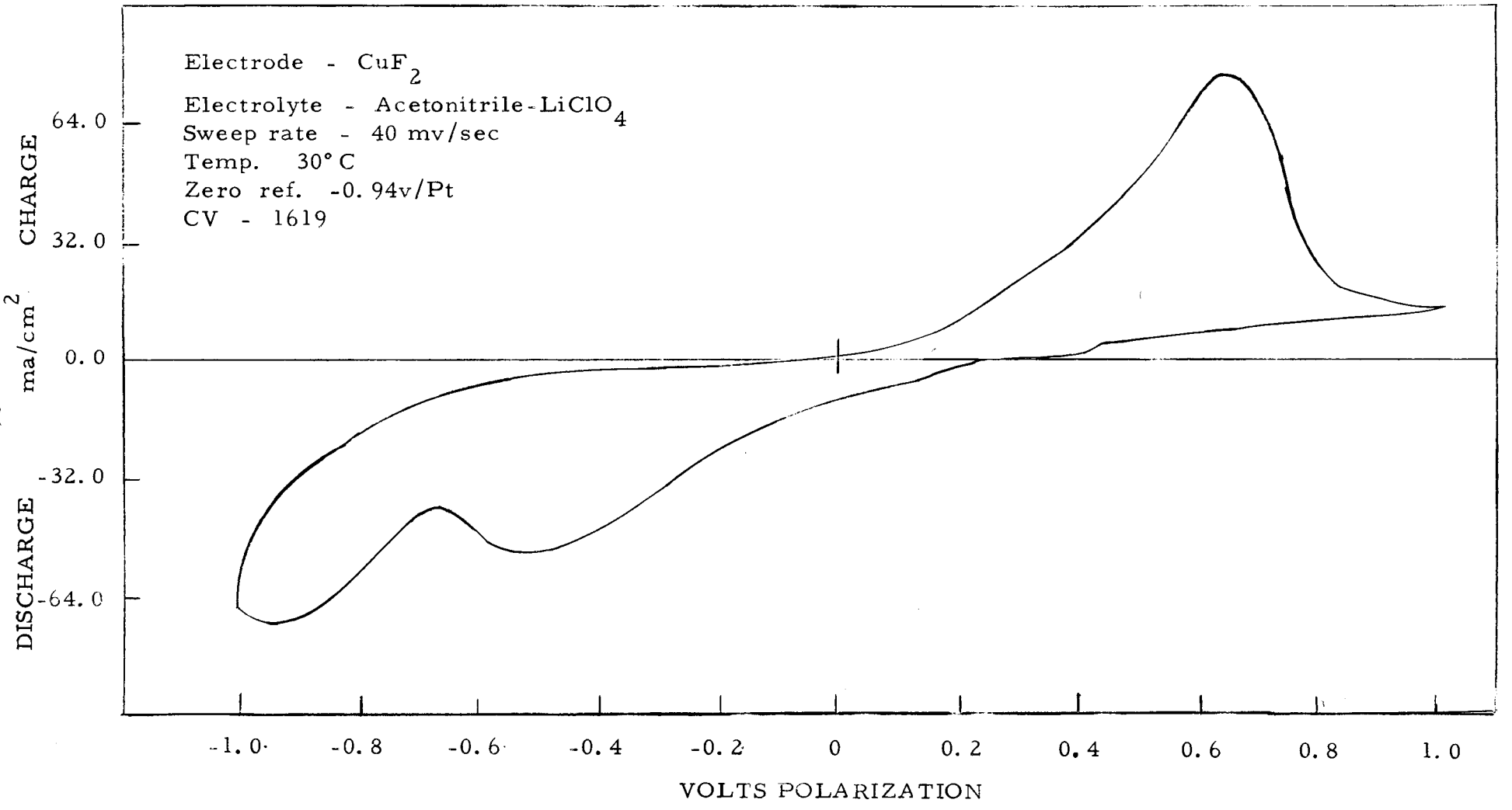
Electrode - CuF_2
Electrolyte - Acetonitrile-$LiClO_4$
Sweep rate - 40 mv/sec
Temp. 30° C
Zero ref. -0.94v/Pt
CV - 1619
64.0
32.0
0.0
-32.0
-64.0
CHARGE
DISCHARGE
ma/cm^2
-1.0
-0.8
-0.6
-0.4
-0.2
0
0.2
0.4
0.6
0.8
1.0
VOLTS POLARIZATION

Figure 9

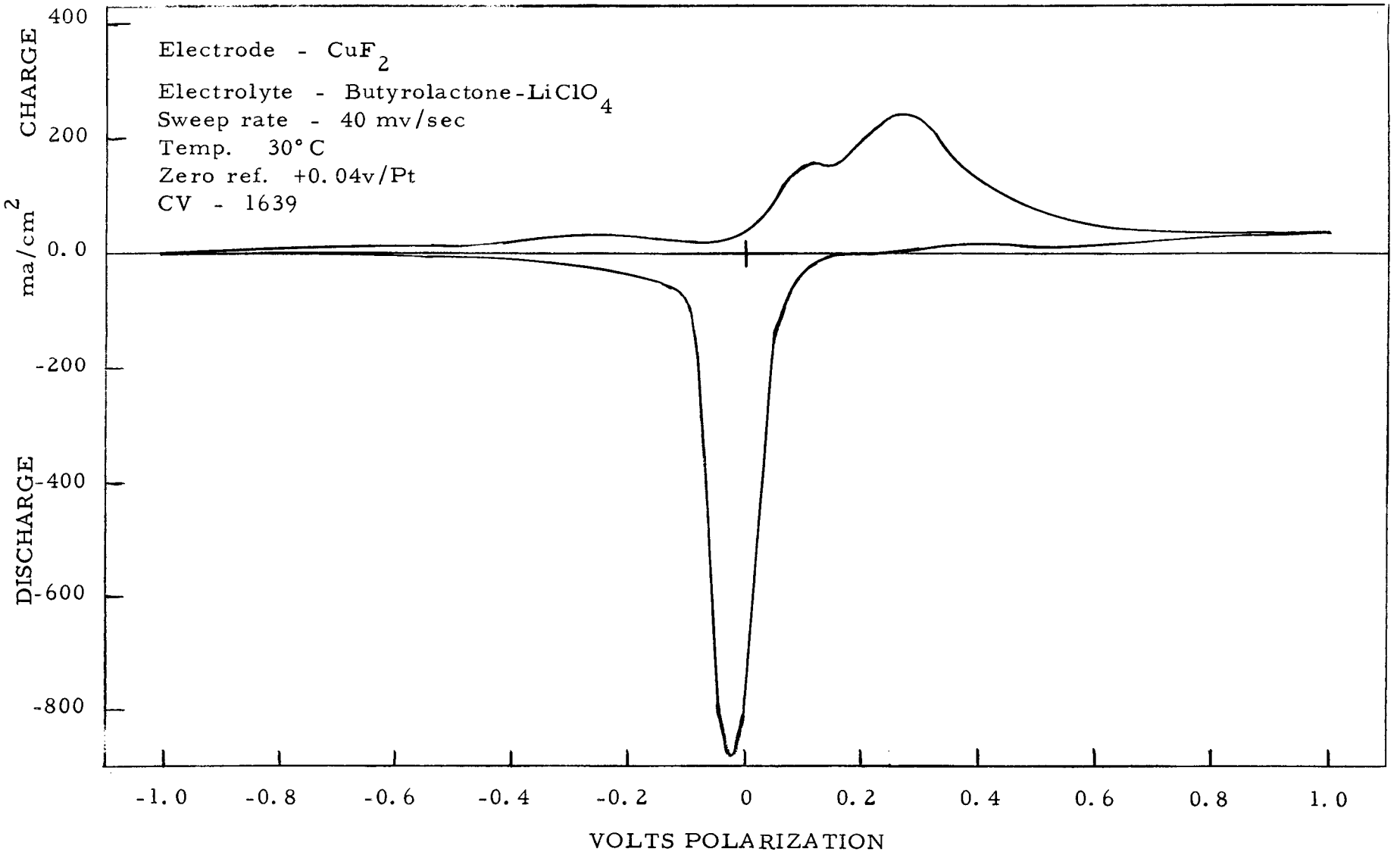
Electrode - CuF_2
Electrolyte - Butyrolactone-$LiClO_4$
Sweep rate - 40 mv/sec
Temp. 30° C
Zero ref. +0.04v/Pt
CV - 1639
CHARGE
DISCHARGE
ma/cm^2
400
200
0.0
-200
-400
-600
-800
-1.0
-0.8
-0.6
-0.4
-0.2
0
0.2
0.4
0.6
0.8
1.0
VOLTS POLARIZATION

Figure 10

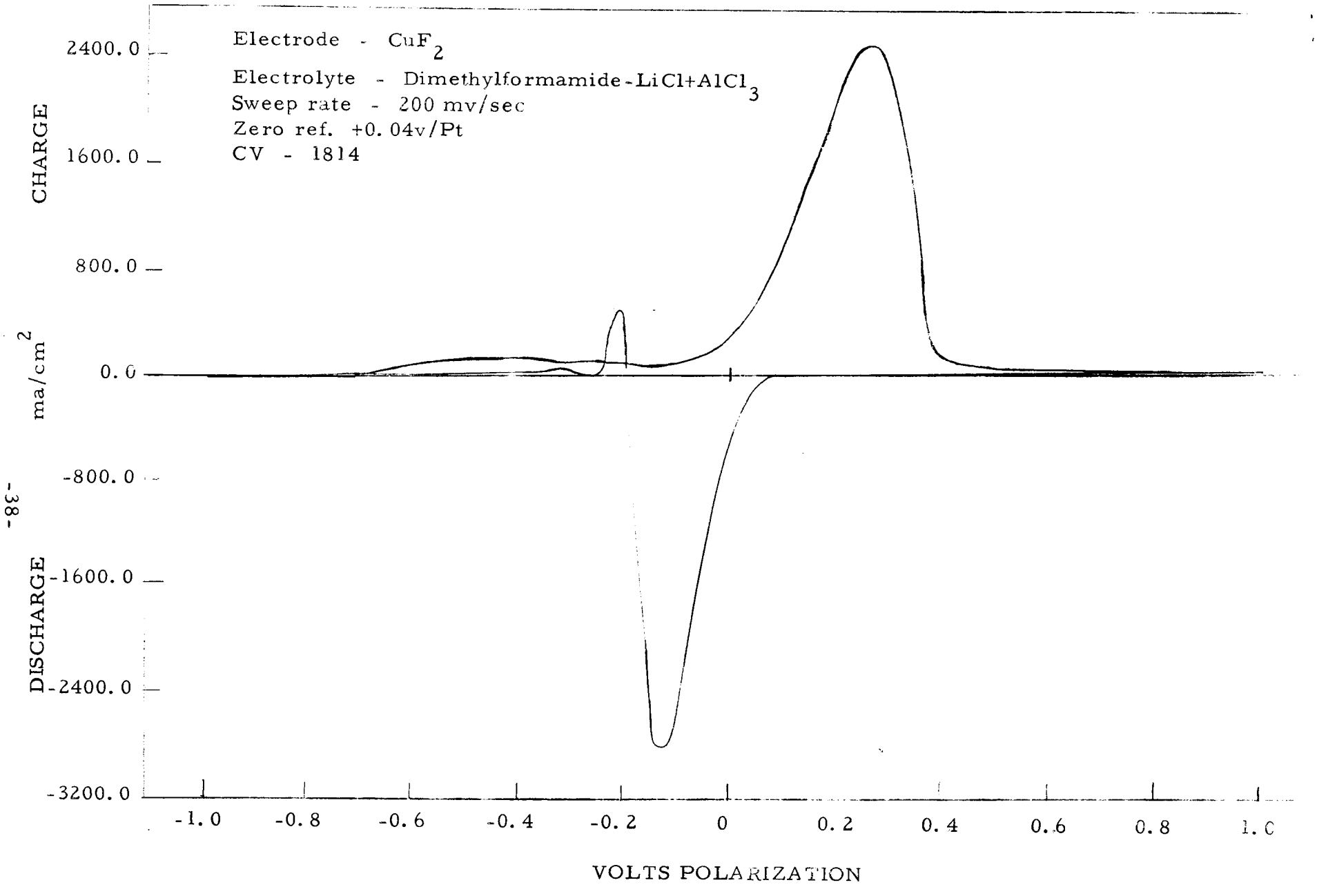
Electrode - CuF_2
Electrolyte - Dimethylformamide-$LiCl+AlCl_3$
Sweep rate - 200 mv/sec
Zero ref. +0.04v/Pt
CV - 1814
CHARGE
DISCHARGE
ma/cm^2
2400.0
1600.0
800.0
0.0
-800.0
-1600.0
-2400.0
-3200.0
-1.0
-0.8
-0.6
-0.4
-0.2
0
0.2
0.4
0.6
0.8
1.0
VOLTS POLARIZATION

Figure 11

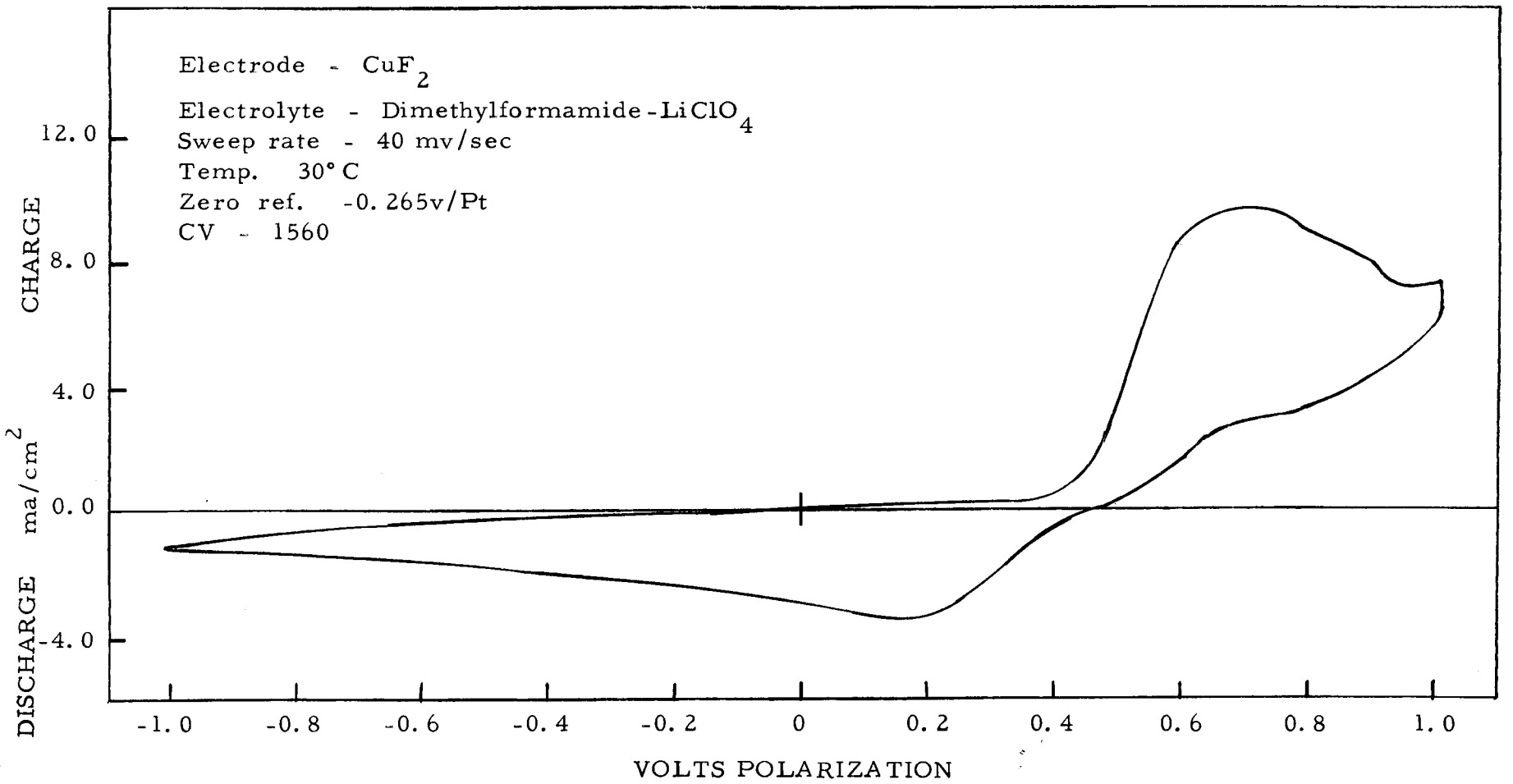
Electrode - CuF_2
Electrolyte - Dimethylformamide-$LiClO_4$
Sweep rate - 40 mv/sec
Temp. 30° C
Zero ref. -0.265v/Pt
CV - 1560
12.0
8.0
4.0
0.0
-4.0
CHARGE
DISCHARGE
ma/cm^2
-1.0
-0.8
-0.6
-0.4
-0.2
0
0.2
0.4
0.6
0.8
1.0
VOLTS POLARIZATION

Figure 12

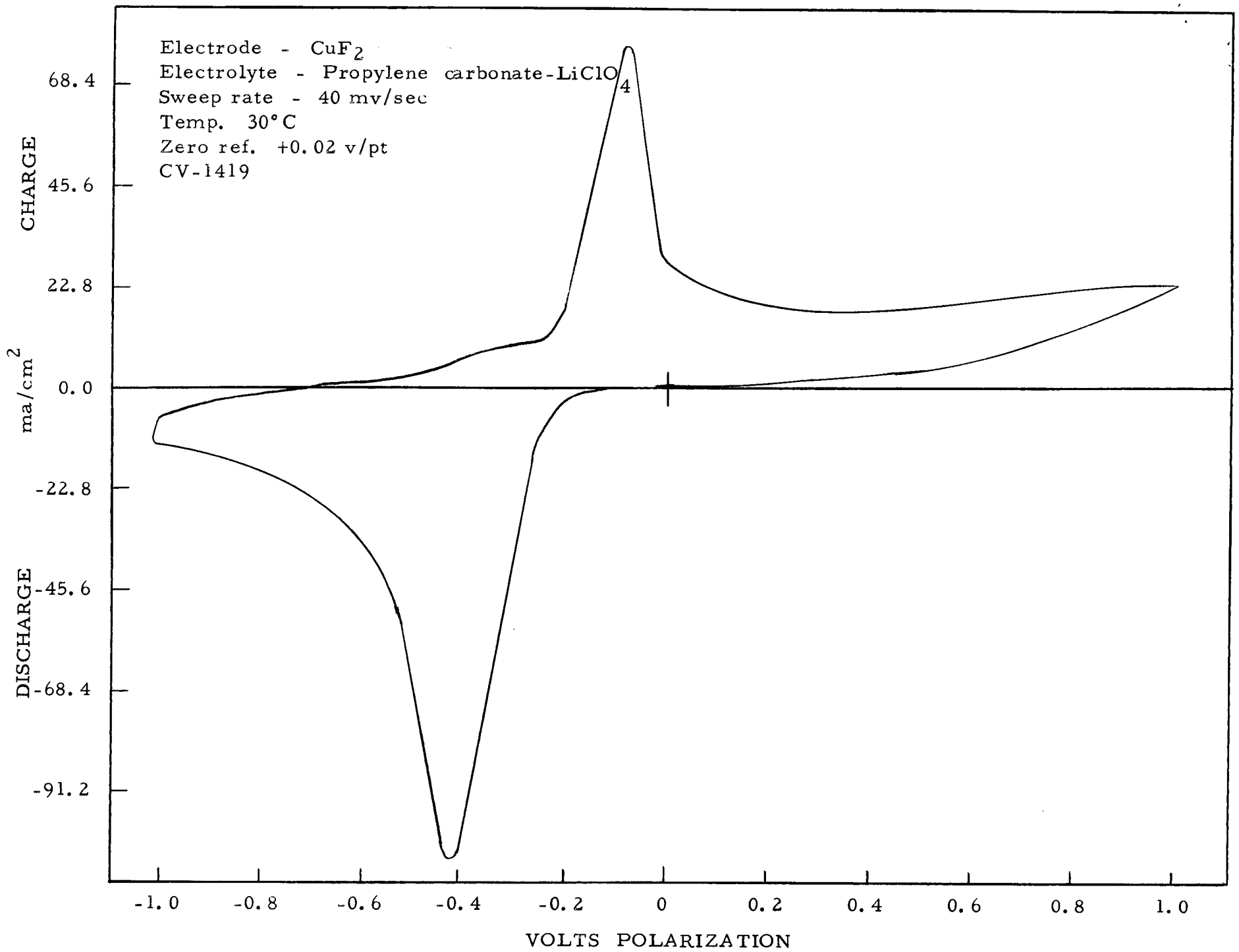
Electrode - CuF_2
Electrolyte - Propylene carbonate-$LiClO_4$
Sweep rate - 40 mv/sec
Temp. 30°C
Zero ref. +0.02 v/pt
CV-1419
CHARGE
DISCHARGE
ma/cm^2
68.4
45.6
22.8
0.0
-22.8
-45.6
-68.4
-91.2
-1.0
-0.8
-0.6
-0.4
-0.2
0
0.2
0.4
0.6
0.8
1.0
VOLTS POLARIZATION

Figure 13

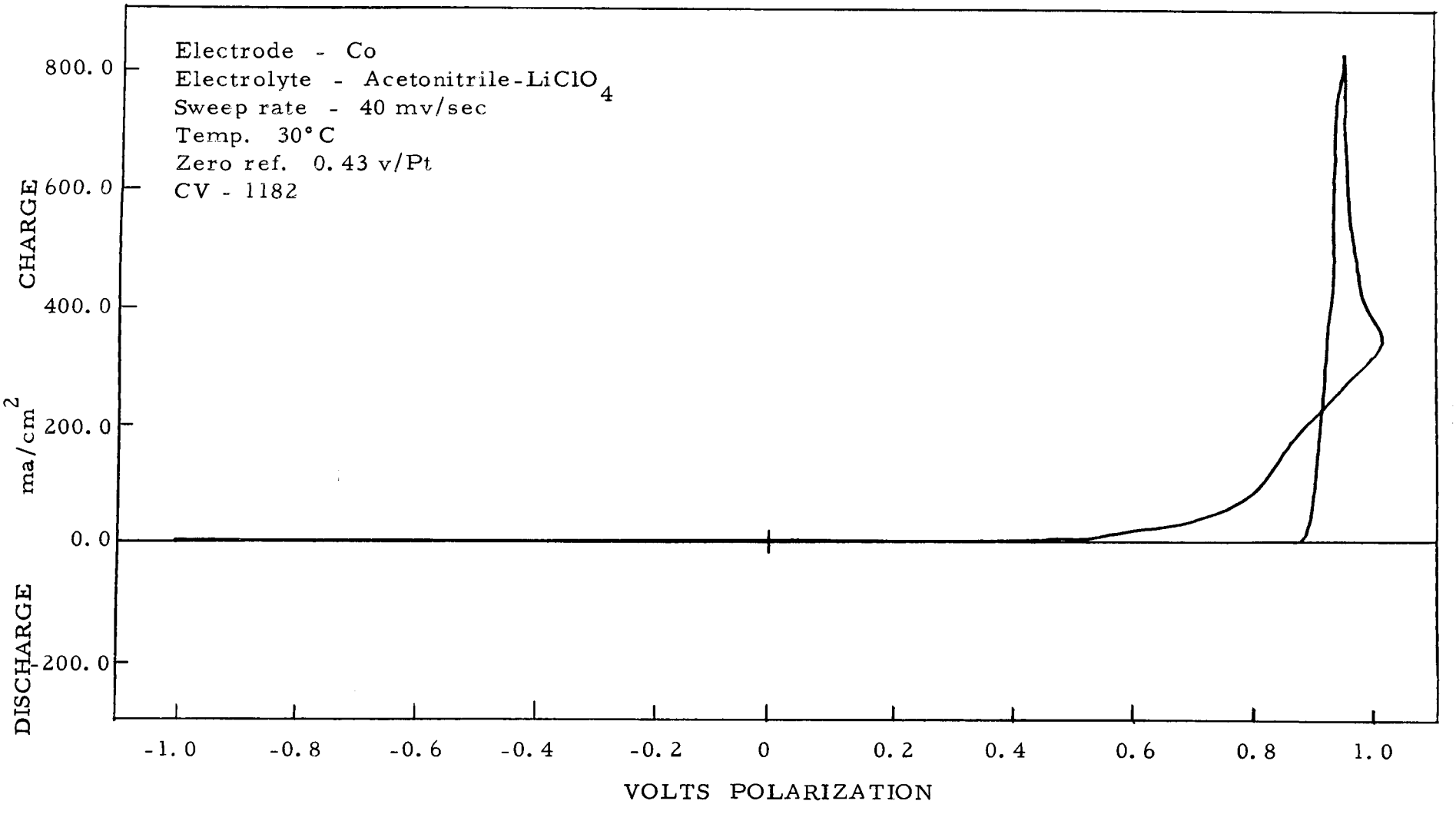
Electrode - Co
Electrolyte - Acetonitrile-LiClO4
Sweep rate - 40 mv/sec
Temp. 30° C
Zero ref. 0.43 v/Pt
CV - 1182
800.0
600.0
400.0
200.0
0.0
-200.0
CHARGE
DISCHARGE
ma/cm2
-1.0
-0.8
-0.6
-0.4
-0.2
0
0.2
0.4
0.6
0.8
1.0
VOLTS POLARIZATION

Figure 14

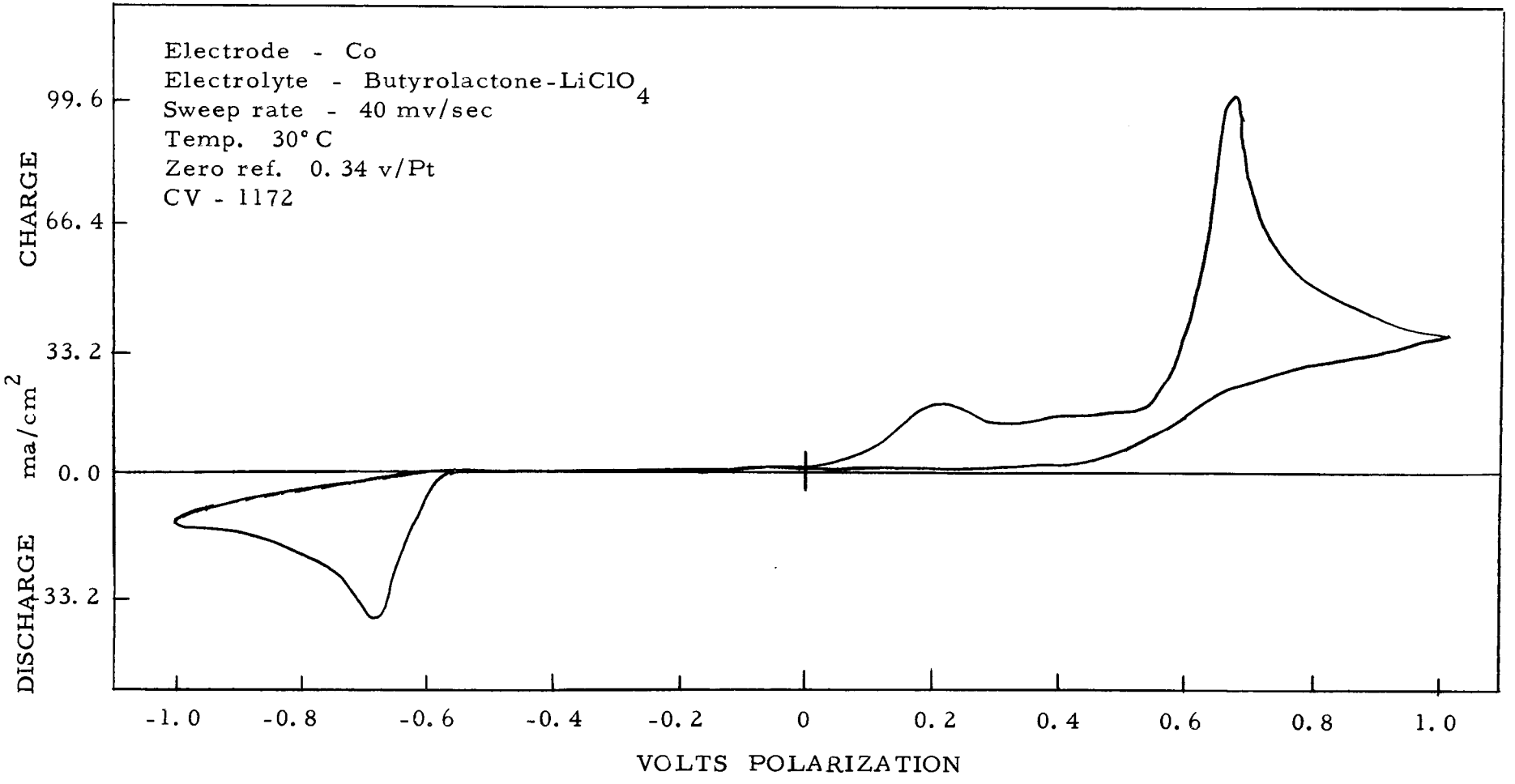
Electrode - Co
Electrolyte - Butyrolactone-LiClO4
Sweep rate - 40 mv/sec
Temp. 30° C
Zero ref. 0.34 v/Pt
CV - 1172
CHARGE
DISCHARGE
ma/cm2
99.6
66.4
33.2
0.0
33.2
-1.0
-0.8
-0.6
-0.4
-0.2
0
0.2
0.4
0.6
0.8
1.0
VOLTS POLARIZATION

Figure 15

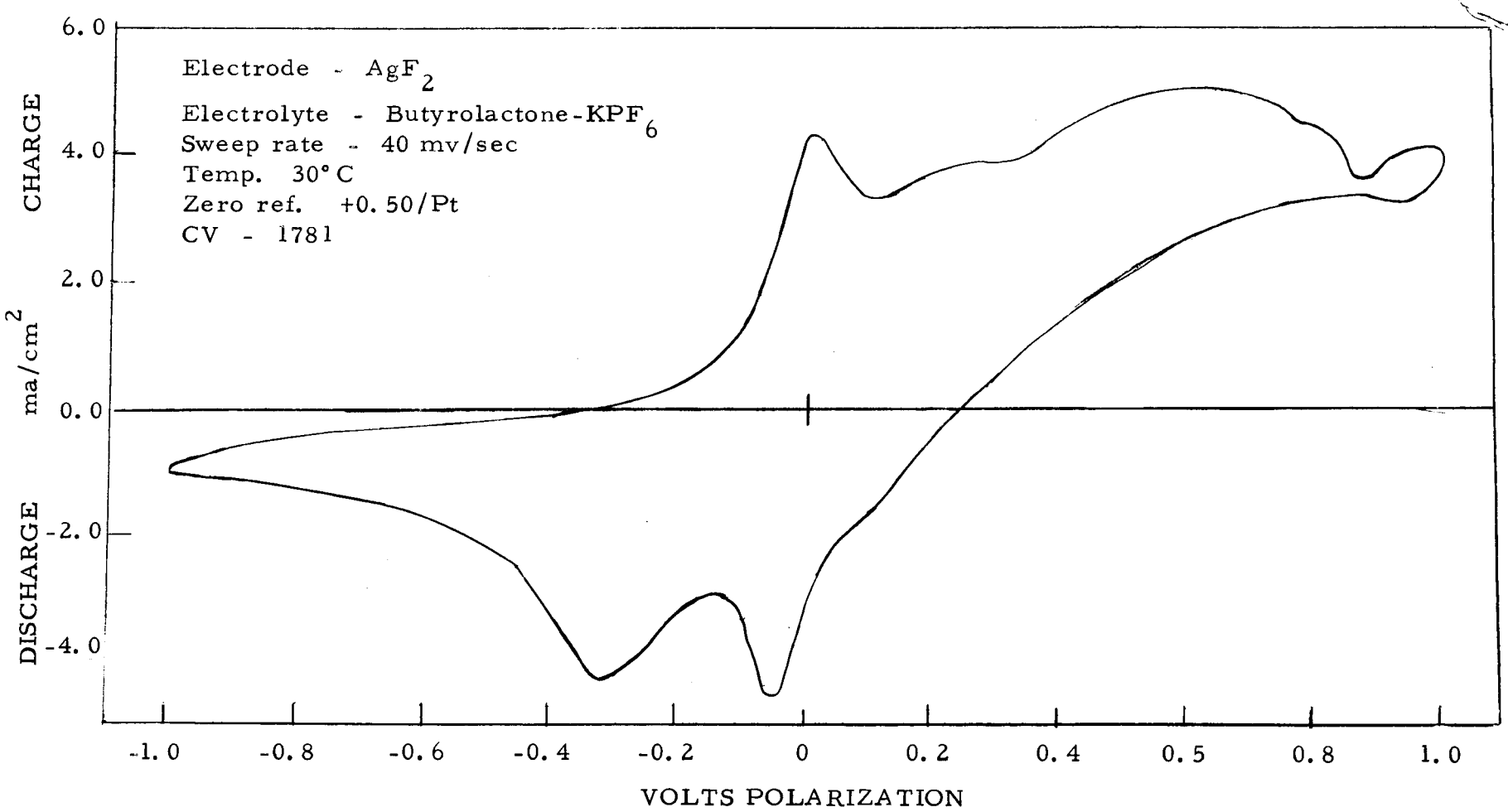
Electrode - AgF_2
Electrolyte - Butyrolactone-KPF_6
Sweep rate - 40 mv/sec
Temp. 30° C
Zero ref. +0.50/Pt
CV - 1781
CHARGE
DISCHARGE
ma/cm^2
6.0
4.0
2.0
0.0
-2.0
-4.0
-1.0
-0.8
-0.6
-0.4
-0.2
0
0.2
0.4
0.5
0.8
1.0
VOLTS POLARIZATION

Figure 16

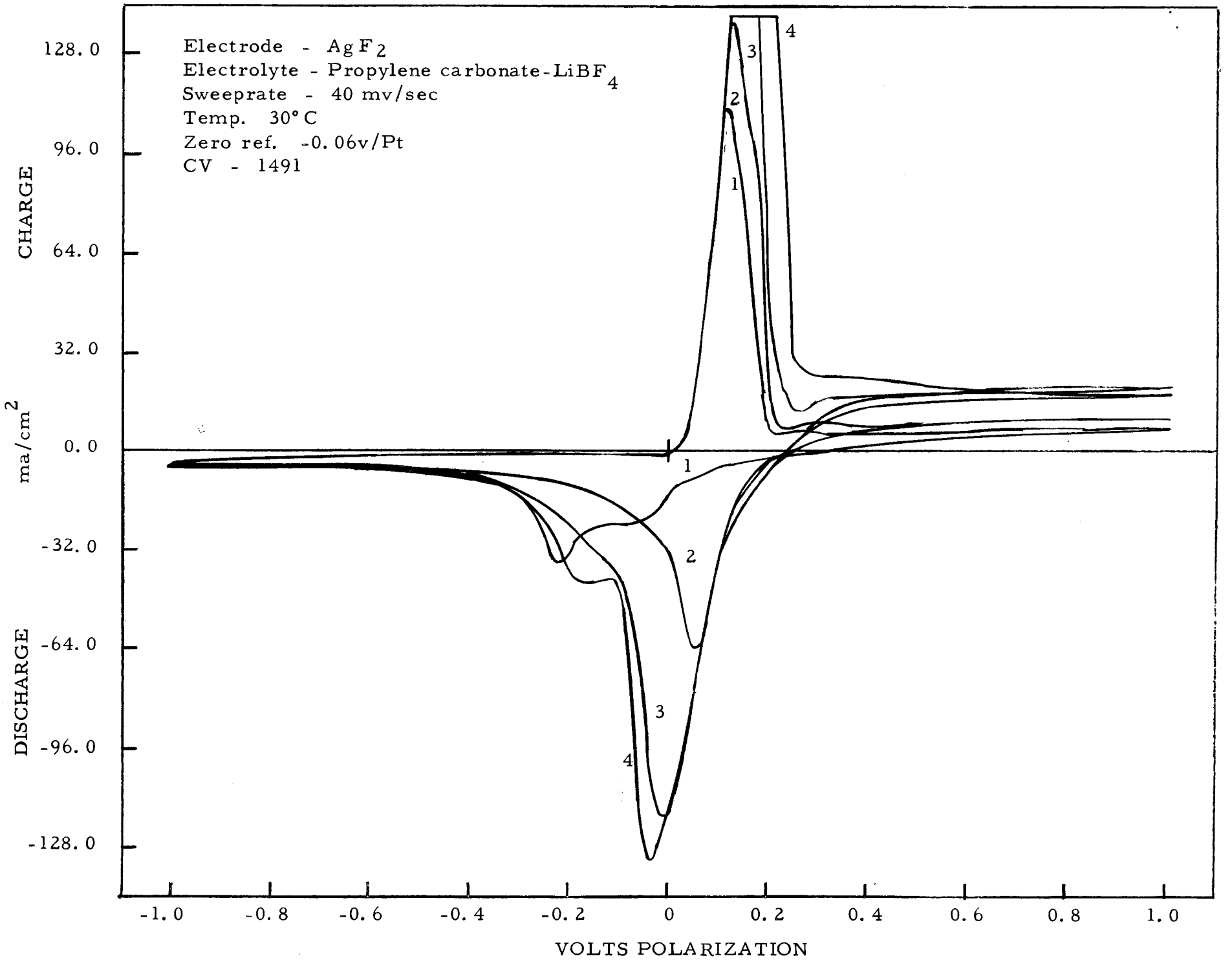
Electrode - AgF_2
Electrolyte - Propylene carbonate-$LiBF_4$
Sweeprate - 40 mv/sec
Temp. 30° C
Zero ref. -0.06v/Pt
CV - 1491
CHARGE
DISCHARGE
ma/cm^2
128.0
96.0
64.0
32.0
0.0
-32.0
-64.0
-96.0
-128.0
-1.0
-0.8
-0.6
-0.4
-0.2
0
0.2
0.4
0.6
0.8
1.0
VOLTS POLARIZATION
1
2
3
4

Figure 17

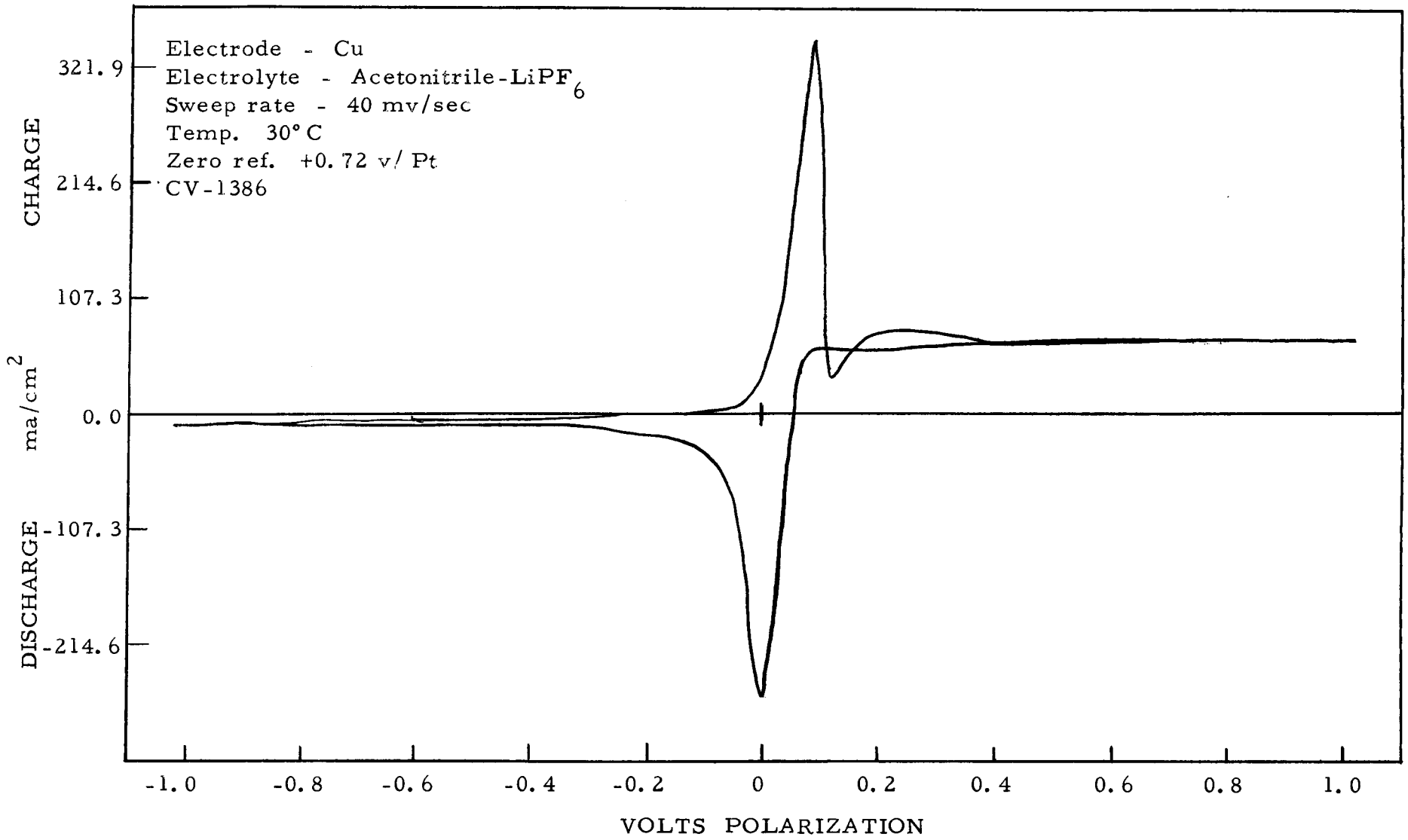
Electrode - Cu
Electrolyte - Acetonitrile-LiPF6
Sweep rate - 40 mv/sec
Temp. 30° C
Zero ref. +0.72 v/ Pt
CV-1386
CHARGE
DISCHARGE
ma/cm2
321.9
214.6
107.3
0.0
-107.3
-214.6
-1.0
-0.8
-0.6
-0.4
-0.2
0
0.2
0.4
0.6
0.8
1.0
VOLTS POLARIZATION

Figure 18

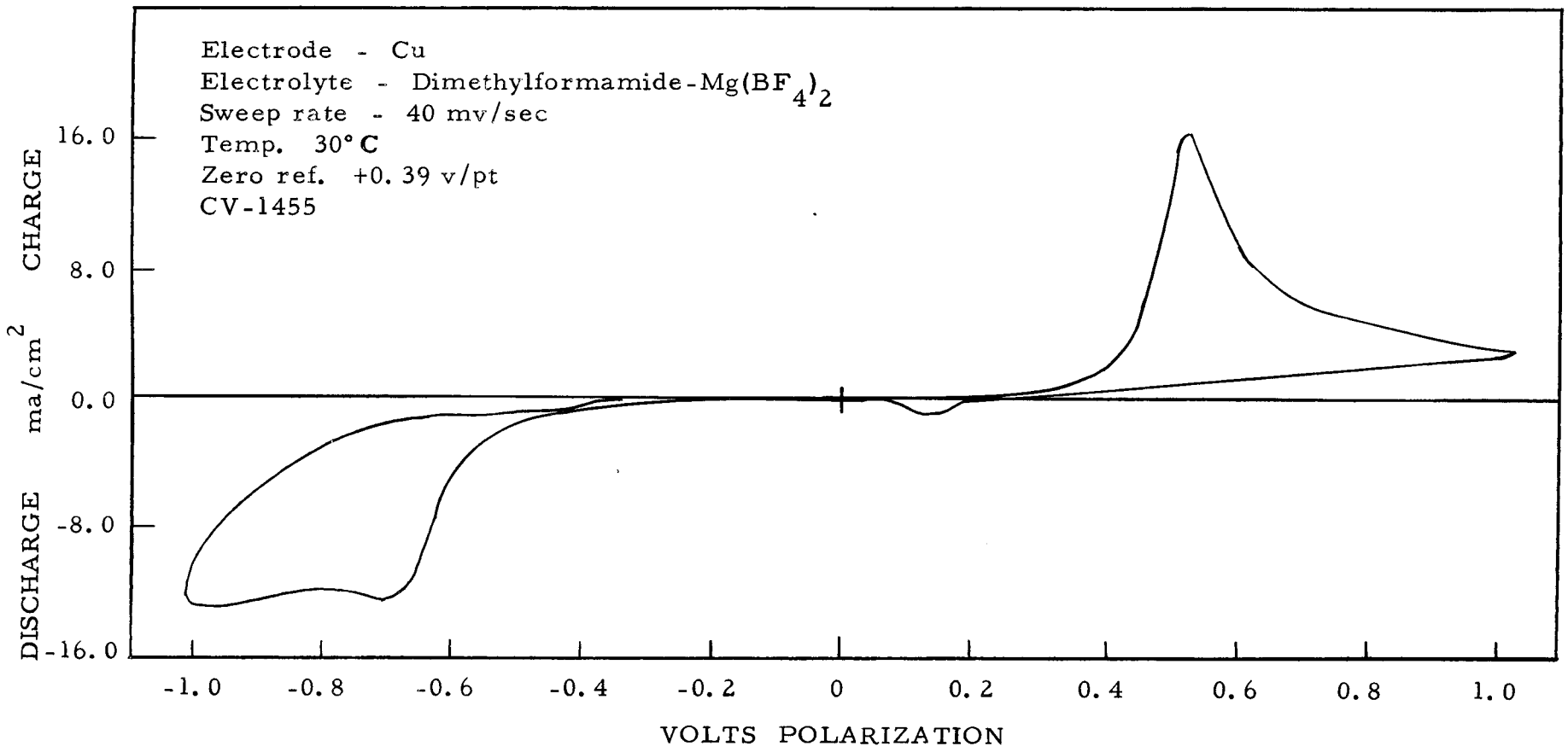
Electrode - Cu
Electrolyte - Dimethylformamide-Mg(BF4)2
Sweep rate - 40 mv/sec
Temp. 30° C
Zero ref. +0.39 v/pt
CV-1455
16.0
8.0
0.0
-8.0
-16.0
CHARGE
ma/cm2
DISCHARGE
-1.0
-0.8
-0.6
-0.4
-0.2
0
0.2
0.4
0.6
0.8
1.0
VOLTS POLARIZATION

Figure 19

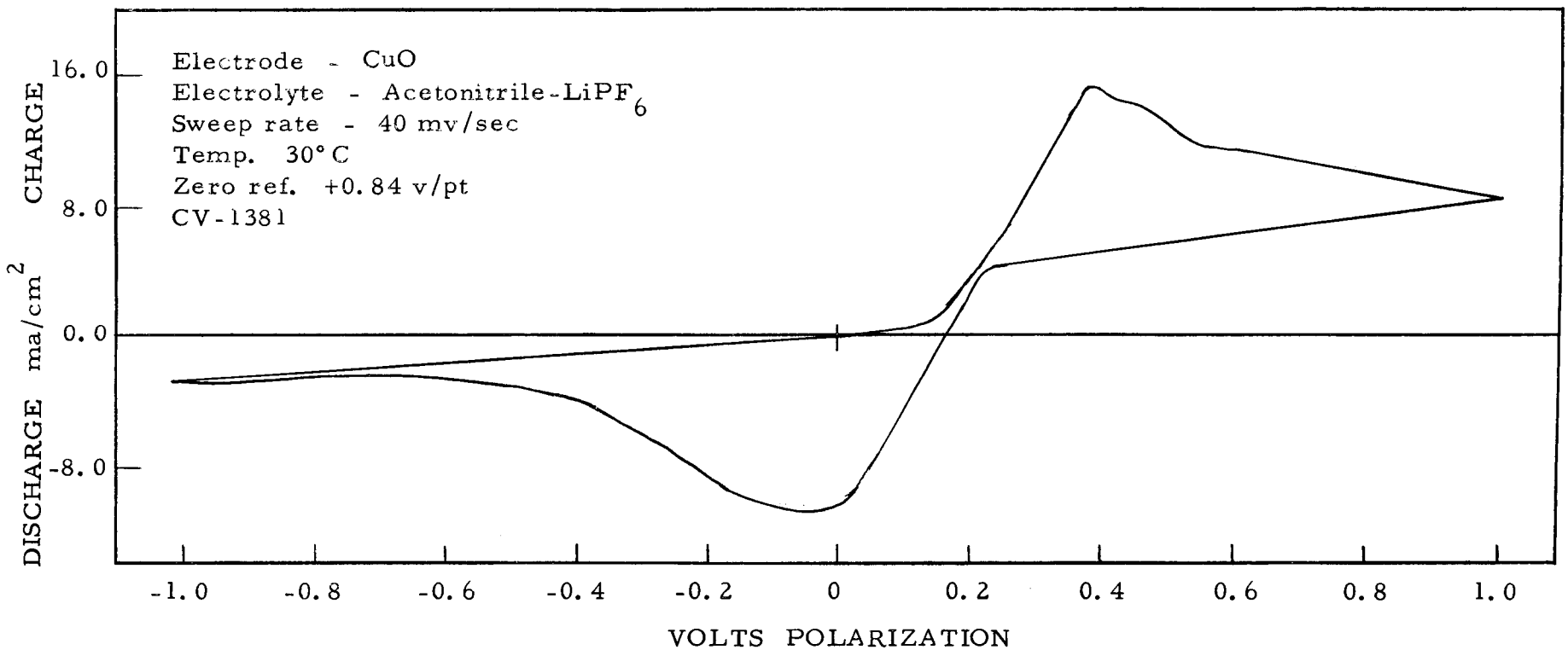
Electrode - CuO
Electrolyte - Acetonitrile-LiPF6
Sweep rate - 40 mv/sec
Temp. 30° C
Zero ref. +0.84 v/pt
CV-1381
CHARGE
DISCHARGE ma/cm2
16.0
8.0
0.0
-8.0
-1.0
-0.8
-0.6
-0.4
-0.2
0
0.2
0.4
0.6
0.8
1.0
VOLTS POLARIZATION

Figure 20

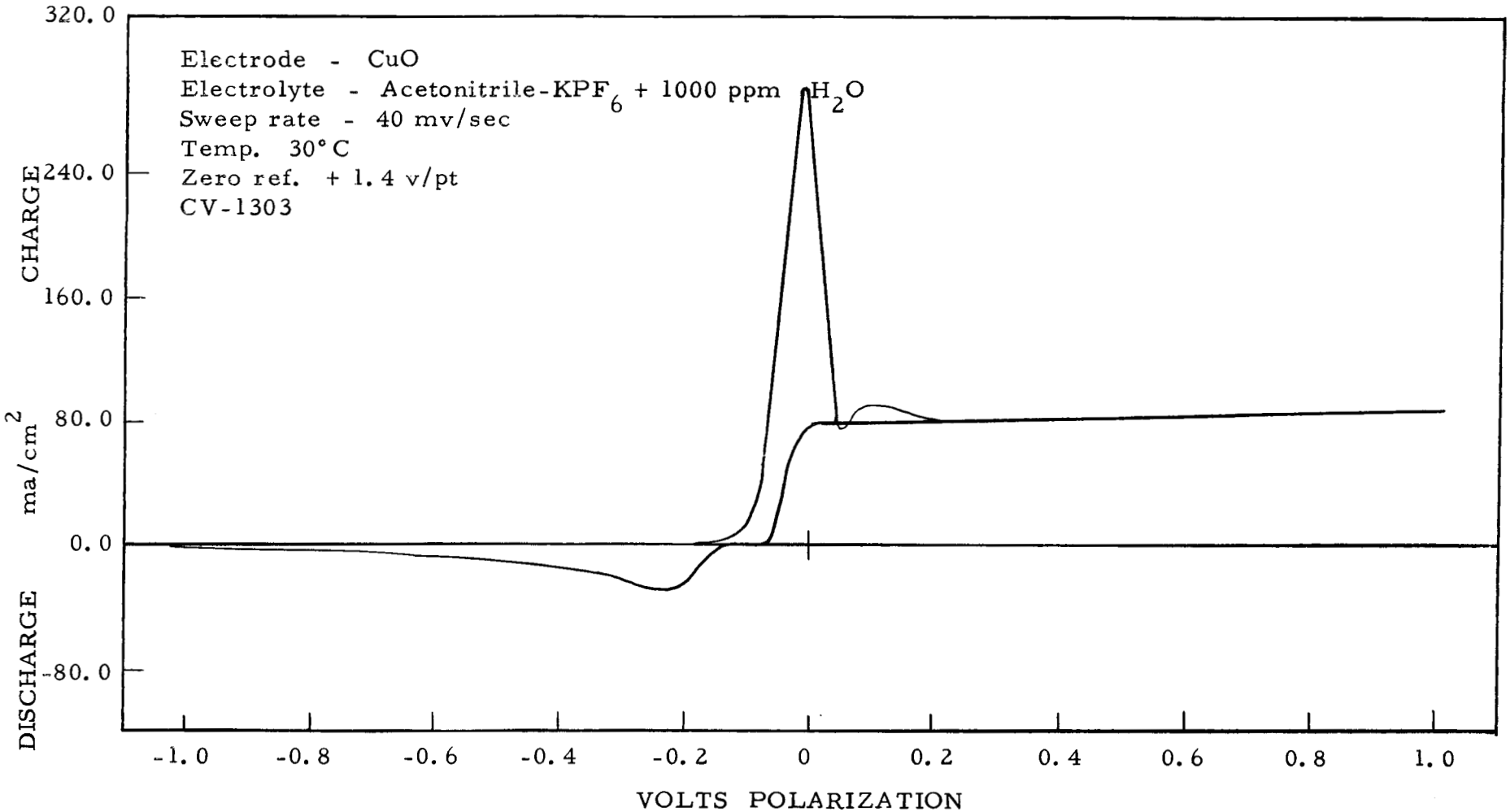
Electrode - CuO
Electrolyte - Acetonitrile-KPF6 + 1000 ppm H2O
Sweep rate - 40 mv/sec
Temp. 30° C
Zero ref. + 1.4 v/pt
CV-1303
320.0
240.0
160.0
80.0
0.0
-80.0
CHARGE
DISCHARGE
ma/cm2
-1.0
-0.8
-0.6
-0.4
-0.2
0
0.2
0.4
0.6
0.8
1.0
VOLTS POLARIZATION

Figure 21

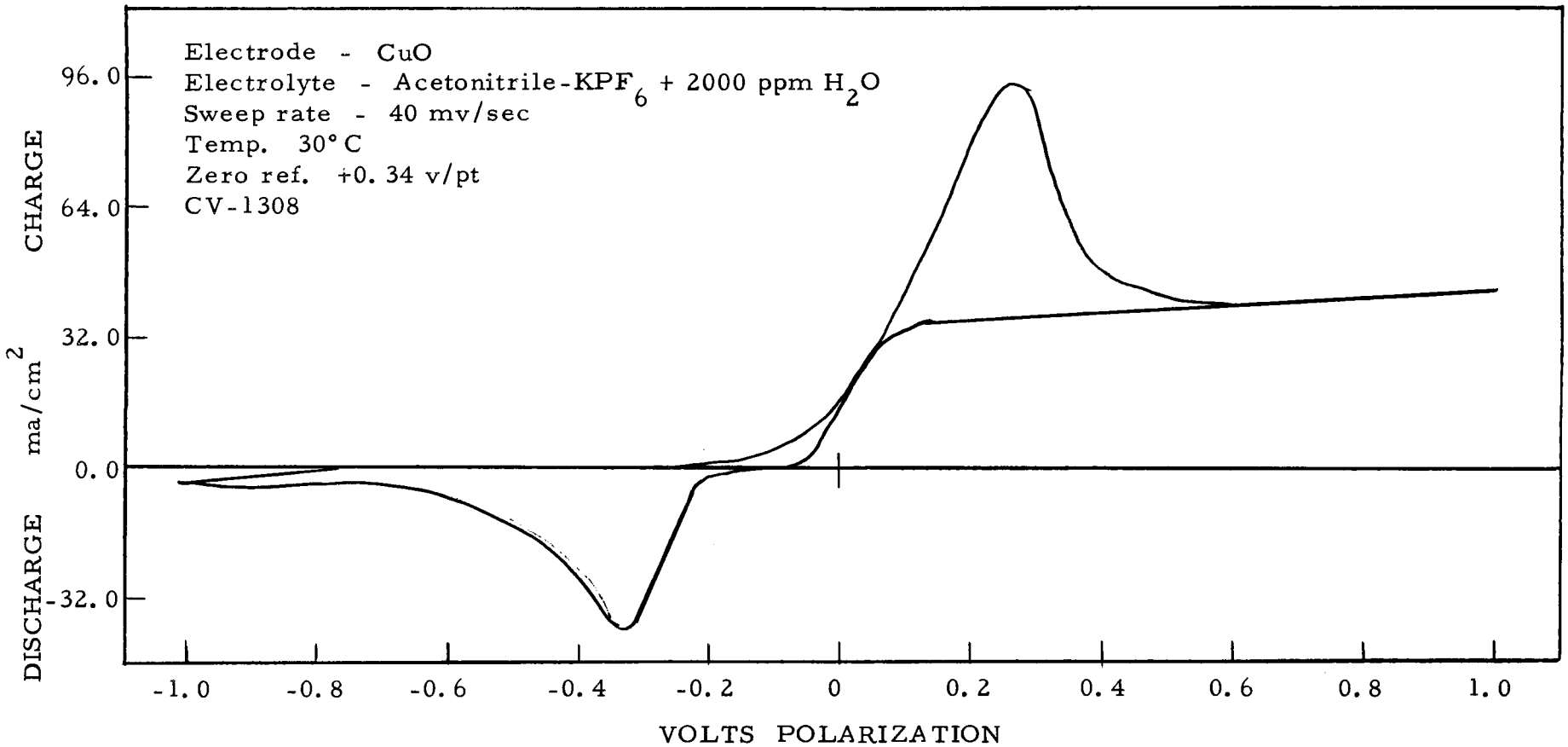
Electrode - CuO
Electrolyte - Acetonitrile-KPF6 + 2000 ppm H2O
Sweep rate - 40 mv/sec
Temp. 30° C
Zero ref. +0.34 v/pt
CV-1308
96.0
64.0
32.0
0.0
-32.0
CHARGE
ma/cm2
DISCHARGE
-1.0
-0.8
-0.6
-0.4
-0.2
0
0.2
0.4
0.6
0.8
1.0
VOLTS POLARIZATION

Figure 22

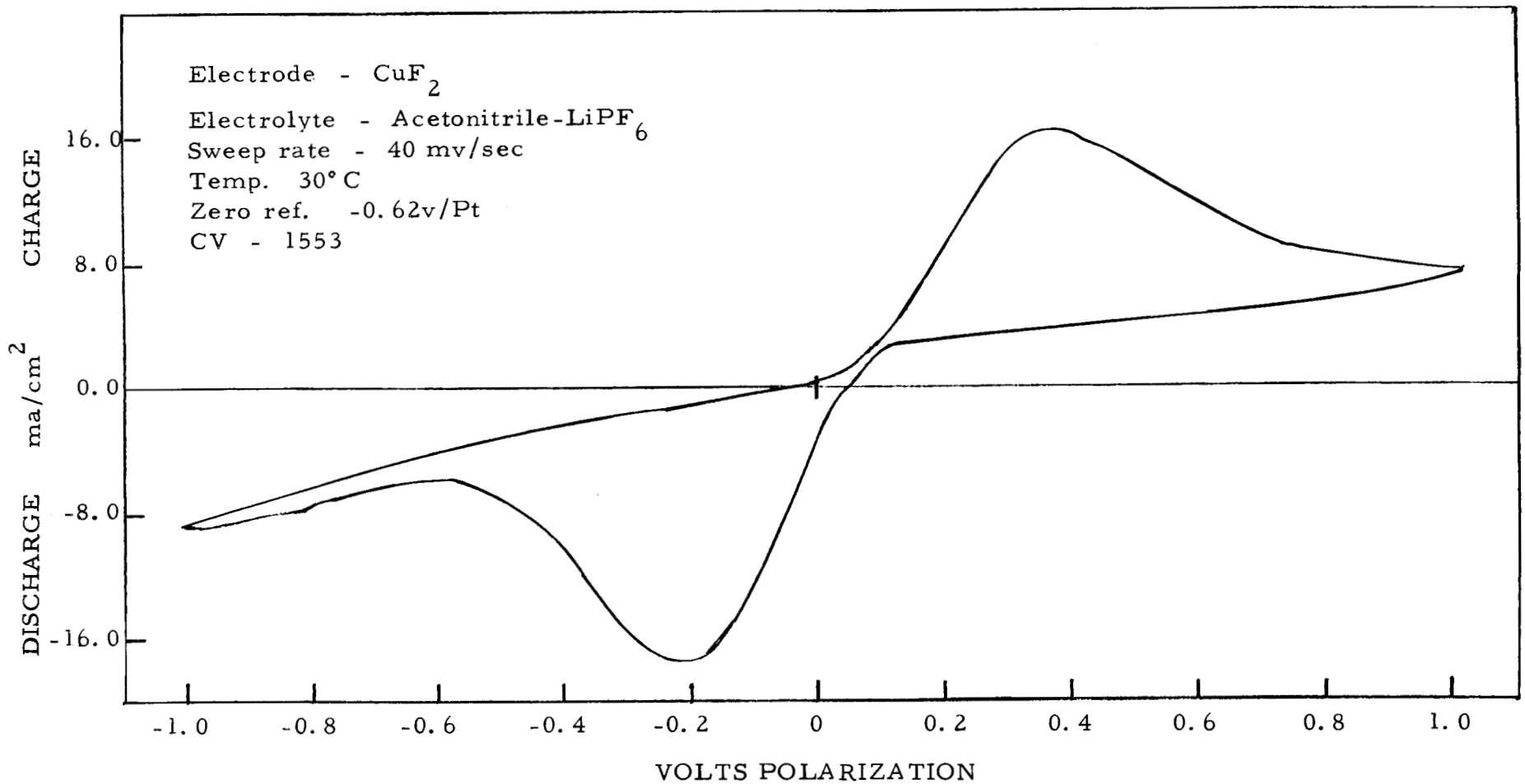
Electrode - CuF_2
Electrolyte - Acetonitrile-$LiPF_6$
Sweep rate - 40 mv/sec
Temp. 30° C
Zero ref. -0.62v/Pt
CV - 1553
CHARGE
DISCHARGE
ma/cm^2
16.0
8.0
0.0
-8.0
-16.0
-1.0
-0.8
-0.6
-0.4
-0.2
0
0.2
0.4
0.6
0.8
1.0
VOLTS POLARIZATION

Figure 23

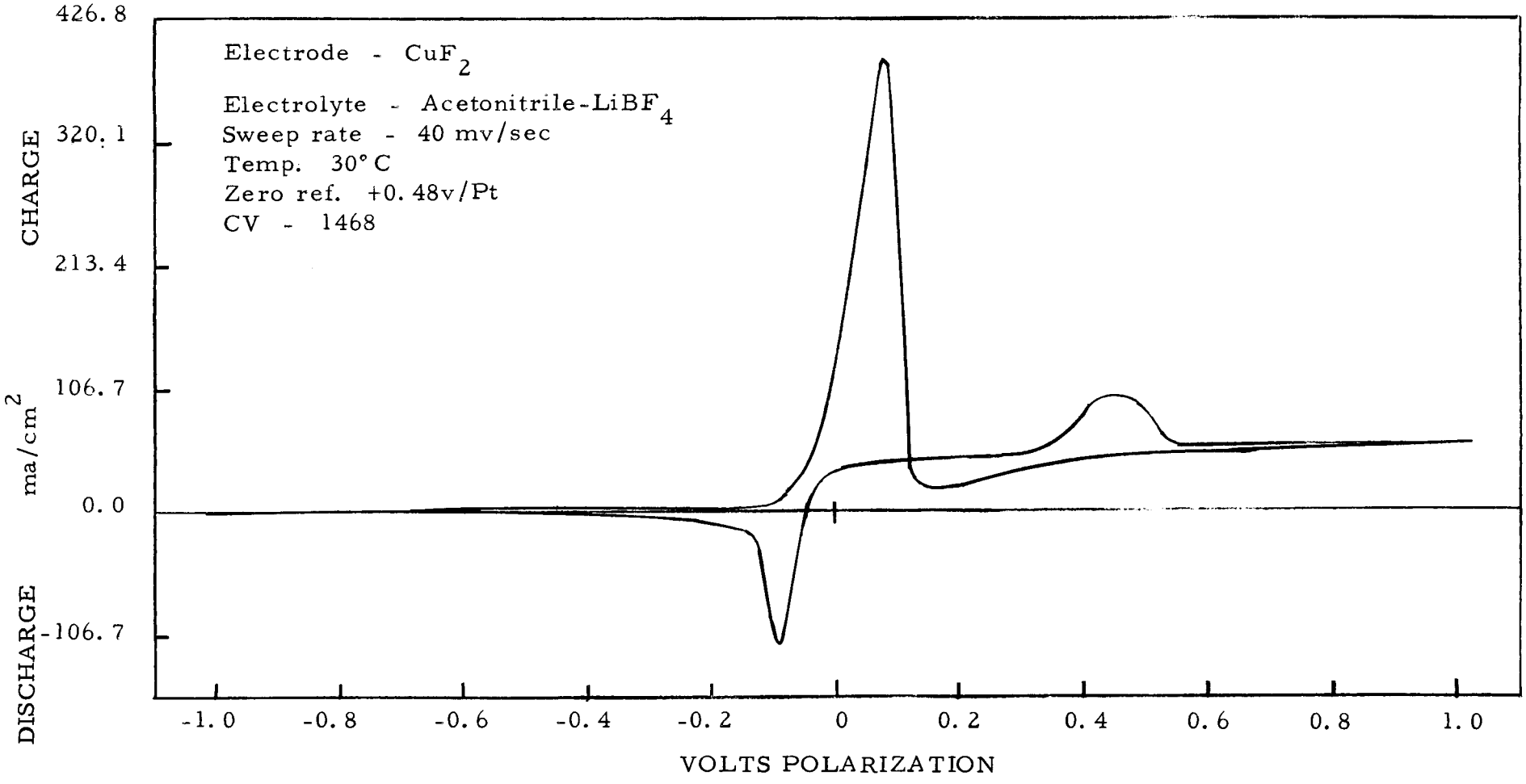
Electrode - CuF_2
Electrolyte - Acetonitrile-$LiBF_4$
Sweep rate - 40 mv/sec
Temp. 30° C
Zero ref. +0.48v/Pt
CV - 1468
426.8
320.1
213.4
106.7
0.0
-106.7
CHARGE
DISCHARGE
ma/cm^2
-1.0
-0.8
-0.6
-0.4
-0.2
0
0.2
0.4
0.6
0.8
1.0
VOLTS POLARIZATION

Figure 24

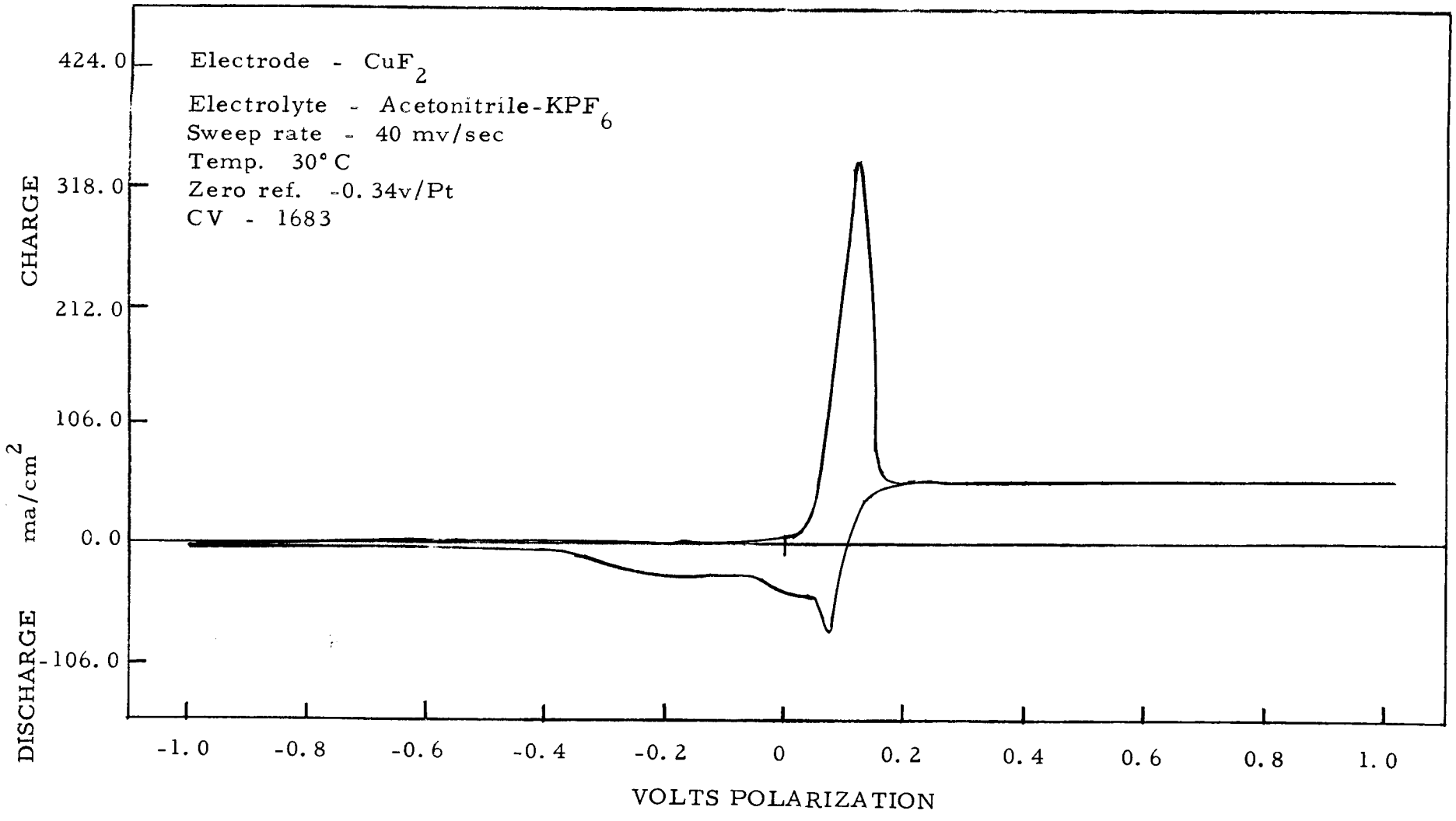
Electrode - CuF_2
Electrolyte - Acetonitrile-KPF_6
Sweep rate - 40 mv/sec
Temp. 30° C
Zero ref. -0.34v/Pt
CV - 1683
424.0
318.0
212.0
106.0
0.0
-106.0
CHARGE
ma/cm^2
DISCHARGE
-1.0
-0.8
-0.6
-0.4
-0.2
0
0.2
0.4
0.6
0.8
1.0
VOLTS POLARIZATION

Figure 25

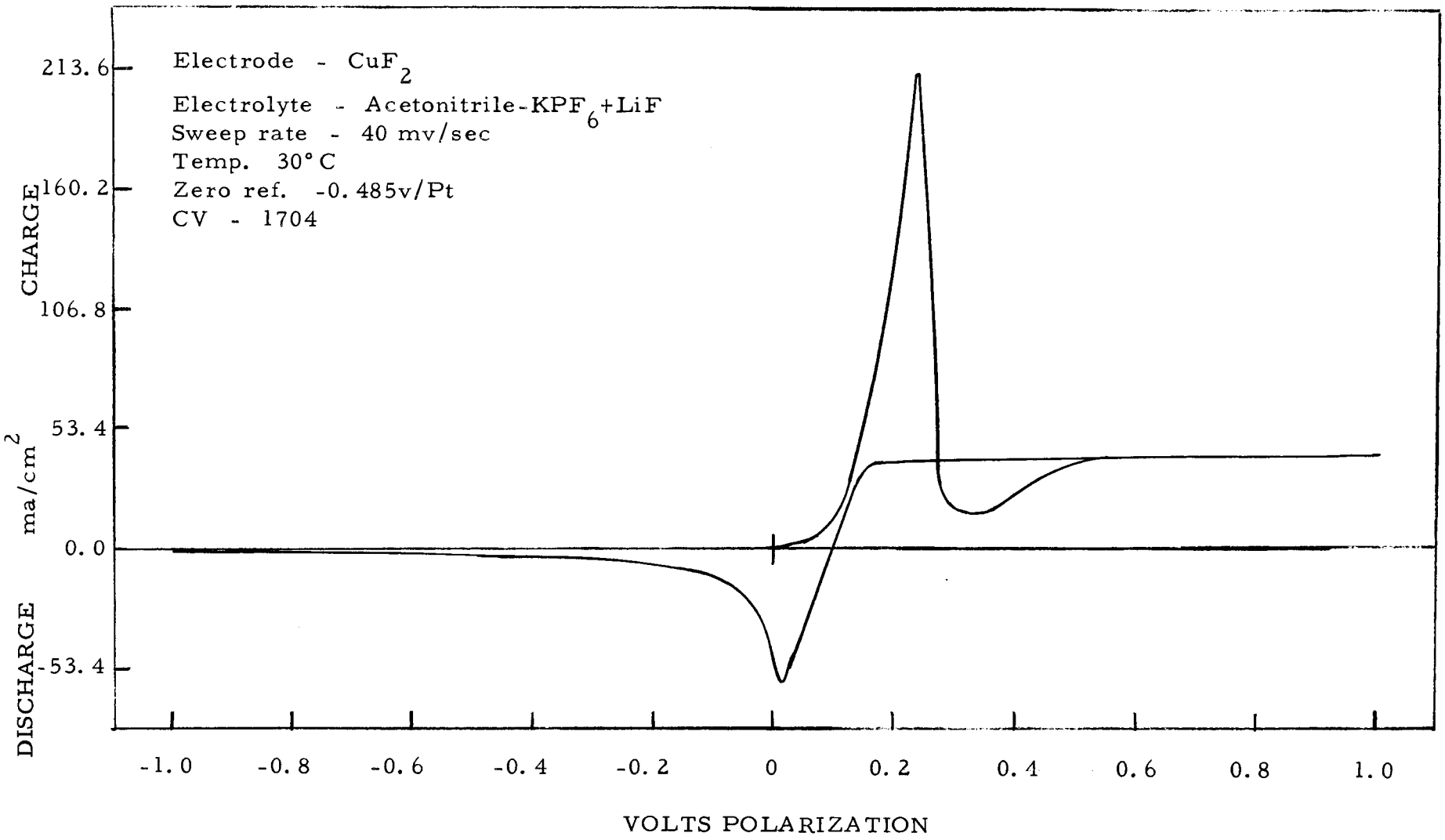
Electrode - CuF_2
Electrolyte - Acetonitrile-KPF_6+LiF
Sweep rate - 40 mv/sec
Temp. 30° C
Zero ref. -0.485v/Pt
CV - 1704
213.6
160.2
106.8
53.4
0.0
-53.4
CHARGE
DISCHARGE
ma/cm^2
-1.0
-0.8
-0.6
-0.4
-0.2
0
0.2
0.4
0.6
0.8
1.0
VOLTS POLARIZATION

Figure 26

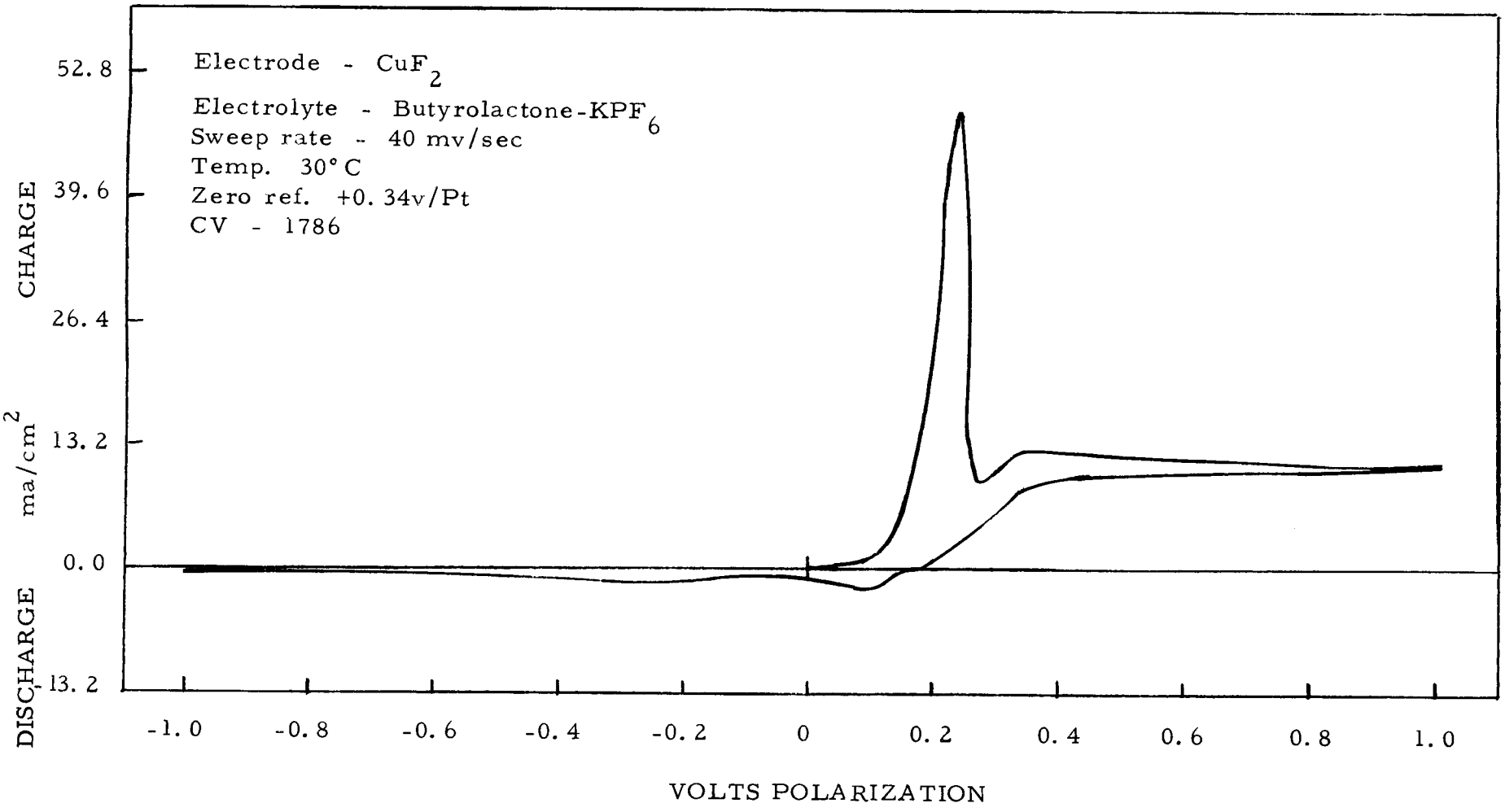
Electrode - CuF_2
Electrolyte - Butyrolactone-KPF_6
Sweep rate - 40 mv/sec
Temp. 30° C
Zero ref. +0.34v/Pt
CV - 1786
52.8
39.6
26.4
13.2
0.0
-13.2
CHARGE
ma/cm^2
DISCHARGE
-1.0
-0.8
-0.6
-0.4
-0.2
0
0.2
0.4
0.6
0.8
1.0
VOLTS POLARIZATION

Figure 27

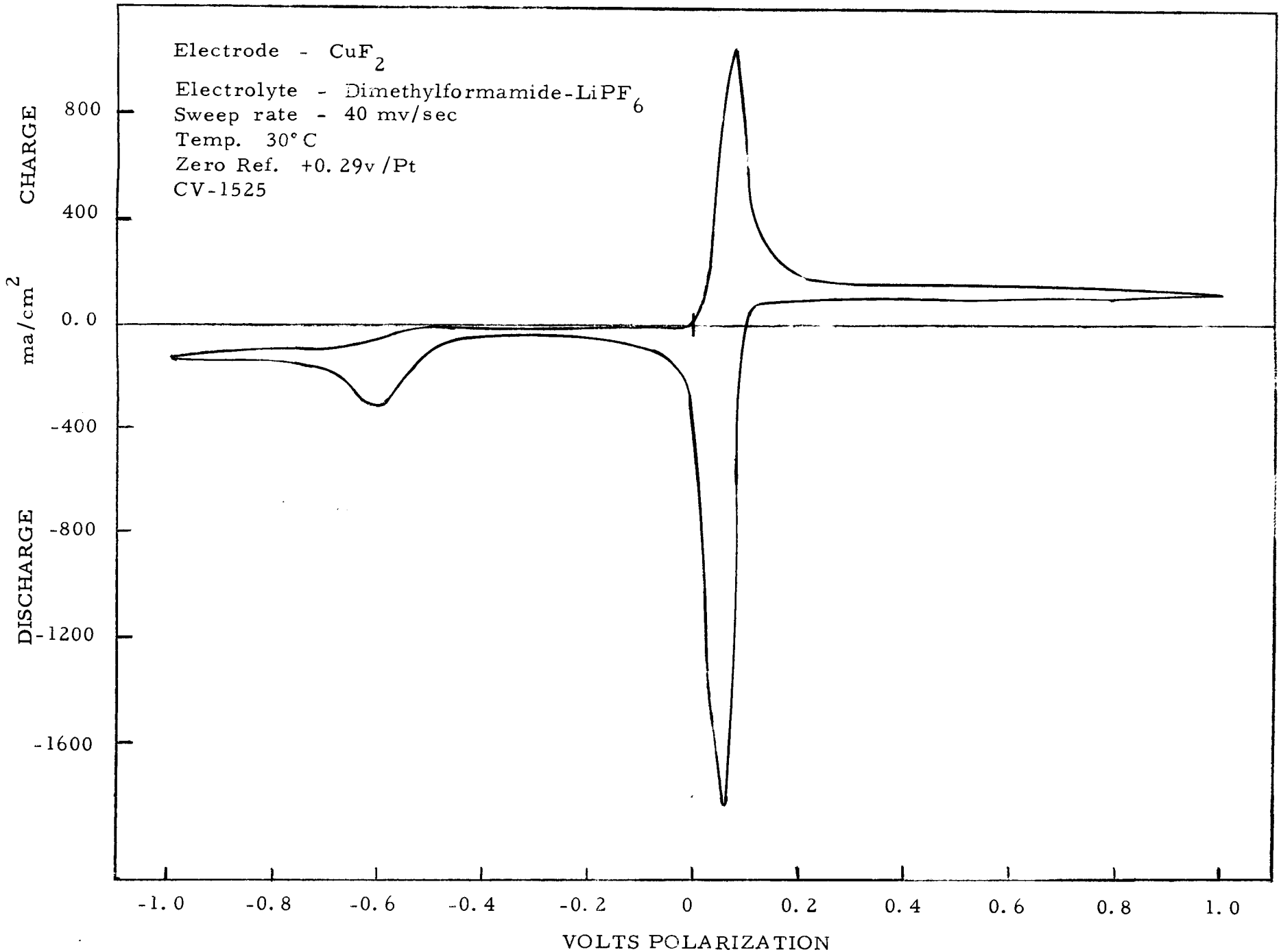
Electrode - CuF_2
Electrolyte - Dimethylformamide-$LiPF_6$
Sweep rate - 40 mv/sec
Temp. 30° C
Zero Ref. +0.29v /Pt
CV-1525
CHARGE
DISCHARGE
ma/cm^2
800
400
0.0
-400
-800
-1200
-1600
-1.0
-0.8
-0.6
-0.4
-0.2
0
0.2
0.4
0.6
0.8
1.0
VOLTS POLARIZATION

Figure 28

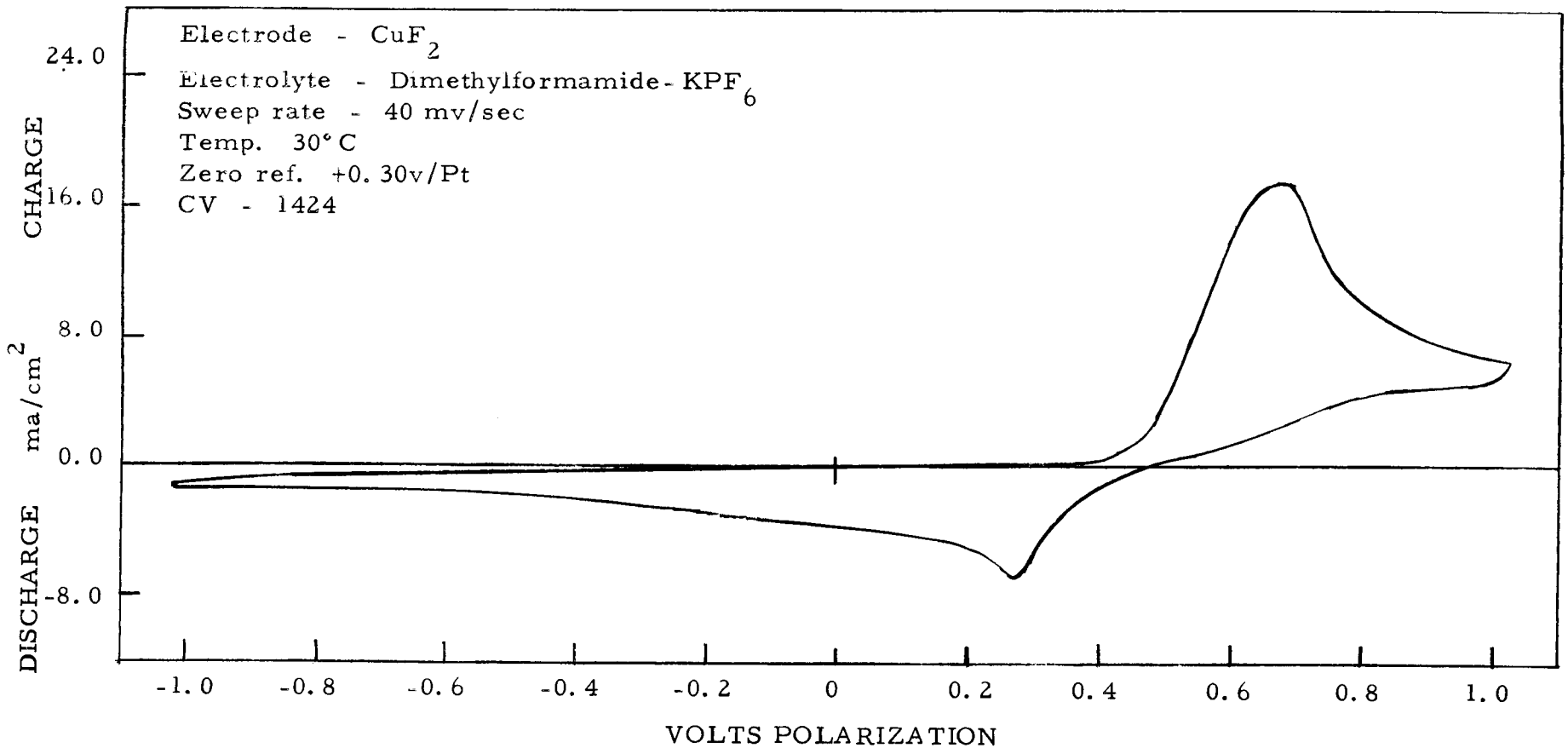
Electrode - CuF_2
Electrolyte - Dimethylformamide - KPF_6
Sweep rate - 40 mv/sec
Temp. 30° C
Zero ref. +0.30v/Pt
CV - 1424
CHARGE
DISCHARGE
ma/cm^2
24.0
16.0
8.0
0.0
-8.0
-1.0
-0.8
-0.6
-0.4
-0.2
0
0.2
0.4
0.6
0.8
1.0
VOLTS POLARIZATION

Figure 29

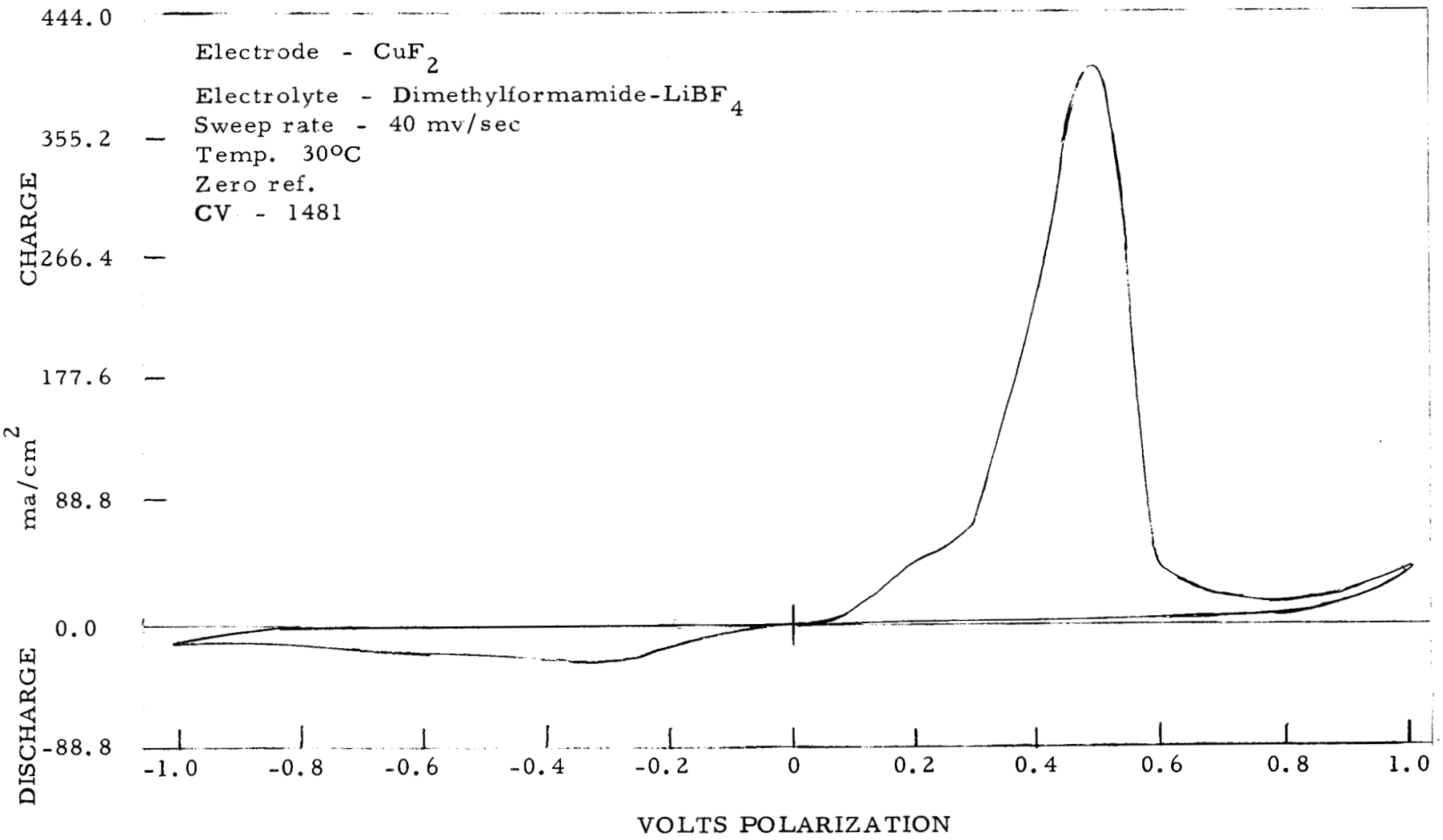
Electrode - CuF_2
Electrolyte - Dimethylformamide-$LiBF_4$
Sweep rate - 40 mv/sec
Temp. 30°C
Zero ref.
CV - 1481
444.0
355.2
266.4
177.6
88.8
0.0
-88.8
CHARGE
DISCHARGE
ma/cm^2
-1.0
-0.8
-0.6
-0.4
-0.2
0
0.2
0.4
0.6
0.8
1.0
VOLTS POLARIZATION

Figure 30

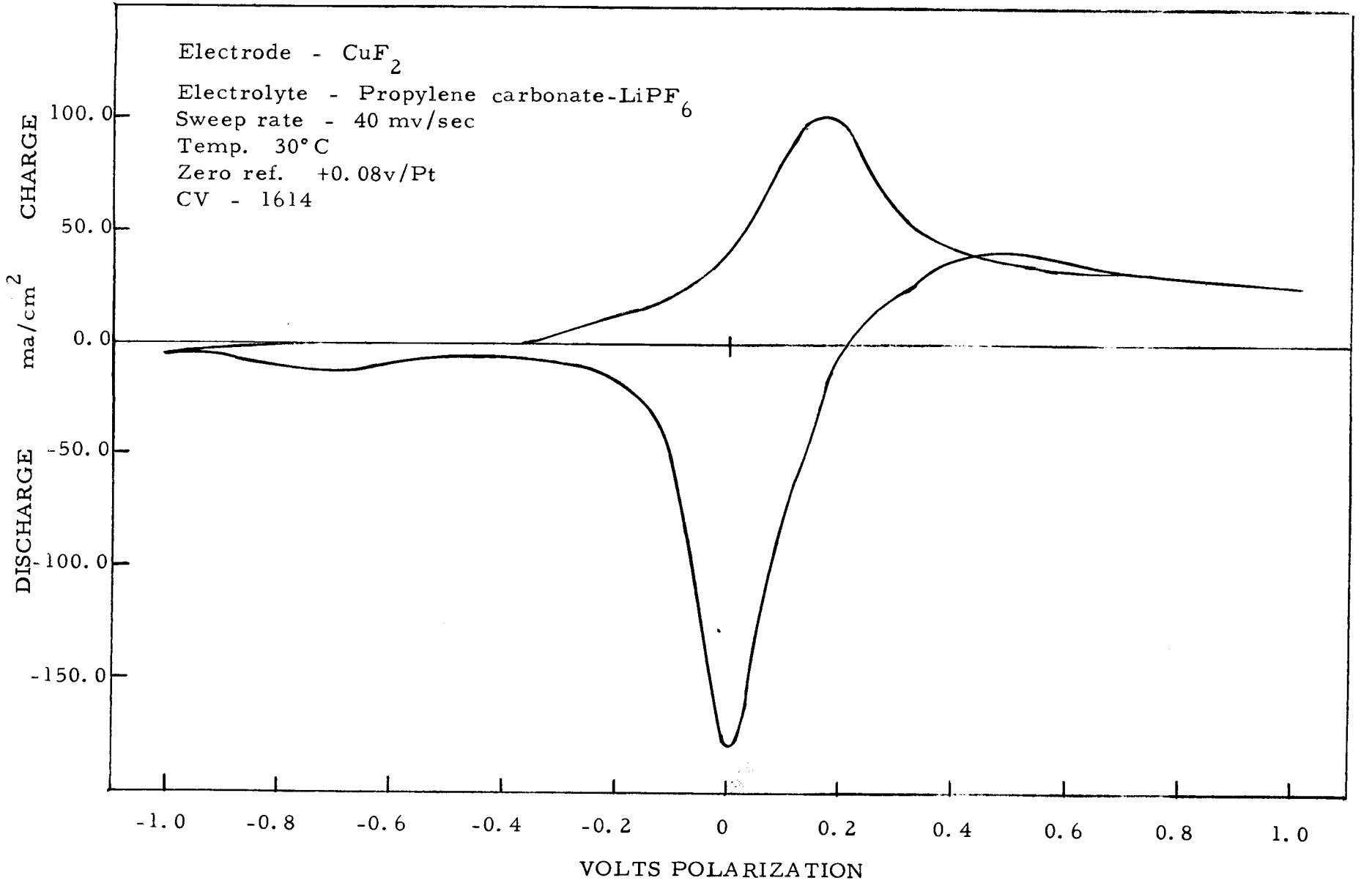
Electrode - CuF_2
Electrolyte - Propylene carbonate-$LiPF_6$
Sweep rate - 40 mv/sec
Temp. 30° C
Zero ref. +0.08v/Pt
CV - 1614
CHARGE
DISCHARGE
ma/cm^2
100.0
50.0
0.0
-50.0
-100.0
-150.0
-1.0
-0.8
-0.6
-0.4
-0.2
0
0.2
0.4
0.6
0.8
1.0
VOLTS POLARIZATION

Figure 31

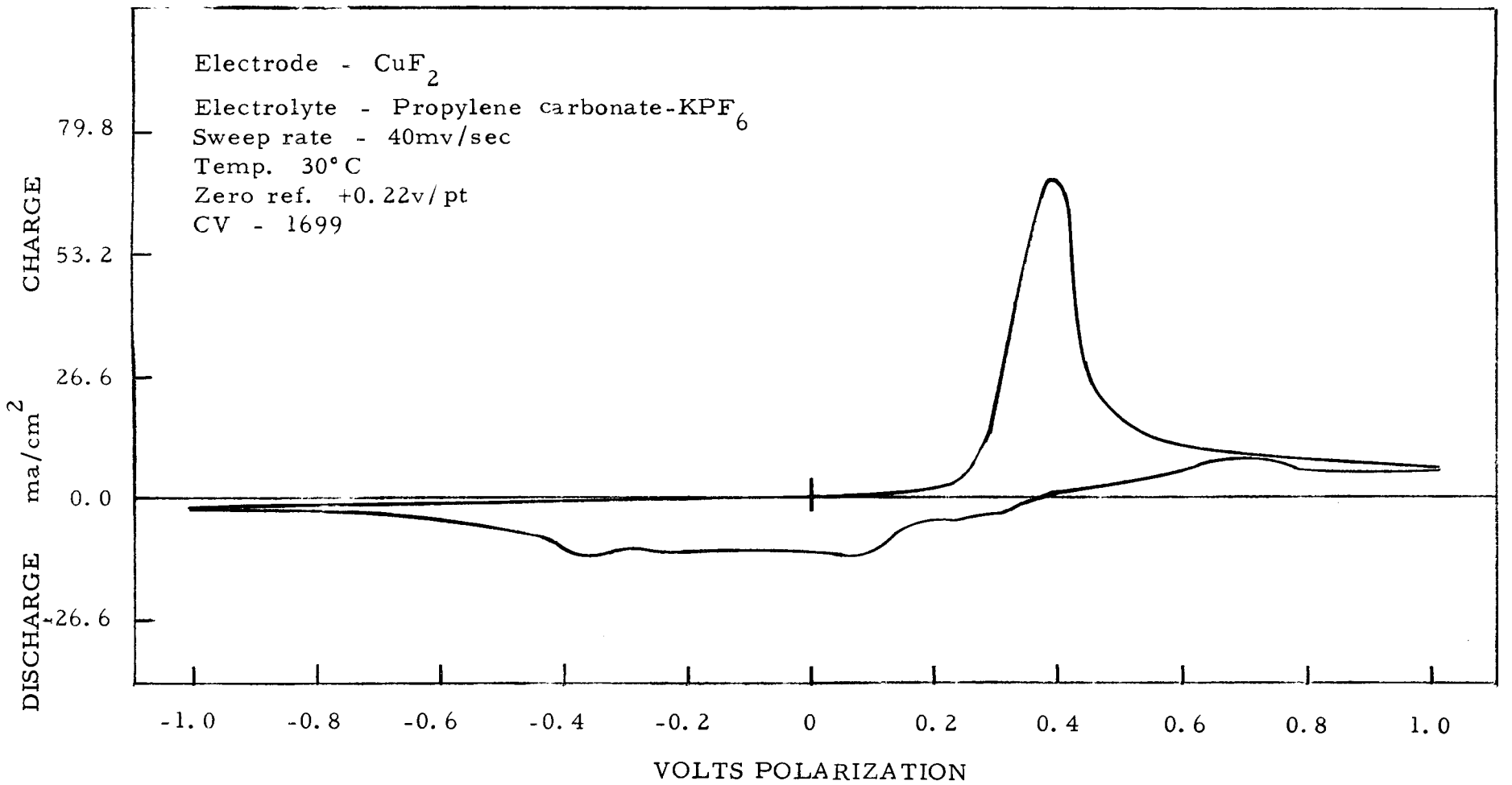
Electrode - CuF_2
Electrolyte - Propylene carbonate-KPF_6
Sweep rate - 40mv/sec
Temp. 30° C
Zero ref. +0.22v/pt
CV - 1699
79.8
53.2
26.6
0.0
-26.6
CHARGE
ma/cm^2
DISCHARGE
-1.0
-0.8
-0.6
-0.4
-0.2
0
0.2
0.4
0.6
0.8
1.0
VOLTS POLARIZATION

Figure 32

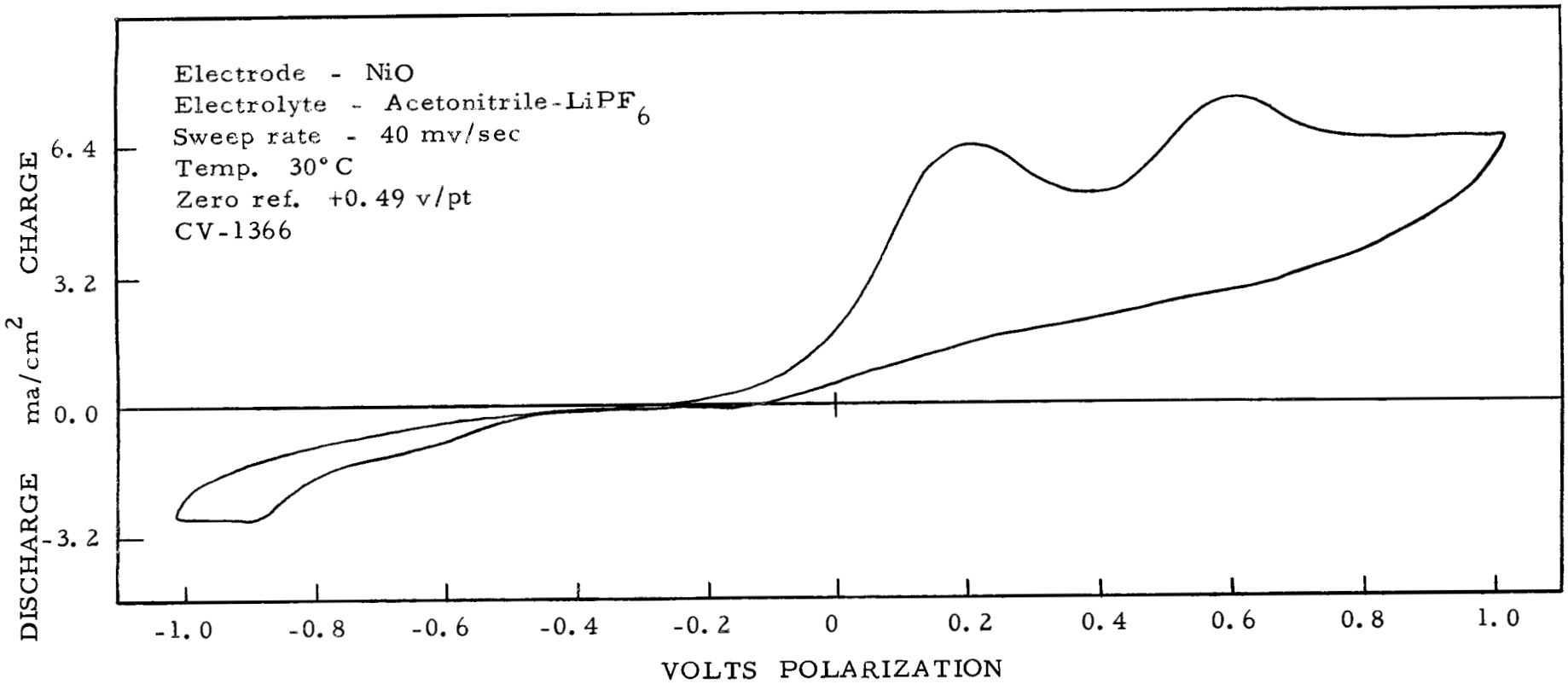
Electrode - NiO
Electrolyte - Acetonitrile-LiPF6
Sweep rate - 40 mv/sec
Temp. 30° C
Zero ref. +0.49 v/pt
CV-1366
CHARGE
ma/cm2
DISCHARGE
6.4
3.2
0.0
-3.2
-1.0
-0.8
-0.6
-0.4
-0.2
0
0.2
0.4
0.6
0.8
1.0
VOLTS POLARIZATION

Figure 33

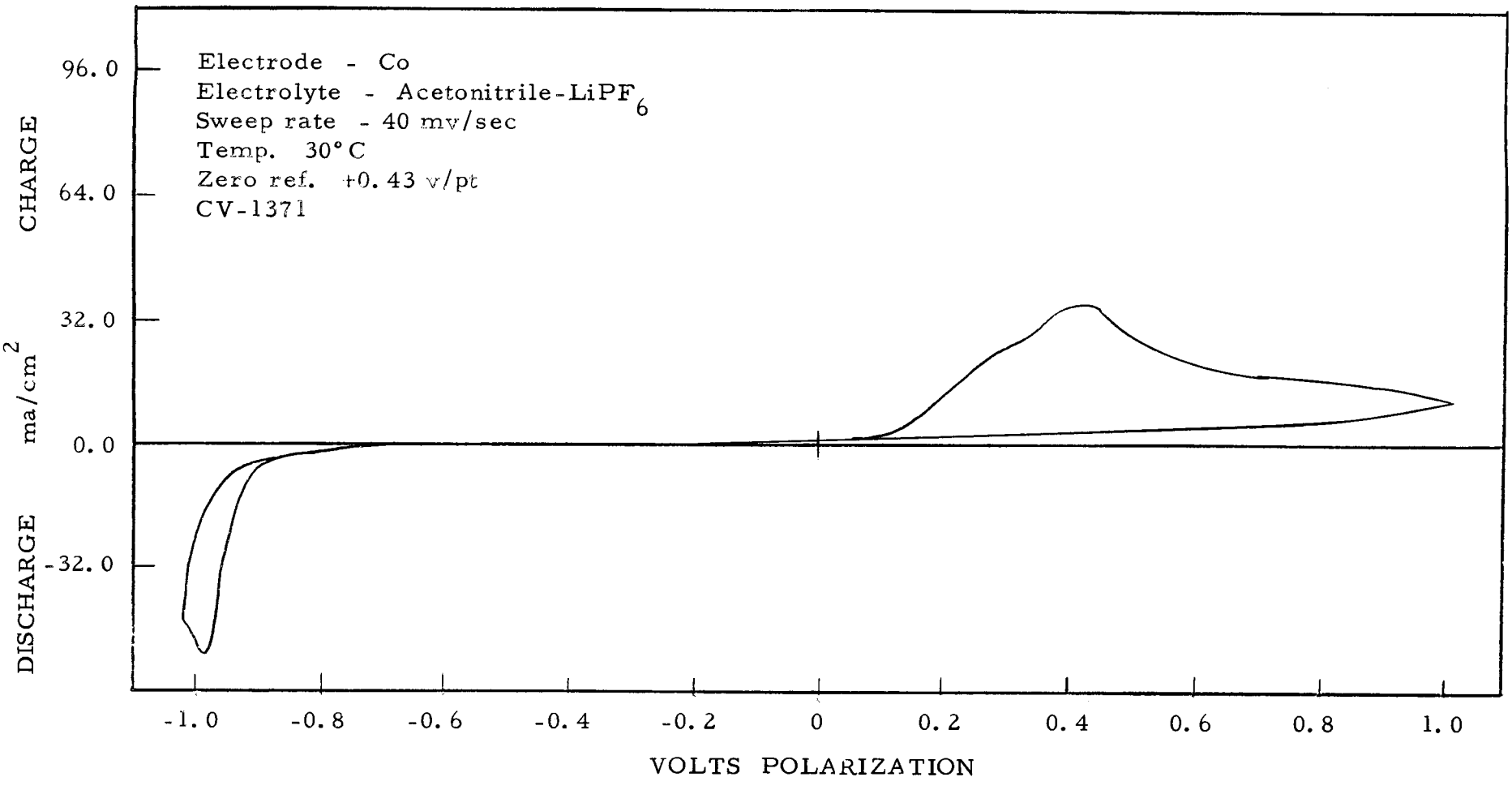
Electrode - Co
Electrolyte - Acetonitrile-LiPF6
Sweep rate - 40 mv/sec
Temp. 30° C
Zero ref. +0.43 v/pt
CV-1371
96.0
64.0
32.0
0.0
-32.0
CHARGE
ma/cm2
DISCHARGE
-1.0
-0.8
-0.6
-0.4
-0.2
0
0.2
0.4
0.6
0.8
1.0
VOLTS POLARIZATION

Figure 34

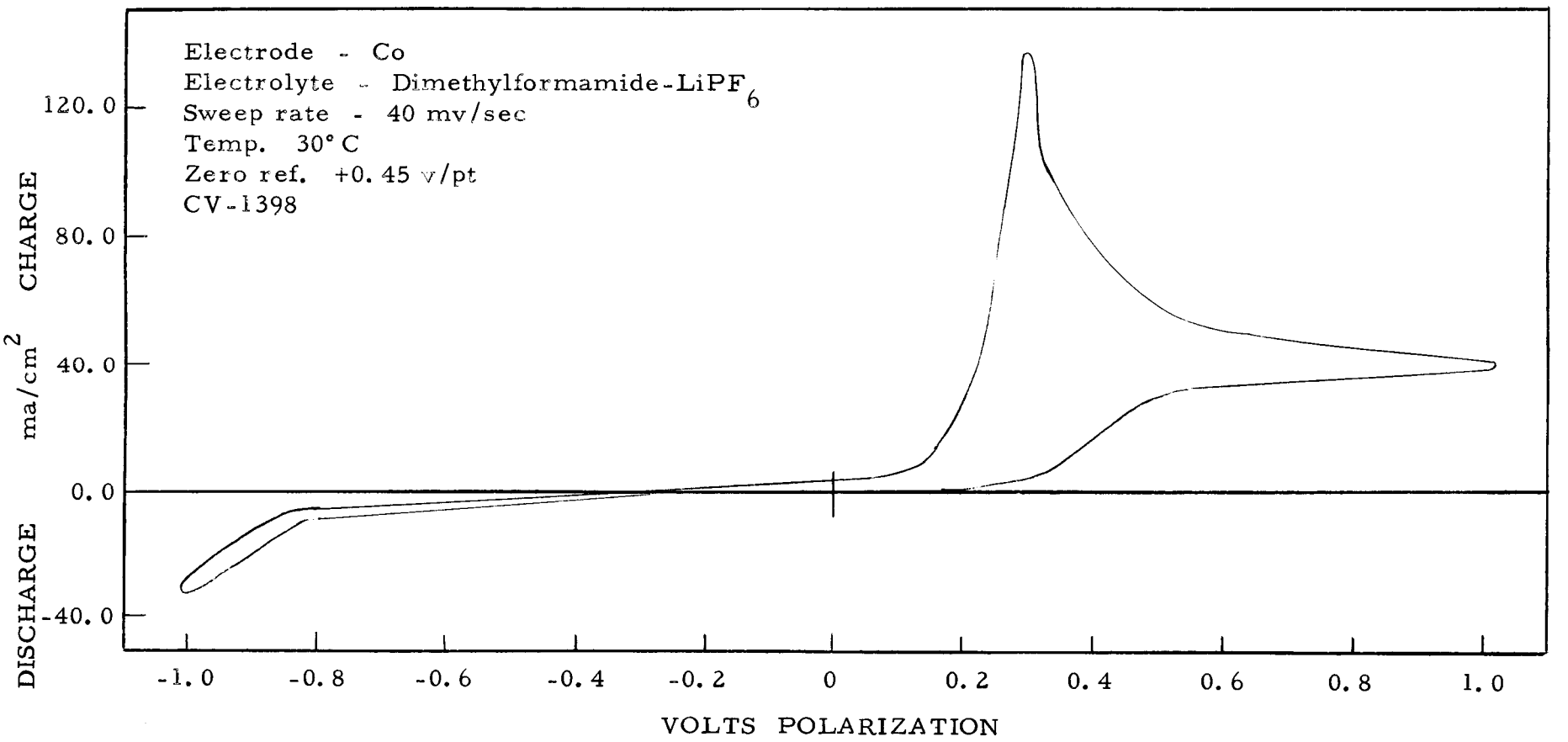
Electrode - Co
Electrolyte - Dimethylformamide-LiPF6
Sweep rate - 40 mv/sec
Temp. 30° C
Zero ref. +0.45 v/pt
CV-1398
120.0
80.0
40.0
0.0
-40.0
CHARGE
ma/cm2
DISCHARGE
-1.0
-0.8
-0.6
-0.4
-0.2
0
0.2
0.4
0.6
0.8
1.0
VOLTS POLARIZATION

Figure 35

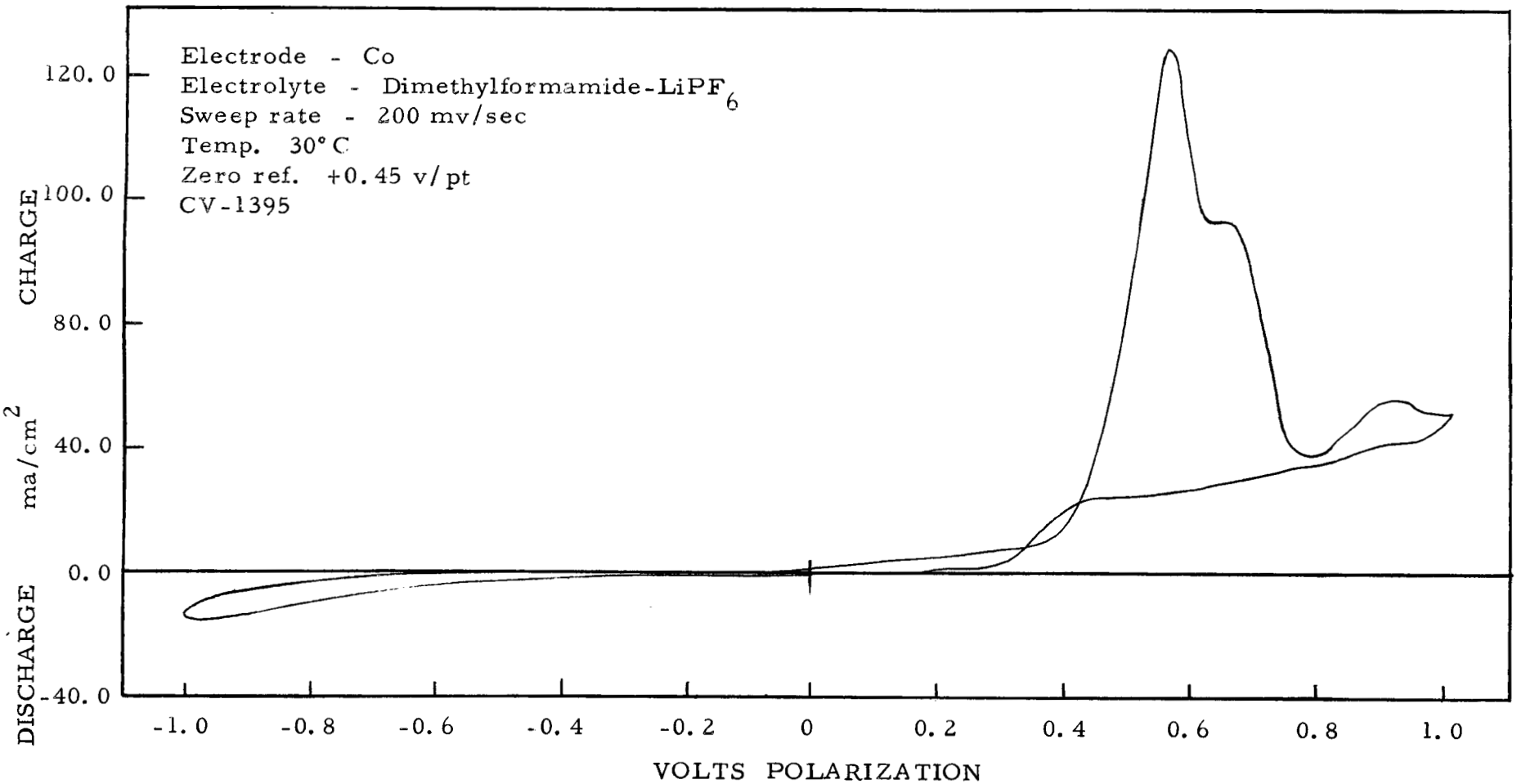
Electrode - Co
Electrolyte - Dimethylformamide-LiPF6
Sweep rate - 200 mv/sec
Temp. 30° C
Zero ref. +0.45 v/pt
CV-1395
120.0
100.0
80.0
40.0
0.0
-40.0
CHARGE
ma/cm2
DISCHARGE
-1.0
-0.8
-0.6
-0.4
-0.2
0
0.2
0.4
0.6
0.8
1.0
VOLTS POLARIZATION

Figure 36

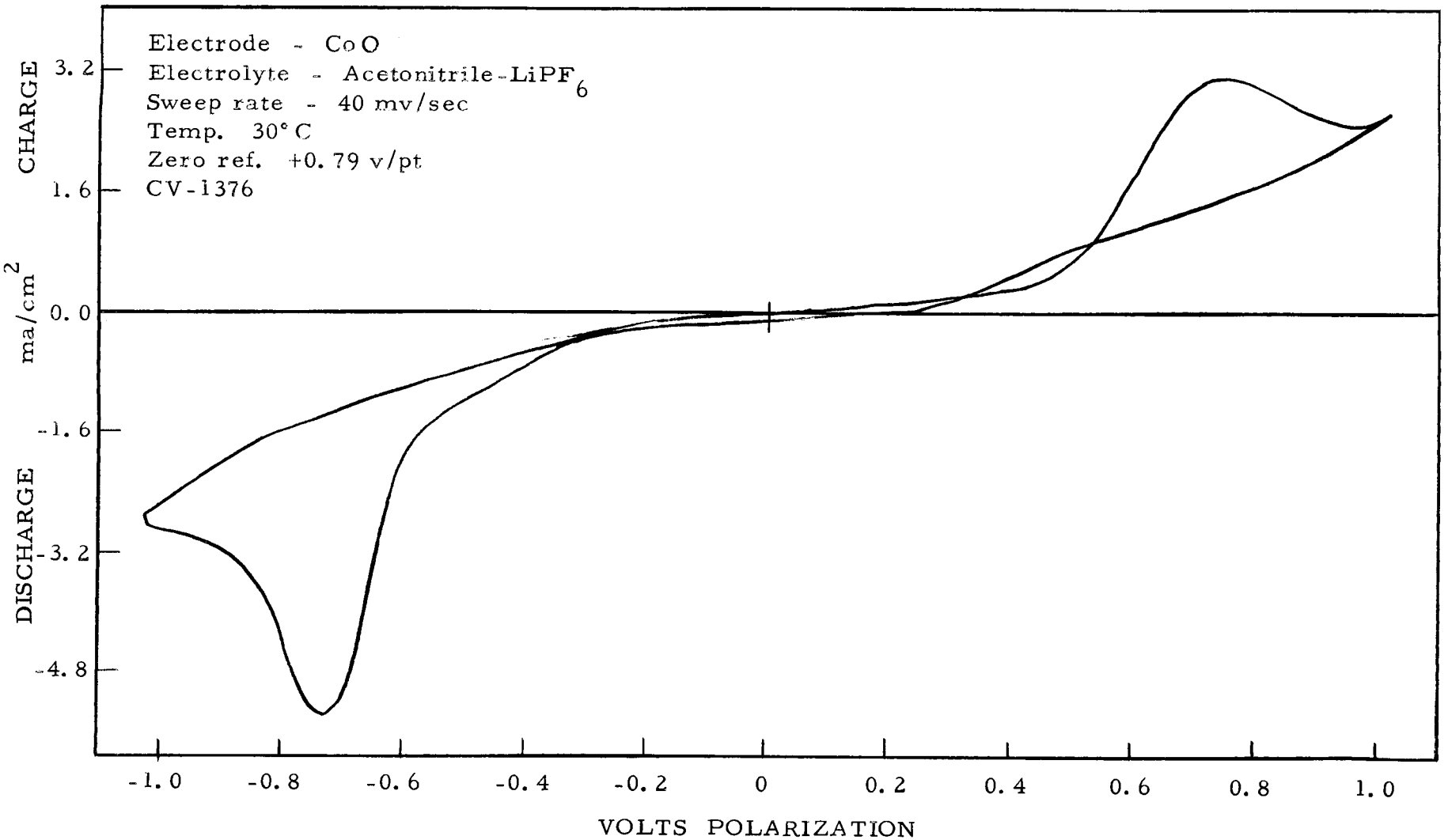
Electrode - CoO
Electrolyte - Acetonitrile-LiPF6
Sweep rate - 40 mv/sec
Temp. 30° C
Zero ref. +0.79 v/pt
CV-1376
CHARGE
DISCHARGE
ma/cm2
3.2
1.6
0.0
-1.6
-3.2
-4.8
-1.0
-0.8
-0.6
-0.4
-0.2
0
0.2
0.4
0.6
0.8
1.0
VOLTS POLARIZATION

Figure 37

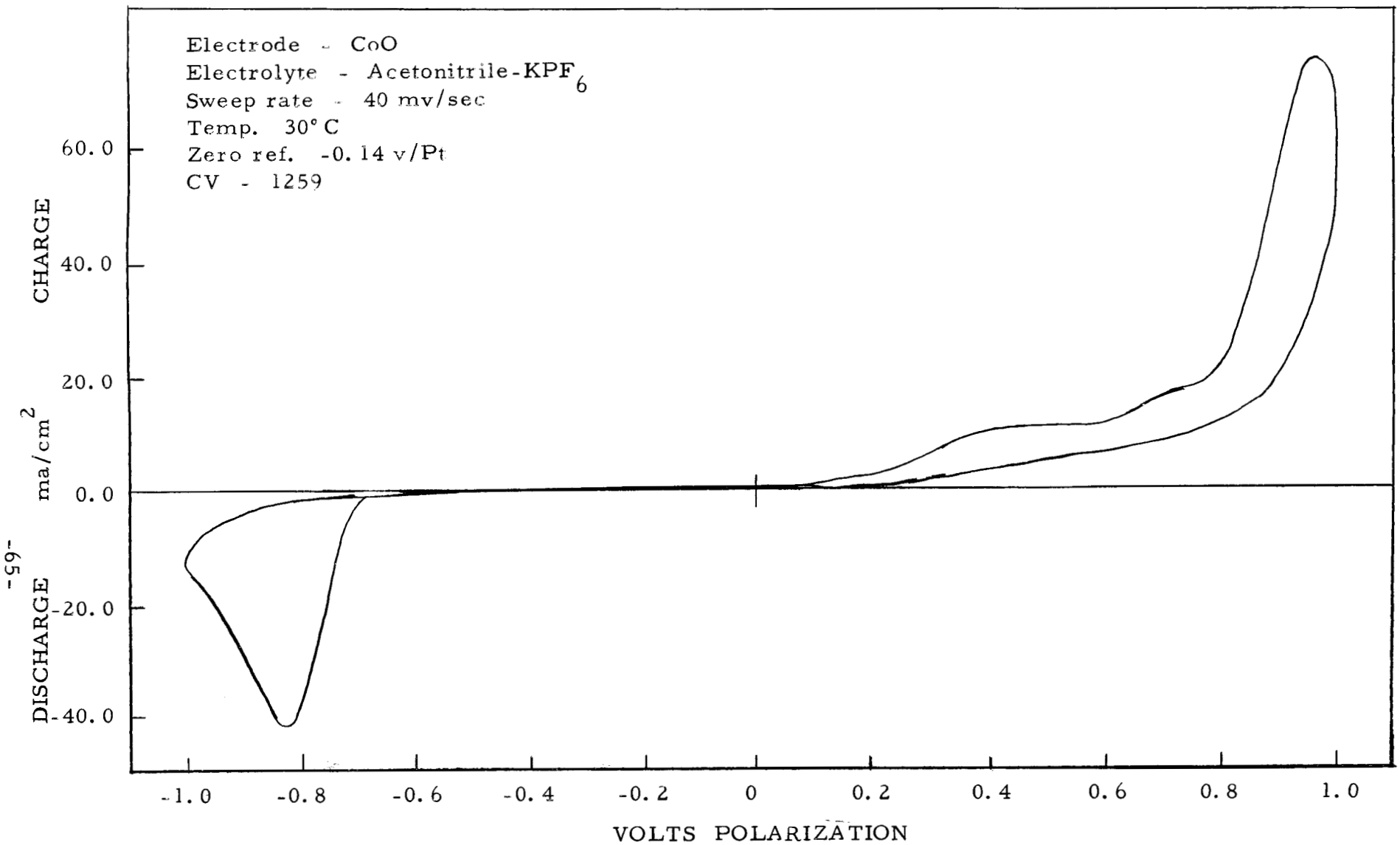
Electrode - CoO
Electrolyte - Acetonitrile-KPF6
Sweep rate - 40 mv/sec
Temp. 30° C
Zero ref. -0.14 v/Pt
CV - 1259
60.0
40.0
20.0
0.0
-20.0
-40.0
CHARGE
ma/cm2
DISCHARGE
-1.0
-0.8
-0.6
-0.4
-0.2
0
0.2
0.4
0.6
0.8
1.0
VOLTS POLARIZATION

Figure 38

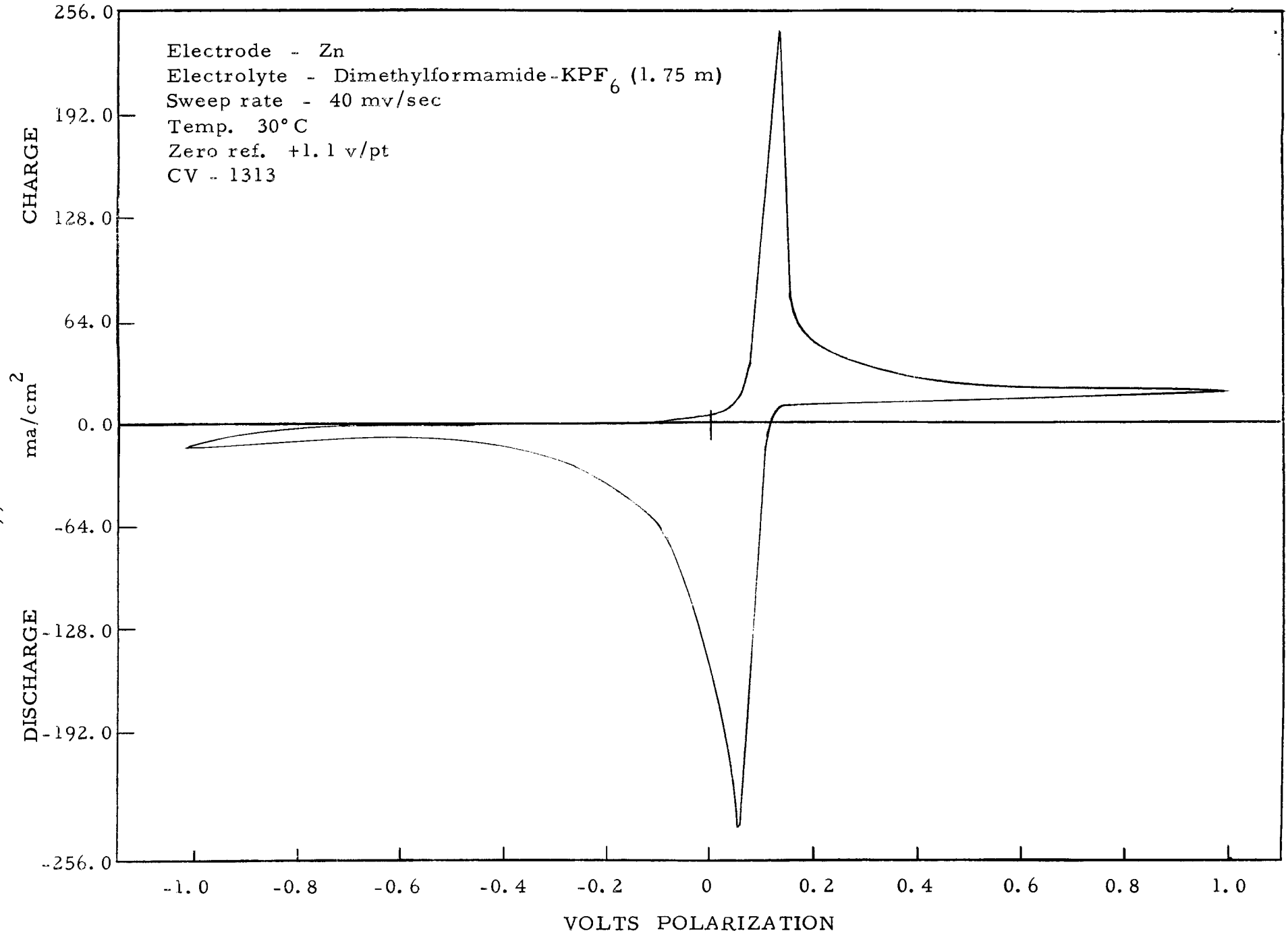
Electrode - Zn
Electrolyte - Dimethylformamide-KPF6 (1.75 m)
Sweep rate - 40 mv/sec
Temp. 30° C
Zero ref. +1.1 v/pt
CV - 1313
256.0
192.0
128.0
64.0
0.0
-64.0
-128.0
-192.0
-256.0
CHARGE
DISCHARGE
ma/cm2
-1.0
-0.8
-0.6
-0.4
-0.2
0
0.2
0.4
0.6
0.8
1.0
VOLTS POLARIZATION

Figure 39

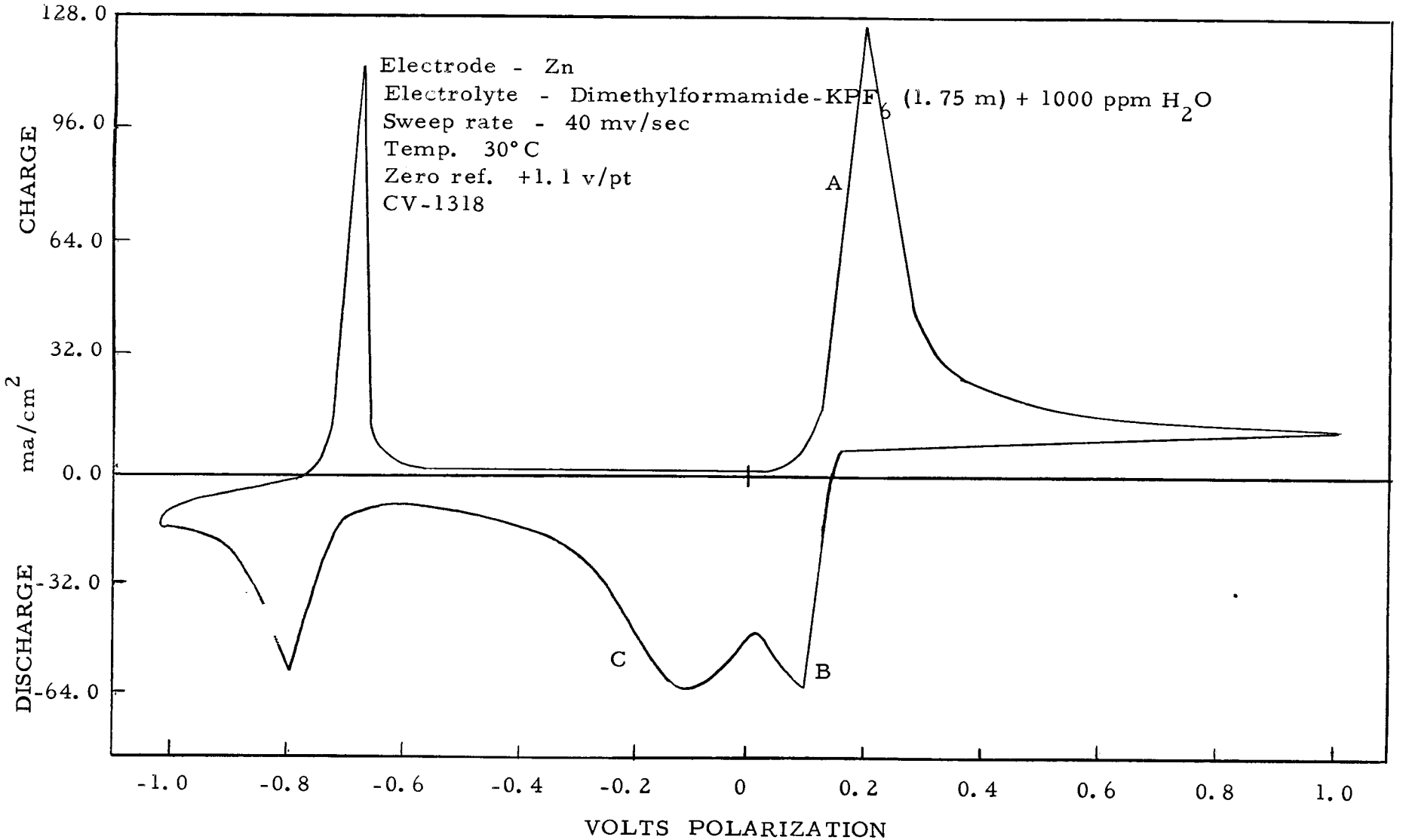
Electrode - Zn
Electrolyte - Dimethylformamide-KPF_6 (1.75 m) + 1000 ppm H_2O
Sweep rate - 40 mv/sec
Temp. 30°C
Zero ref. +1.1 v/pt
CV-1318
A
B
C
128.0
96.0
64.0
32.0
0.0
-32.0
-64.0
CHARGE
DISCHARGE
ma/cm^2
-1.0
-0.8
-0.6
-0.4
-0.2
0
0.2
0.4
0.6
0.8
1.0
VOLTS POLARIZATION

Figure 40

C. TABLES OF CYCLIC VOLTAMMETRIC DATA

Included in this section are tables listing parameters derived from the cyclic voltammograms. These parameters are as follows:

1. Sweep index

This is a relative figure of merit taking into account peak height, sweep rate, and discharge capacity. This parameter is described in more detail in an earlier report (Ref. 2, p. 80).

2. Peak current density range

Relative magnitude of peak currents classified according to page 7.

3. Cathode compatibility with electrolyte

A measure of degree of solubility of the cathode material relative to the cycling time, and hence the sweep rate.

4. Charge-discharge efficiency

Ratio of discharge coulombs to charge coulombs.

5. ΔV_p

Peak-to-peak displacement in volts of charge and discharge reactions giving a measure of overall electrode reversibility, or in more practical terms, a measure of suitability of the electrochemical system for secondary battery application.

Also included is Table IV listing the maximum current range of systems causing voltage overload of the instrumentation so that cyclic voltammograms could not be recorded.

TABLE IV

SYSTEMS CAUSING VOLTAGE OVERLOAD OF INSTRUMENTATION

System	CV	Maximum Anodic Current Density ma/cm^2	Maximum Cathodic Current Density ma/cm^2
$Ag/AN-PF_5$	1328	nr*	nr
$Ag/AN-BF_3$	1399	80	40
$Ag/AN-Mg(BF_4)_2$	1436	440	400
$Ag/BL-PF_5$	1340	nr	nr
$Ag/BL-BF_3$	1430	360	200
$Ag/DMF-PF_5$	1324	nr	nr
$Ag/DMF-BF_3$	1403	600	200
$Ag/DMF-Mg(BF_4)_2$	1444	800	800
$Ag/PC-PF_5$	1350	nr	nr
$Ag/PC-BF_3$	1409	nr	nr
$AgO/DMF-LiPF_6$	1387	1200	800
$AgO/PC-LiPF_6$	1571	1000	920
$AgF_2/DMF-LiBF_4$	1486	1600	400
$Cu/AN-MgCl_2$	1151	nr	nr
$Cu/AN-BF_3$	1402	nr	nr
$Cu/AN-Mg(BF_4)_2$	1443	nr	nr
$Cu/BL-PF_5$	1349	nr	nr
$Cu/BL-BF_3$	1435	nr	nr
$Cu/DMF-PF_5$	1327	nr	nr

AN - Acetonitrile
BL - Butyrolactone
DMF - Dimethylformamide
PC - Propylene carbonate

* nr - not recorded

TABLE IV (Cont'd)

SYSTEMS CAUSING VOLTAGE OVERLOAD OF INSTRUMENTATION

System	CV	Maximum Anodic Current Density ma/cm^2	Maximum Cathodic Current Density ma/cm^2
$Cu/DMF-BF_3$	1408	720	640
$Cu/PC-PF_5$	1360	nr*	nr
$Cu/PC-BF_3$	1414	nr	nr
$CuO/DMF-LiClO_4$	1133	nr	nr
$Ni/AN-BF_3$	1400	200	40
$Ni/AN-Mg(BF_4)_2$	1441	nr	nr
$Ni/DMF-PF_5$	1325	nr	nr
$Ni/PC-PF_5$	1354	nr	nr
$Co/AN-PF_5$	1334	nr	nr
$Co/AN-BF_3$	1401	400	80
$Co/AN-Mg(BF_4)_2$	1442	nr	nr
Co/BL-LiCl	1152	nr	nr
$Co/BL-BF_3$	1434	320	40
$Co/DMF-LiCl+AlCl_3$	1823	3200	nr
$Co/DMF-PF_5$	1326	nr	nr
$Co/DMF-BF_3$	1407	700	0
$Co/DMF-Mg(BF_4)_2$	1450	600	200
$Co/PC-BF_3$	1413	nr	nr

AN - Acetonitrile
BL - Butyrolactone
DMF - Dimethylformamide
PC - Propylene carbonate

* nr - not recorded

TABLE V

PEAK CURRENT DENSITY RANGE
CHLORIDE AND PERCHLORATE ELECTROLYTES

System	CV	Anodic	Cathodic
$Ag/AN-MgCl_2$	1147	low	low
$AgF_2/AN-LiClO_4$	1634	very low	very low
$AgF_2/BL-LiClO_4$	1644	low	low
$AgF_2/PC-LiClO_4$	1659	very low	very low
Cu/DMF-LiCl	1116	high	med. high
$CuO/PC-LiCl+AlCl_3$	1111	med. low	med. low
$CuF_2/AN-LiClO_4$	1619	med. high	med. high
$CuF_2/BL-LiClO_4$	1639	high	very high
$CuF_2/DMF-LiCl+AlCl_3$	1817	very high	very high
$CuF_2/DMF-LiClO_4$	1560	low	low
$CuF_2/PC-LiClO_4$	1419	med. high	high
$Co/BL-LiClO_4$	1172	med. high	med. low
$Co/BL-LiCl+LiClO_4$	1208	low	low
CoO/BL-LiCl	1152	high	low
$CoO/BL-LiCl+LiClO_4$	1213	very low	very low
CoO/DMF-LiCl	1167	very low	very low

AN - Acetonitrile
BL - Butyrolactone
DMF - Dimethylformamide
PC - Propylene carbonate

TABLE VI

PEAK CURRENT DENSITY RANGE
FLUORIDE ELECTROLYTES

System	CV	Anodic	Cathodic
$AgO/PC-LiF+KPF_6$	1286	med. high	med. low
$AgF_2/AN-KPF_6$	1678	low	very low
$AgF_2/AN-LiF+KPF_6$	1719	low	low
$AgF_2/BL-KPF_6$	1781	low	low
$AgF_2/BL-LiF+KPF_6$	1807	low	low
$AgF_2/DMF-KPF_6$	1737	med. low	low
$AgF_2/DMF-LiF+KPF_6$	1745	med. low	med. low
$AgF_2/PC-LiPF_6$	1609	low	very low
$AgF_2/PC-KPF_6$	1694	low	low
$AgF_2/PC-LiF+KPF_6$	1763	low	low
$AgF_2/PC-LiBF_4$	1491	high	high
$Cu/AN-LiPF_6$	1386	very high	high
$Cu/DMF-Mg(BF_4)_2$	1455	med. low	med. low
$CuO/AN-LiPF_6$	1381	med. low	med. low
$CuO/PC-LiPF_6$	1570	med. low	med. low
$CuO/PC-LiF+KPF_6$	1281	med. low	low
$CuF_2/AN-LiPF_6$	1553	med. low	med. low
$CuF_2/AN-KPF_6$	1683	very high	med. high
$CuF_2/AN-LiF+KPF_6$	1704	high	med. high
$CuF_2/AN-LiBF_4$	1468	very high	high

AN - Acetonitrile
BL - Butyrolactone
DMF - Dimethylformamide
PC - Propylene carbonate

TABLE VI (Cont'd)

PEAK CURRENT DENSITY RANGE
FLUORIDE ELECTROLYTES

System	CV	Anodic	Cathodic
CuF_2/BL-KPF_6	1786	med. high	low
CuF_2/BL-LiF+KPF_6	1812	high	med. low
CuF_2/DMF-$LiPF_6$	1525	very high	very high
CuF_2/DMF-KPF_6	1424	med. low	low
CuF_2/DMF-LiF+KPF_6	1429	low	low
CuF_2/DMF-$LiBF_4$	1481	very high	med. low
CuF_2/PC-$LiPF_6$	1614	high	high
CuF_2/PC-KPF_6	1699	med. high	med. low
CuF_2/PC-LiF+KPF_6	1768	med. high	med. low
NiO/AN-$LiPF_6$	1366	low	low
NiF_2/DMF-$LiBF_4$	1510	low	low
Co/AN-$LiPF_6$	1371	med. low	med. low
Co/AN-$LiBF_4$	1460	very high	med. low
Co/BL-KPF_6	1228	low	low
Co/DMF-KPF_6	1242	low	very low
Co/DMF-$LiBF_4$	1477	high	med. low
Co/PC-$LiPF_6$	1596	low	low
CoO/AN-$LiPF_6$	1376	low	low
CoO/AN-KPF_6	1259	med. high	med. low
Zn/DMF-KPF_6	1313	high	high

AN - Acetonitrile
BL - Butyrolactone
DMF - Dimethylformamide
PC - Propylene carbonate

TABLE VII

SWEEP INDEX *

System	CV	Anodic $ohm^{-1}\ cm^{-2}$	Cathodic $ohm^{-1}\ cm^{-2}$
AgF_2/DMF-LiF+KPF_6	1745	11.2	7.3
Cu/AN-$LiPF_6$	1386	141	251
CuO/AN-$LiPF_6$	1381	3.0	2.0
CuF_2/AN-$LIPF_6$	1553	2.0	2.0
CuF_2/AN-LiF+KPF_6	1704	55.3	37.0
CuF_2/AN-$LiBF_4$	1468	192.0	25.0
CuF_2/BL-LiF+KPF_6	1812	35.8	3.2
CuF_2/DMF-$LiPF_6$	1525	364	2570
CuF_2/DMF-KPF_6	1424	5.0	8.0
CuF_2/PC-$LiPF_6$	1614	13.0	80.0
CuF_2/PC-LiF+KPF_6	1768	12.4	2.0
Zn/DMF-KPF_6	1313	125	134
Cu/DMF-LiCl	1116	31.6	158
CuF_2/BL-$LiClO_4$	1639	-	1290
CuF_2/DMF-LiCl+$AlCl_3$	1817	-	652
CuF_2/DMF-$LiClO_4$	1560	1.0	0.3
CuF_2/PC-$LiClO_4$	1419	14.0	46.0

AN - Acetonitrile
BL - Butyrolactone
DMF - Dimethylformamide
PC - Propylene carbonate

$$* \frac{(\text{peak c.d.})^2 \times 100}{\text{sweep rate} \times \text{coul/cm}^2}$$

TABLE VIII

CATHODE COMPATIBILITY IN CHLORIDE ELECTROLYTES

System	CV	Cathode Stability
$Ag/AN-MgCl_2$	1147	Insoluble
$AgF_2/AN-LiClO_4$	1634	Insoluble
$AgF_2/BL-LiClO_4$	1644	Insoluble
$AgF_2/PC-LiClO_4$	1659	Insoluble
Cu/DMF-LiCl	1116	Soluble
$CuO/PC-LiCl+AlCl_3$	1111	Soluble
$CuF_2/AN-LiClO_4$	1619	Insoluble
$CuF_2/BL-LiClO_4$	1639	Insoluble
$CuF_2/DMF-LiCl+AlCl_3$	1817	Soluble
$CuF_2/DMF-LiClO_4$	1560	Soluble
$CuF_2/PC-LiClO_4$	1419	Insoluble
$Co/BL-LiClO_4$	1172	Soluble
$Co/BL-LiCl+LiClO_4$	1208	Insoluble
CoO/BL-LiCl	1152	Insoluble
$CoO/BL-LiCl+LiClO_4$	1213	Insoluble
CoO/DMF-LiCl	1167	Insoluble

AN - Acetonitrile
BL - Butyrolactone
DMF - Dimethylformamide
PC - Propylene carbonate

TABLE IX

CATHODE COMPATIBILITY IN FLUORIDE ELECTROLYTES

System	CV	Cathode Stability
$AgO/PC-LiF+KPF_6$	1286	Soluble
$AgF_2/AN-KPF_6$	1678	Insoluble
$AgF_2/AN-LiF+KPF_6$	1719	Insoluble
$AgF_2/BL-KPF_6$	1781	Insoluble
$AgF_2/BL-LiF+KPF_6$	1807	Insoluble
$AgF_2/DMF-KPF_6$	1737	Soluble
$AgF_2/DMF-LiF+KPF_6$	1745	Soluble
$AgF_2/PC-LiPF_6$	1609	Insoluble
$AgF_2/PC-KPF_6$	1694	Insoluble
$AgF_2/PC-LiF+KPF_6$	1763	Insoluble
$AgF_2/PC-LiBF_4$	1491	Soluble
$Cu/AN-LiPF_6$	1386	Insoluble
$Cu/DMF-Mg(BF_4)_2$	1455	Insoluble
$CuO/AN-LiPF_6$	1381	Insoluble
$CuO/PC-LiPF_6$	1570	Insoluble
$CuO/PC-LiF+KPF_6$	1281	Insoluble
$CuF_2/AN-LiPF_6$	1553	Insoluble
$CuF_2/AN-KPF_6$	1683	Insoluble
$CuF_2/AN-LiF+KPF_6$	1704	Soluble
$CuF_2/AN-LiBF_4$	1468	Insoluble

AN - Acetonitrile
BL - Butyrolactone
DMF - Dimethylformamide
PC - Propylene carbonate

TABLE IX (Cont'd)

CATHODE COMPATIBILITY IN FLUORIDE ELECTROLYTES

System	CV	Cathode Stability
CuF_2/BL-KPF_6	1786	Soluble
CuF_2/BL-LiF+KPF_6	1812	Insoluble
CuF_2/DMF-$LiPF_6$	1525	Insoluble
CuF_2/DMF-KPF_6	1424	Insoluble
CuF_2/DMF-LiF+KPF_6	1429	Insoluble
CuF_2/DMF-$LiBF_4$	1481	Insoluble
CuF_2/PC-$LiPF_6$	1614	Insoluble
CuF_2/PC-KPF_6	1699	Soluble
CuF_2/PC-LiF+KPF_6	1768	Soluble
NiO/AN-$LiPF_6$	1366	Insoluble
NiF_2/DMF-$LiBF_4$	1510	Insoluble
Co/AN-$LiPF_6$	1371	Insoluble
Co/AN-$LiBF_4$	1460	Soluble
Co/BL-KPF_6	1228	Insoluble
Co/DMF-KPF_6	1242	Insoluble
Co/DMF-$LiBF_4$	1477	Soluble
Co/PC-$LiPF_6$	1596	Insoluble
CoO/AN-$LiPF_6$	1376	Insoluble
CoO/AN-KPF_6	1259	Insoluble
Zn/DMF-KPF_6	1313	Insoluble

AN - Acetonitrile
BL - Butyrolactone
DMF - Dimethylformamide
PC - Propylene carbonate

TABLE X

ΔV_p AND CHARGE-DISCHARGE EFFICIENCY
CHLORIDE ELECTROLYTES

System	CV	ΔV_p *	Charge-Discharge Efficiency %
$Ag/AN\text{-}MgCl_2$	1147	1.05	-
$AgF_2/AN\text{-}LiClO_4$	1634	0.35	-
$AgF_2/BL\text{-}LiClO_4$	1644	1.10	-
$AgF_2/PC\text{-}LiClO_4$	1659	0.95	-
Cu/DMF-LiCl	1116	0.08	4.3
$CuF_2/AN\text{-}LiClO_4$	1619	1.10	-
$CuF_2/BL\text{-}LiClO_4$	1639	0.25	67
$CuF_2/DMF\text{-}LiCl+AlCl_3$	1817	0.10	-
$CuF_2/DMF\text{-}LiClO_4$	1560	0.50	56
$CuF_2/PC\text{-}LiClO_4$	1419	0.33	58
$Co/BL\text{-}LiClO_4$	1172	0.89	23
$Co/BL\text{-}LiCl+LiClO_4$	1208	1.55	-
$CoO/BL\text{-}LiCl+LiClO_4$	1213	1.02	-

* - Voltage separating anodic and cathodic peaks.

AN - Acetonitrile
BL - Butyrolactone
DMF - Dimethylformamide
PC - Propylene carbonate

TABLE XI

ΔV_p AND CHARGE-DISCHARGE EFFICIENCY
FLUORIDE ELECTROLYTES

System	CV	ΔV_p*	Charge-Discharge Efficiency %
$AgO/PC-LiF+KPF_6$	1286	0.65	-
$AgF_2/AN-KPF_6$	1678	0.88	-
$AgF_2/AN-LiF+KPF_6$	1719	0.94	-
$AgF_2/BL-LiF+KPF_6$	1807	0.45	-
$AgF_2/DMF-LiF+KPF_6$	1745	0.65	64
$AgF_2/PC-LiPF_6$	1609	1.20	-
$AgF_2/PC-LiBF_4$	1491	0.20	-
$Cu/AN-LiPF_6$	1386	0.09	33
$CuO/AN-LiPF_6$	1381	0.41	66
$CuO/PC-LiPF_6$	1570	0.25	-
$CuF_2/AN-LiPF_6$	1553	0.56	94
$CuF_2/AN-KPF_6$	1683	0.04	15
$CuF_2/AN-LiF+KPF_6$	1704	0.23	11
$CuF_2/AN-LiBF_4$	1468	0.20	13

* - Voltage separating anodic and cathodic peaks.

AN - Acetonitrile
BL - Butyrolactone
DMF - Dimethylformamide
PC - Propylene carbonate

TABLE XI (Cont'd)

ΔV_p AND CHARGE-DISCHARGE EFFICIENCY
FLUORIDE ELECTROLYTES

System	CV	ΔV_p*	Charge-Discharge Efficiency %
CuF_2/BL-KPF_6	1786	0.15	-
CuF_2/DMF-$LiPF_6$	1525	0.02	43
CuF_2/DMF-KPF_6	1424	0.41	71
CuF_2/DMF-LiF+KPF_6	1429	0.64	-
CuF_2/DMF-$LiBF_4$	1481	0.77	-
CuF_2/PC-$LiPF_6$	1614	0.17	51
CuF_2/PC-LiF+KPF_6	1768	0.97	48
NiF_2/DMF-$LiBF_4$	1510	1.18	-
Co/AN-$LiPF_6$	1371	1.40	-
Co/AN-$LiBF_4$	1460	1.50	-
Co/BL-KPF_6	1228	1.10	-
Co/DMF-KPF_6	1242	1.20	-
Co/DMF-$LiBF_4$	1477	1.80	-
Co/PC-$LiPF_6$	1596	1.80	-
CoO/AN-$LiPF_6$	1376	1.46	-
Zn/DMF-KPF_6	1313	0.07	98

* - Voltage separating anodic and cathodic peaks.

AN - Acetonitrile
BL - Butyrolactone
DMF - Dimethylformamide
PC - Propylene carbonate

II. EXPERIMENTAL

A. MATERIAL PURIFICATION AND CHARACTERIZATION

As previously reported, all materials handling, unless otherwise indicated, was accomplished under nitrogen in an atmosphere chamber maintained at 30 ±1°C by a recirculating gas heating system. Characterization and preparation of solutions of such materials as LiCl, $AlCl_3$ and KPF_6 have been previously detailed.

1. Distillation of Solvents

Minor modifications have been made in the distillation procedure. Solvents were distilled at the indicated temperature and pressure in the same apparatus. Usually 1500 ml portions were distilled, with about 100 ml comprising the main cut, the remainder being divided between the head fraction and pot residue. The distillation apparatus consisted of 1 inch by 3 feet vacuum jacketed (and silvered) column packed with 3/8" beryl saddles, and equipped with a total reflux return head. The head was connected to a revolving type multiple distillation receiver through a stopcock which was used to adjust the take-off rate. Connection was also made to the usual vacuum manifold consisting of rough and fine manometers connected in series with a Cartesian manostat, dry ice-trap and vacuum pump. After distillation start-up and removal of low boiling impurities, the column was purposely flooded to insure proper wetting. It was then allowed to equilibrate over a 1-2 hours period and fractionation commenced. The main fractions were usually taken over a 48-hour period at a reflux ratios of 20-25/1. Use of higher reflux ratios did not improve the fractionation characteristics.

Propylene carbonate was distilled at 108-110°/10 mm. Following the initial distillation, the main cut was dried over calcium sulfate and redistilled under

the same conditions. Butyrolactone was distilled at 91-93°/17 mm. A somewhat larger head fraction (300-400 ml) was usually taken in order to avoid possible trace contamination of a high boiling impurity previously revealed by VPC analysis. Acetonitrile was distilled at 80-82°C. Dimethylformamide was not redistilled since previous work had indicated less than 100 ppm of water in the "as received" material (MCB, Spectroquality grade).

2. Solution Preparation

a. PF_5 solutions

The stainless steel gas manifold used for the preparation of PF_5 solutions is shown in Figure 41. The manifold was conditioned by evacuating for several hours at 0.05 mm, refilling with PF_5 to 15 psig, and re-evacuation to remove any gaseous reaction products.

After filling the three-neck flask with about 240 ml of solvent in the inert atmosphere chamber, the pyrex gas inlet tube of the flask was connected to the manifold by means of a short Tygon connector. The entire system was then flushed with nitrogen. After removal of nitrogen by evacuation, the gas bulbs were filled to 60 psig with PF_5. The latter was then slowly introduced to the solvent at a rate allowing complete absorption of the gas. The amount of gas being absorbed was monitored by the oil-filled bubbler on the gas exit tube. Following solution preparation, the gas exit tube was replaced by a special dip tube which allowed direct transfer of the solution to the CV measuring cell by means of nitrogen pressurization. For electrochemical measurements involving either PF_5 or BF_3 solutions, the cell was not placed in the inert atmosphere chamber in order to avoid possible contamination of the chamber with these gases.

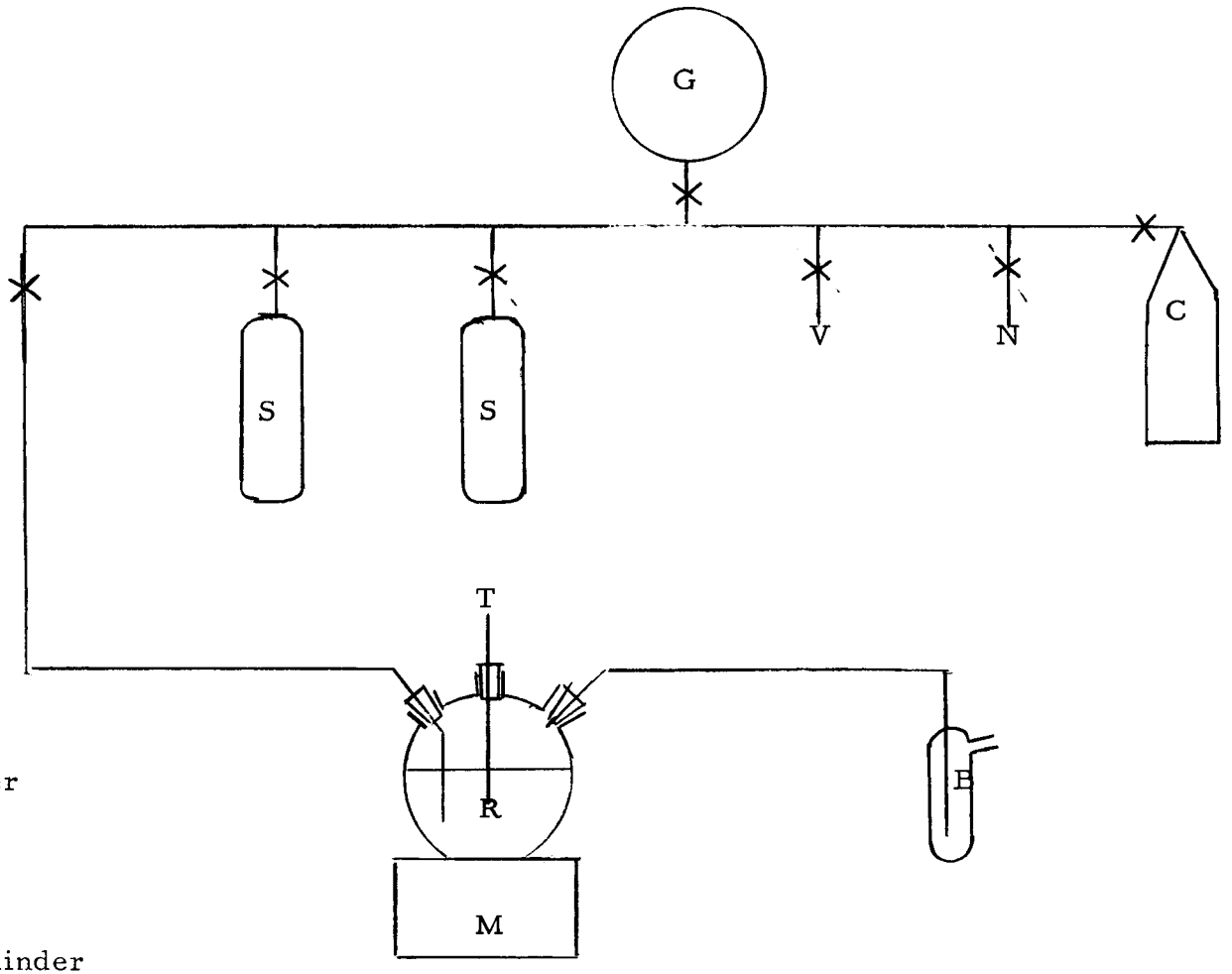

G - gauge
B - bubbler
M - magnetic stirrer
R - reaction flask
S - storage bulb
V - vacuum
N - nitrogen
C - PF_5 or BF_3 cylinder
T - thermometer

Figure 41 Schematic of apparatus for preparing fluoride electrolytes

All solutions were prepared at room temperature. In the case of dimethylformamide, propylene carbonate, and acetonitrile, there was evidence of deposition of a solid complex on the walls of the gas addition tube. (The complex was apparently soluble in the solvent). Solutions of PF_5 in dimethylformamide and propylene carbonate were colorless and did not discolor after several hours. The PF_5-acetonitrile solutions were yellow. This color persisted for several hours but could be removed by the addition of LiF. The addition of PF_5 to butyrolactone caused immediate discoloration of the solution which intensified on longer standing.

b. BF_3 solutions

Solutions of BF_3 were prepared in the same manner as for PF_5 except for the fact that the solvent temperature was usually maintained at 8-10°C in order to increase the apparent rate of solution. After BF_3 addition was completed, the solution was allowed to warm to room temperature before transferring to the conductance or CV measuring cell. As in the case of PF_5, addition of BF_3 to butyrolactone caused extensive discoloration.

c. $LiPF_6$ and $LiBF_4$ solutions

Solutions of $LiPF_6$ and $LiBF_4$ were prepared in a manner similar to that described above except that a known quantity of LiF was suspended in the solvent before addition of the PF_5 or BF_3 respectively. Essentially all of the LiF dissolved on addition of equimolar quantities of the gases, indicating relatively complete formation of the complex fluoride salts. Additions were carried out at 8-10°C.

Since PF_5 appeared to react in a deleterious manner with butyrolactone, the preparation of $LiPF_6$ *in situ* was not deemed advisable so that direct reaction of LiF with PF_5 was attempted without success. A 5.0g sample of LiF was placed in a nickel tube connected to the gas manifold. The tube was

evacuated and filled with PF_5 to 25 psig. This quantity of PF_5 was insufficient to react with all of the LiF. Even after slowly heating to 290°C, no pressure drop was observed, indicating little or no formation of $LiPF_6$ under these conditions. An alternate procedure, involving solution of LiF in liquid PF_5 at -88.5°C afforded no product.

d. $Mg(BF_4)_2$ solutions

Preparation of $Mg(BF_4)_2$ by addition of BF_3 to LiF suspension of solvent was attempted. From the amount of material remaining after the addition of 2 moles of BF_3 per mole of MgF_2, incomplete reaction was indicated. However, it is not known at this time whether the residual solid is unreacted MgF_2 or precipitated $Mg(BF_4)_2$.

3. Electrode Preparation

Fluoride electrodes were prepared by exposing short lengths of wire of the desired metal to pure fluorine in a nickel reactor at 30 psia (20°C) under the conditions given in Table XII. Evidence of reaction was indicated by a 1-2% weight gain and a change in visual appearance. (A typical weight gain was 15 mg for a 3-inch length of Cu wire).

TABLE XII

FLUORINATION CONDITIONS

Metal	Exposure Time (hours)	Temperature °C
Ag	5	100
Co	7	480
Cu	4	480
Ni	14	600

B. CYCLIC VOLTAMMETRIC MEASUREMENTS

A detailed description of the instrumentation, measuring cell, and measurement procedure, is thoroughly described in an earlier report (Ref. 2). Minor modification including use of a newly designed cell is described in a later report (Ref. 1).

1. Instrument Overloading

The instrumentation which has been employed in the cyclic voltammetric measurements is based upon operational amplifier modules. Since the modular instrumentation is limited to ±20 ma, a Harrison 6823A amplifier is used to extend the working range. This amplifier is rated at 20 v and ±500 ma. In the past, a number of electrochemical systems have resulted in currents in excess of this value, causing current overload of the amplifier. This in turn drives the voltage to an overload condition. During this reporting period many of the BF_3 and PF_5 solutions have resulted in voltage overload, but without the accompanying current overload. This is due to the relatively low electrolyte conductance accompanied by an appreciable current so that the 20 v limit of the instrument is exceeded. Voltage overload did not occur in the earlier reporting periods on MgF_2 systems for instance, even though the solution resistance was 10 to 100 times greater, since the currents were exceedingly low, owing to poor availability of electroactive species (very low solute solubility). In the case of the PF_5 and BF_3 solutions, however, there is sufficient anodic or cathodic activity to produce current densities from the medium low to very high range, but still less than 500 ma total current, which with the relatively high solution resistance will cause voltage overload.

In both cases (currents less and greater than 500 ma) the amplifier suffers a voltage overload. For purposes of recording however, and to distinguish

systems having currents greater than 500 ma (irrespective of the solution conductivity) from those in which the currents are sufficiently high (but less than 500 ma) but which possess a relatively low conductance, the term current overload will be reserved for the former, and voltage overload for the latter. The approximate maximum current (both anodic and cathodic) for the latter systems is indicated on the amplifier meter, and in a number of cases was noted and recorded. Because of the large frequency of occurrence of such systems, recording of the magnitude and direction of this current will be standard procedure for continuing measurements.

A maximum current of 500 ma corresponds to a current density of 2.0 amps/cm^2 for a 1/4 inch length electrode. Prior to the availability of the Harrison amplifier, the Wenking potentiostat was used as a current amplifier. With this instrument the maximum permissible current was 500 ma anodic, and 300 ma cathodic. A new Harrison amplifier will shortly be available which will extend the current capability to 1.0 amp and the voltage limit to 50 v.

III. REFERENCES

1. Whittaker Corporation, Narmco Research and Development Division, Second Quarterly Report, NASA Contract NAS 3-8509, NASA Report CR-72138, November 1966.

2. Whittaker Corporation, Narmco Research and Development Division, First Quarterly Report, NASA Contract NAS 3-8509, NASA Report CR-72069, August 1966.

DISTRIBUTION LIST

National Aeronautics and Space Admin.
Washington, D. C. 20546
Attn: E. M. Cohn/RNW
A. M. Greg Andrus/PC

National Aeronautics and Space Admin.
Goddard Space Flight Center
Greenbelt, Maryland 20771
Attn: T. Hennigan, Code 716.2
J. Sherfey, Code 735
P. Donnelly, Code 636.2
E. R. Stroup, Code 636.2

National Aeronautics and Space Admin.
Langley Research Center
Instrument Research Division
Hampton, Virginia 23365
Attn: J. L. Patterson, MS 234
M. B. Seyffert, MS 112

National Aeronautics and Space Admin.
Langley Research Center
Langley Station
Hampton, Virginia 23365
Attn: S. T. Peterson
Harry Ricker

National Aeronautics and Space Admin.
Lewis Research Center
21000 Brookpark Road
Cleveland, Ohio 44135
Attn: Library, MS 60-3
N. D. Sanders, MS 302-1
John E. Dilley, MS 500-309
B. Lubarsky, MS 500-201
H. J. Schwartz, MS 500-201
R. B. King, MS 500-202
V. F. Hlavin, MS 3-14 (Final only)
M. J. Saari, MS 500-202
J. J. Weber, MS 3-19
Report Control, MS 5-5
S. Fordyce, MS 302-1

National Aeronautics and Space Admin.
Scientific and Technical Information Facility
P. O. Box 33
College Park, Maryland 20740
Attn: Acquisitions Branch (SQT-34054)
(2 cys. + 1 repro.)

National Aeronautics and Space Admin.
George C. Marshall Space Flight Center
Huntsville, Alabama 35812
Attn: Philip Youngblood
R. Boehme, Bldg. 4487-BB,
M-ASTR-EC

National Aeronautics and Space Admin.
Manned Spacecraft Center
Houston, Texas 77058
Attn: W. R. Dusenbury, Propulsion
and Energy Systems
R. Cohen, Gemini Project Office
R. Ferguson (EP-5)
J. T. Kennedy (EE-5)
F. E. Eastman (EE-4)

National Aeronautics and Space Admin.
Ames Research Center
Pioneer Project
Moffett Field, California 94035
Attn: J. R. Swain
A. S. Hertzog
J. Rubenzer, Biosatellite Project

Jet Propulsion Laboratory
4800 Oak Grove Drive
Pasadena, California 91103
Attn: A. Uchiyama

U. S. Army Engineer R and D Labs.
Fort Belvoir, Virginia 22060
Attn: Electrical Power Branch.
SMOFB-EP

Commanding Officer
U. S. Army Electronics R and D Labs.
Fort Monmouth, New Jersey 07703
Attn: Power Sources Div., Code SELRA/PS

Research Office
R and D Directorate
Army Weapons Command
Rock Island, Illinois 61201
Attn: G. Riensmith, Chief

U. S. Army Research Office
Box CM, Duke Station
Durham, North Carolina 27706
Attn: Dr. W. Jorgensen

U. S. Army Research Office
Chief, R and D
Department of the Army
3 D 442, The Pentagon
Washington, D. C. 20546

Harry Diamond Laboratories
Room 300, Bldg. 92
Conn. Ave. and Van Ness St., NW
Washington, D. C. 20438
Attn: N. Kaplan

Army Materiel Command
Research Division
AMCRD-RSCM-T-7
Washington, D. C. 20315
Attn: J. W. Crellin

Army Materiel Command
Development Division
AMCRO-DE-MO-P
Washington, D. C. 20315
Attn: M. D. Aiken

U. S. Army TRECOM
Fort Eustis, Virginia 23604
Attn: Dr. R. L. Echols (SMOFE-PSG)
L. M. Bartone (SMOFE-ASE)

U. S. Army Mobility Command
Research Division
Watten, Michigan 48090
Attn: O. Renius (AMSMO-RR)

U. S. Army R and L Liaison Group
(9851 DV) APO 757
New York, New York 10004
Attn: B. R. Stein

Natick Laboratories
Clothing and Organic Materials Division
Natick, Massachusetts 01760
Attn: N. Fertman

Office of Naval Research
Department of the Navy
Washington, D. C. 20360
Attn: Head, Power Branch, Code 429
H. W. Fox, Code 425

Naval Research Laboratory
Washington, D. C. 20390
Attn: Dr. J. C. White, Code 6160

U. S. Navy
Marine Engineering Laboratory
Annapolis, Maryland 21402
Attn: J. H. Harrison

Bureau of Naval Weapons
Department of the Navy
Washington, D. C. 20360
Attn: W. T. Beatson, Code RAAE-52
M. Knight, Code RAAE-50

Naval Ammunition Depot
Crane, Indiana 47522
Attn: E. Bruess
H. Schultz

Naval Ordnance Laboratory
Department of the Navy
Corona, California 91720
Attn: W. C. Spindler, Code 441

Naval Ordnance Laboratory
Department of the Navy
Silver Springs, Maryland 20900
Attn: P. B. Cole, Code WB

Bureau of Ships
Department of the Navy
Washington, D. C. 20360
Attn: B. B. Rosenbaum, Code 340
C. F. Viglotti, Code 660

Space Systems Division
Los Angeles AF Station
Los Angeles, California 90045
Attn: SSSD

Air Force Cambridge Research Lab.
L. G. Hanscom Field
Bedford, Massachusetts 01731
Attn: Commander (CRO)

Flight Vehicle Power Branch
Aero Propulsion Laboratory
Wright-Patterson AFB, Ohio 45433
Attn: J. E. Cooper

Headquarters, USAF (AFRDR-AS)
Washington, D. C. 20546
Attn: Maj. G. Starkey
Lt. Col. W. G. Alexander

Rome Air Development Center, ESD
Griffis AF Base, New York 13442
Attn: F. J. Mollura (RASSM)

National Bureau of Standards
Washington, D. C. 20234
Attn: Dr. W. J. Hamer

Office DDR and E, USE and BSS
The Pentagon
Washington, D. C. 20310
Attn: G. B. Wareham

Army Reactors, DRD
U. S. Atomic Energy Commission
Washington, D. C. 20545
Attn: D. B. Hoatson

Institute for Defense Analyses
R and E Support Division
400 Army-Navy Drive
Arlington, Virginia 22202
Attn: R. Hamilton
Dr. G. C. Szego

U. S. Atomic Energy Commission
Auxiliary Power Branch (SNAP)
Division of Reactor Development
Washington, D. C. 20545
Attn: Lt. Col. G. H. Ogburn, Jr.

Advanced Space Reactor Branch
Division of Reactor Development
U. S. Atomic Energy Commission
Washington, D. C. 20545
Attn: Lt. Col. J. H. Anderson

Office of Technical Services
Department of Commerce
Washington, D. C. 20009

Aerojet-General Corporation
Von Karman Center
Building 312/Dept. 3111
Azusa, California 91703
Attn: Russ Fogle

Aeronutronic Division
Philco Corporation
Ford Road
Newport Beach, California 92660

Aerospace Corporation
P. O. Box 95085
Los Angeles, California 90045
Attn: Library

Aerospace Corporation
Systems Design Division
2350 East El Segundo Boulevard
El Segundo, California 90246
Attn: John G. Krisilas

Allis-Chalmers Manufacturing Company
1100 South 70th Street
Milwaukee, Wisconsin 53201
Attn: Dr. P. Joyner

American University
Massachusetts and Nebraska Avenues, NW
Washington, D. C. 20016
Attn: Dr. R. T. Foley, Chemistry Department

Arthur D. Little, Incorporated
Acorn Park
Cambridge, Massachusetts 02140
Attn: Dr. Ellery W. Stone

Atomics International Division
North American Aviation, Incorporated
8900 DeSoto Avenue
Canoga Park, California 91304
Attn: Dr. H. L. Recht

Battelle Memorial Institute
505 King Avenue
Columbus, Ohio 43201
Attn: Dr. C. L. Faust

Bell Laboratories
Murray Hill, New Jersey 07971
Attn: U. B. Thomas

The Boeing Company
P. O. Box 3707
Seattle, Washington 98124

Borden Chemical Company
Central Research Laboratory
P. O. Box 9524
Philadelphia, Pennsylvania 19124

Burgess Battery Company
Foot of Exchange Street
Freeport, Illinois 61032
Attn: Dr. Howard J. Strauss

C and D Batteries
Division of Electric Autolite Company
Conshohocken, Pennsylvania 19428
Attn: Dr. Eugene Willihnganz

Calvin College
Grand Rapids, Michigan 49506
Attn: Prof. T. P. Dirkse

Catalyst Research Corporation
6101 Falls Road
Baltimore, Maryland 21209
Attn: J. P. Wooley

ChemCell, Incorporated
3 Central Avenue
East Newark, New Jersey 07029
Attn: Peter D. Richman

Delco Remy Division
General Motors Corporation
2401 Columbus Avenue
Anderson, Indiana 46011
Attn: Dr. J. J. Lander

Douglas Aircraft Company, Incorporated
Astropower Laboratory
2121 Campus Drive
Newport Beach, California 92663
Attn: Dr. Carl Berger

Dynatech Corporation
17 Tudor Street
Cambridge, Massachusetts 02138
Attn: R. L. Wentworth

Eagle-Pitcher Company
P. O. Box 47
Joplin, Missouri 64802
Attn: E. M. Morse

Elgin National Watch Company
107 National Street
Elgin, Illinois 60120
Attn: T. Boswell

Electric Storage Battery Company
Missile Battery Division
2510 Louisburg Road
Raleigh, North Carolina 27604
Attn: A. Chreitzberg

Electric Storage Battery Company
Carl F. Norberg Research Center
19 West College Avenue
Yardley, Pennsylvania 19068
Attn: Dr. R. A. Schaefer

Electrochimica Corporation
1140 O'Brien Drive
Menlo Park, California 94025
Attn: Dr. Morris Eisenberg

Electro-Optical Systems, Incorporated
300 North Halstead
Pasadena, California 91107
Attn: E. Findl

Emhart Manufacturing Company
Box 1620
Hartford, Connecticut 06101
Attn: Dr. W. P. Cadogan

Englehard Industries, Incorporated
497 Delancy Street
Newark, New Jersey 07105
Attn: Dr. J. G. Cohn

Dr. Arthur Fleischer
466 South Center Street
Orange, New Jersey 07050

Grumman Aircraft
CPGS Plant 35
Beth Page, Long Island, New York 11101
Attn: Bruce Clark

General Electric Company
Battery Products Section
P. O. Box 114
Gainesville, Florida 32601
Attn: Dr. R. L. Hadley

General Electric Company
Missile and Space Division
Spacecraft Department
P. O. Box 8555
Philadelphia, Pennsylvania 19101
Attn: E. W. Kipp, Rm. T-2513

General Electric Company
Research and Development Center
Schenectady, New York 12301
Attn: Dr. H. Liebhafsky
Dr. R. C. Osthoff, Bldg. 37, Rm 2083

General Motors-Defense Research Labs.
6767 Hollister Street
Santa Barbara, California 93105
Attn: Dr. J. S. Smatko/Dr. C. R. Russell

General Telephone and Electronics Labs.
Bayside, New York 11352
Attn: Dr. Paul Goldberg

Globe-Union, Incorporated
900 East Keefe Avenue
Milwaukee, Wisconsin 53201
Attn: Dr. Warren Towle

Gould-National Batteries, Incorporated
Engineering and Research Center
2630 University Avenue, SE
Minneapolis, Minnesota 55418
Attn: D. L. Douglas

Gulton Industries
Alkaline Battery Division
212 Durham Avenue
Metuchen, New Jersey 08840
Attn: Dr. Robert Shair

Hughes Aircraft Corporation
Centinda Avenue and Teale Street
Culver City, California 90230
Attn: T. V. Carvey

Hughes Aircraft Corporation
Building 366, MS 524
El Segundo, California 90245
Attn: R. B. Robinson

Hughes Research Labs. Corp.
3011 Malibu Canyon Road
Malibu, California 90265
Attn: T. M. Hahn

ITT Federal Laboratories
500 Washington Avenue
Nutley, New Jersey 07110
Attn: Dr. P. E. Lightly

IIT Research Institute
10 West 35 Street
Chicago, Illinois 60616
Attn: Dr. H. T. Francis

Idaho State University
Department of Chemistry
Pocatello, Idaho 83201
Attn: Dr. G. Myron Arcand

Institute of Gas Technology
State and 34 Street
Chicago, Illinois 60616
Attn: B. S. Baker

John Hopkins University
Applied Physics Laboratory
8621 Georgia Avenue
Silver Springs, Maryland 20910
Attn: Richard Cole

Johns-Mansville R and E Center
P. O. Box 159
Manville, New Jersey 08835
Attn: J. S. Parkinson

Leesona Moos Laboratories
Lake Success Park, Community Drive
Great Neck, New York 11021
Attn: Dr. H. Oswin

Livingston Electronic Corporation
Route 309
Montogmeryville, Pennsylvania 18936
Attn: William F. Meyers

Lockheed Missiles and Space Co.
3251 Hanover Street
Palo Alto, California 94304
Attn: Library
Dr. G. B. Adams

Lockheed Missiles and Space Co.
Dept. 52-30
Palo Alto, California 94304
Attn: J. E. Chilton

Lockheed Missiles and Space Co.
Dept. 65-82
Palo Alto, California 94304
Attn: Larry E. Nelson

Magna Corporation
Division of TRW, Incorporated
101 South East Avenue
Anaheim, California 92805
Attn: Dr. G. Rohrbach

P. R. Mallory and Co., Incorporated
Technical Services Laboratory
Indianapolis, Indiana 46206
Attn: A. S. Doty

P. R. Mallory and Co., Incorporated
3029 East Washington Street
Indianapolis, Indiana 46206
Attn: Technical Librarian

Marquardt Corporation
16555 Saticoy Street
Van Nuys, California 91406
Attn: Dr. H. G. Krull

Material Research Corporation
Orangeburg, New York 10962
Attn: V. E. Adler

Melpar
Technical Information Center
3000 Arlington Boulevard
Falls Church, Virginia 22046

Metals and Control Division
Texas Instruments, Incorporated
34 Forest Street
Attleboro, Massachusetts 02703
Attn: Dr. E. M. Jost

Midwest Research Institute
425 Volker Boulevard
Kansas City, Missouri 64110
Attn: Dr. B. W. Beadle

Monsanto Research Corporation
Everett, Massachusetts 02149
Attn: Dr. J. O. Smith

North American Aviation, Incorporated
Rocketdyne Division
6633 Canoga Avenue
Canoga Park, California 91303
Attn: Library

North American Aviation, Incorporated
12214 Lakewood Boulevard
Downey, California 90241
Attn: Burden M. Otzinger

Power Information Center
University of Pennsylvania
Moore School Building
200 South 33rd Street
Philadelphia, Pennsylvania 19104

Philco Corporation
Division of the Ford Motor Company
Blue Bell, Pennsylvania 19422
Attn: Dr. Phillip Cholet

Radiation Applications, Incorporated
36-40 37th Street
Long Island City, New York 11101

Radio Corporation of America
Astro Division
Hightstown, New Jersey 08520
Attn: Seymour Winkler

Radio Corporation of America
P. O. Box 800
Princeton, New Jersey 08540
Attn: I. Schulman

Sonotone Corporation
Saw Mill River Road
Elmsford, New York 10523
Attn: A. Mundel

Texas Instruments, Incorporated
13500 North Central Expressway
Dallas, Texas 75222
Attn: Dr. Isaac Trachtenberg

Thomas A. Edison Research Laboratory
McGraw Edison Company
Watchung Avenue
West Orange, New Jersey 07052
Attn: Dr. P. F. Grieger

TRW Incorporated
TRW Systems Group
One Space Park
Redondo Beach, California 90278
Attn: Dr. A. Drausz, Bldg. 60, Rm 929
R. Sparks

TRW Incorporated
23555 Euclid Avenue
Cleveland, Ohio 44117
Attn: Librarian

Tyco Laboratories, Incorporated
Bear Hill
Hickory Drive
Waltham, Massachusetts 02154
Attn: W. W. Burnett

Union Carbide Corporation
Development Laboratory Library
P. O. Box 6056
Cleveland, Ohio 44101

Union Carbide Corporation
Parma Research Center
P. O. Box 6116
Cleveland, Ohio 44101
Attn: Library

University of California
Space Science Laboratory
Berkeley, California 94720
Attn: Dr. C. W. Tobias

University of Pennsylvania
Electrochemistry Laboratory
Philadelphia, Pennsylvania 19104
Attn: Prof. J. O'M Bockris

Western Electric Company
Suite 802, RCA Building
Washington, D. C. 20006
Attn: R. T. Fiske

Westinghouse Electric Corporation
Research and Development Center
Churchill Borough
Pittsburgh, Pennsylvania 15235
Attn: Dr. A. Langer

Whittaker Corporation
Power Sources Division
3850 Olive Street
Denver, Colorado 80237
Attn: J. W. Reiter

Whittaker Corporation
Narmco Research and Development Division
3540 Aero Court
San Diego, California 92123
Attn: Dr. M. Shaw

Yardney Electric Corporation
40-50 Leonard Street
New York, New York 10013
Attn: Dr. George Dalin